UNDERSTANDING FRACTURE CONDUCTIVITY CREATED BY PROPPANT IN THE AUSTIN CHALK FORMATION

A Thesis

by

ANDREW TRAVIS BRASHEAR

Submitted to the Graduate and Professional School of
Texas A&M University
in partial fulfillment of the requirements for the degree of

MASTER OF SCIENCE

Chair of Committee,	Ding Zhu
Committee Members,	A. Daniel Hill
	Frederick M. Chester
Head of Department,	Akhil Dattagupta

May 2023

Major Subject: Petroleum Engineering

ABSTRACT

Hydraulic fracturing is necessary for all wells in the unconventional reservoirs in the U.S. to be economically viable. Propped hydraulic fracturing involves pumping huge sums of fluid and proppant, at extremely high pressures and rates, down the wellbore and into the formation. This is done so that after the hydraulic pressure that is holding the fractures open is released, the proppant stays in the fractures and "props" the fractures open. This connects the greatly expanded and newly exposed surface area of the reservoir to the wellbore for hydrocarbon production.

The Austin Chalk formation was one of the first formations to incorporate horizontal drilling in the 1980's in the U.S., with the original aim to intersect naturally occurring fractures. This study investigated the fracture conductivity of outcrop and downhole cores from the Austin Chalk formation to help improve completion designs. This is of great interest due to the renewed drilling and completion activity occurring in the Austin Chalk formation.

From the results gathered in this study, it was concluded that lower proppant concentration can provide higher fracture conductivity, excluding the unpropped case. These results are due to a partial mono-layer of proppant distribution in the fracture. Although lower proppant concentrations had the higher fracture conductivities starting out, they also decreased the quickest with increasing closure stress. This is from a higher percentage of proppant crushing at lower proppant concentrations and less grains of proppant having to support the same closure stress. Downhole core samples gave slightly higher fracture conductivity values than outcrop samples with similar decline behavior.

Outcrop samples can therefore be used as proxies for downhole core samples in determining the lower limit for fracture conductivity. Fracture conductivities of sawcut and fractured samples were nearly identical at a proppant concentration of 0.20lbs/ft^2 but varied at proppant concentrations of 0.10lbs/ft^2 and 0.05lbs/ft^2.

This study provides useful information for proppant selection and fracture design in the Austin Chalk formation.

DEDICATION

I would like to dedicate this work to my parents Kevin and Sue. Their wisdom and support have allowed me to persevere in achieving my goals. I know they understand how much it means to me to pursue my dream of a career in Oil & Gas.

ACKNOWLEDGEMENTS

I would like to thank my committee chair, Dr. Ding Zhu, and my committee members, Dr. Daniel Hill, and Dr. Frederick Chester, for their guidance and support throughout the course of this research.

Thanks also go to my friends and colleagues in Richardson 714 and the department faculty and staff for making my time at Texas A&M University a great experience. I would like to specifically say thank you to Tohoko Tajima whose help was instrumental in trouble shooting and completing the experimental work. Thank you also to Mr. John Maldonado for his help in the laboratory.

Finally, thanks to Mrs. Eleanor Schuler whose suggestion led to my introduction to Dr. Ding Zhu and allowed this amazing life experience to occur.

CONTRIBUTORS AND FUNDING SOURCES

Contributors

This work was supervised by a thesis committee consisting of advisors: Dr. Ding Zhu and Dr. Daniel Hill of the Harold Vance Department of Petroleum Engineering and Dr. Frederick Chester of the Department of Geology & Geophysics.

Technical assistance was provided by Tohoko Tajima of the Harold Vance Department of Petroleum Engineering.

All other work conducted for the thesis was completed by the student independently.

Funding Sources

Graduate study was supported by a fellowship from Texas A&M University and a graduate research assistantship in the Harold Vance Department of Petroleum Engineering.

This work was also made possible in part by funding provided by the U.S. Department of Energy Office of Fossil Energy and Carbon Management and the National Energy Technology Laboratory under Award No DE-FE0031579. Its contents are solely the responsibility of the authors and do not necessarily represent the official views of the Department of Energy.

NOMENCLATURE

A	Cross sectional area (in^2)
C_f	Fracture Conductivity (md-ft)
C_p	Proppant concentration (lbs/ft^2)
$\frac{dP}{dL}$	change in pressure per unit length (psi/in)
h_f	Fracture height (in)
k_f	Fracture permeability (md)
L	Length of the fracture (in)
$\dot{m}$	Mass flow rate (kg/s)
M_g	Molar mass (kg/mol)
P_1	Upsteam pressure (psi)
P_2	Downstream pressure (psi)
P_{atm}	Atmosperic pressure (psi)
R	Universal gas constant (J/mol-K)
T	Temperature (K)
v	Fluid velocity (ft/s)
w_f	Fracture width (in)
Z	Gas compressibility factor (dimensionless)
ΔP	Differential pressure (psi)
μ	Fluid viscosity (cP)
ρ	Density (kg/m^3, lbm/ft^3)

ϕ	Porosity (% or dimensionless)

TABLE OF CONTENTS

Page

LIST OF FIGURES

Page

LIST OF TABLES

Page

1. INTRODUCTION*

1.1. Background of the Research

This section will review the background information relevant to the study through a literature survey.

1.1.1. Hydraulic Fracturing

The first hydraulic fracture was performed by Stanolind Oil, a division of Standard Oil of Indiana, in the Hugoton field in Grant County, Kansas in 1947 (Kamal, 2020). A picture of the first hydraulic fracture can be seen in Figure 1. This process was known as "Hydrafrac", and the hydraulic fracture treatment performed consisted of 1,000 gallons of gasoline-based napalm gel frac fluid (Palisch et al., 2008).

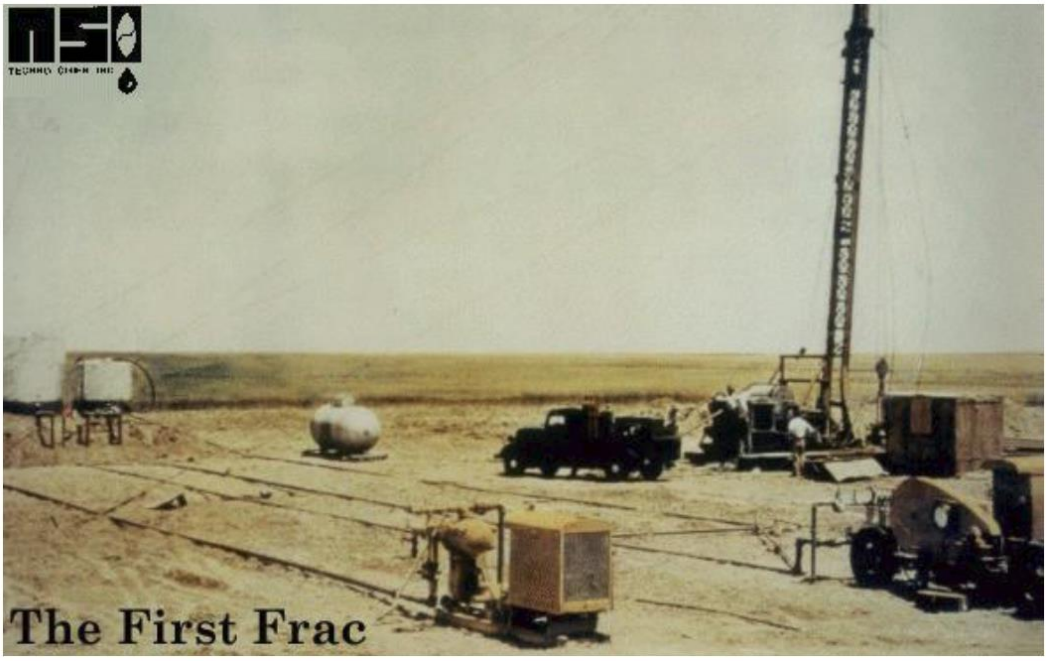

Figure 1. The first hydraulic fracture in the Hugoton field in Grant County, Kansas (Reprinted from Kamal, 2020).

* Used with permission of Society of Petroleum Engineers (SPE), from Fracture Conductivity Created by Proppants and Acid in the Austin Chalk Formation, A. T. Brashear; A. D. Hill; D. Zhu; E. Kerr; R. Scofield; D. Jordan; E. Estrada; T. Tajima, 2022; permission conveyed through Copyright Clearance Center, Inc.

The following is an excerpt from Green (2022) of the American Petroleum Institute: “A patent was issued in 1949, with an exclusive license granted to the Halliburton Oil Well Cementing Company (Howco) to pump the new Hydrafrac process. Howco performed the first two commercial fracturing treatments—one, costing $900, in Stephens County, Oklahoma, and the other, costing $1,000, in Archer County, Texas—on March 17, 1949 … In the first year, 332 wells were treated, with an average production increase of 75%. Applications of the fracturing process grew rapidly and increased the supply of oil in the United States far beyond anything anticipated. Treatments reached more than 3,000 wells a month for stretches during the mid-1950s.”

Hydraulic fracturing grew in popularity and eventually became a common practice. These hydraulic fractures were being performed on vertical wells though, as shown in Figure 2, and were usually pumped in only one stage. Some vertical wells had multiple hydraulic fracturing stages performed when multiple producing zones were completed and produced from. As the treatment volume increases, some of the single stage, vertical well treatments performed in Wyoming (Wamsutter & Frontier formations) actually communicated with offset wells over a mile away (Kamal, 2020). Other wells in the Barnett formation proved fracture half lengths on the order of 2,500 feet, killing 5 surrounding wells’ production (Fisher, 2002). The same data also gave rise to the concept of complex fracture networks, described in Figure 3. This concept deviates from the traditional thought that the hydraulic fractures created were planar, bi-wing fractures. The concept of a complex fracture network in comparison to only a planar bi-wing fracture being created indicates that a tremendously large surface area of the reservoir has been exposed to the fracture and ultimately back to the wellbore for production.

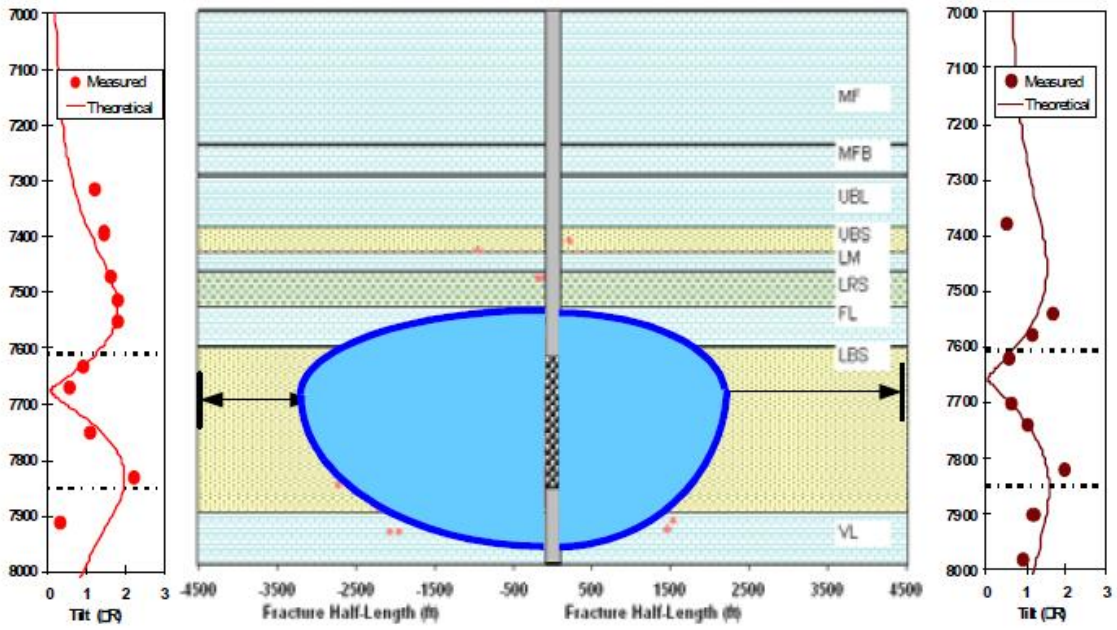

Figure 2. Example of a vertical bi-wing fracture (Reprinted from Fisher et al., 2002).

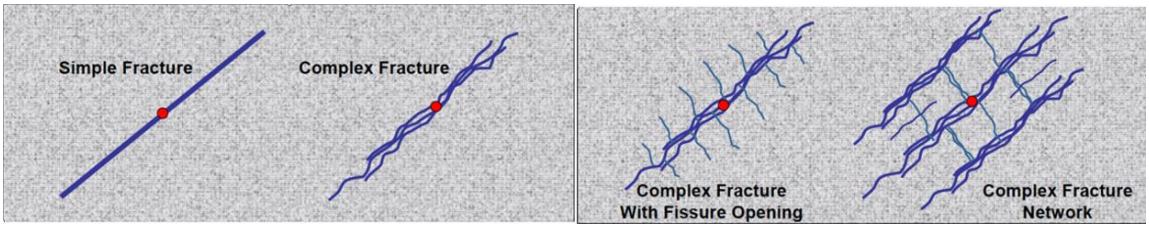

Figure 3. Conceptual view of simple to complex fracture networks (Modified from Warpinski et al., 2008).

Roughly 20 years after the first hydraulic fracture, the next step change advancement in hydraulic fracturing occurred with the introduction of crosslinked gel fluid systems. These crosslinked gel fluid systems were able to achieve greater fracture widths allowing for higher concentrations of proppant without screening out the well. Treatments routinely consisted of proppant being pumped down the wellbore in excess of 2 million pounds, and incorporated fluid systems of 60 pptg guar borate crosslinked gel (Palisch, 2008). Examples of the dry powder base

for making gel out of guar, hydroxypropyl guar, and carboxymethyl hydroxypropyl guar can be seen in Figure 4.

Figure 4. Left – Guar (Reprinted from polymersco.com, 2022). Center - Hydroxypropyl Guar (HPG) (Reprinted from alibaba.com, 2022). Right - Carboxymethyl Hydroxypropyl Guar (CMHPG) (Reprinted from made-in-china.com, 2022).

Borate crosslinked gels were first developed and sufficient for a time. Later, when crosslinked fluid systems needed to last longer before breaking in ever increasing temperature ranges, metallic crosslinked fluid systems were developed. An example of a borate crosslinked gel can be seen in Figure 5.

Figure 5. Borate crosslinked gel (Reprinted from Beckwith, 2012).

By the 1980's hydraulic fracturing treatments had grown tremendously in size. It was with the advent of horizontal drilling that hydraulic fracture stimulations grew in the number of stages and total volume. In the late 1990's Mayerhofer et al. (1997) surprised the industry and

communicated real world production numbers showing better production from zero proppant water fracs than from proppant laden previous completion designs. From that point forward, completion designs tended towards slickwater completion designs or hybrid completion designs. A slickwater completion design refers to using a hydraulic fracturing fluid system that has much lower viscosity than traditional gel or crosslinked gel fluid systems, usually consisting of friction reducer in the form of polyacrylamide. Hybrid completion designs start with slickwater, then move to gel, and end with crosslinked fluid all in the same pumping stage. Most slickwater-only completion designs consisted of using friction reducer in the form of polyacrylamide and modest maximum proppant concentrations in the range of 2-3 ppg (Palisch et al., 2008). This gave rise to the overwhelming majority of completion designs in use today comprising of 150 - 300 foot stage spacings, slickwater fluid systems using either friction reducer or high viscosity friction reducer, 40 – 70 barrels of fluid per lateral length completed, and 2000 – 4000 pounds of proppant per foot of lateral length completed. Some wells require close to 50 million pounds of proppant in today's completion designs, (15,000ft lateral at 3,000lbs/ft). A modern-day hydraulic fracturing pad site can be seen in Figure 6.

Figure 6. Modern day hydraulic fracturing pad site (Reprinted from hartenergy.com, 2022).

1.1.2. Fracture Conductivity

According to Cooke (1973) fracture conductivity is defined as the fracture width multiplied by the permeability of the proppant pack in the fracture. An increase in fracture conductivity can improve the completion design, as shown in Figure 7 (Sun et al., 2014). This beneficial effect does have dimenishing returns though (Mayerhofer et al., 2006). The American Petroleum Institute, API, has developed a procedure to measure the short term fracture conductivity (API RP-61, 1989). It has been shown that short term fracture conductivity can be reduced by up to 99% at elevated temperature, fracturing fluid residues, proppant embedment, and formation fines migration (Palisch, 2007). Due to this reduction in short term fracture conductivity, a long term fracture conductivity measurement procedure has also been developed by the API and accepted by the International Organization for Standardization to provide more realistic fracture

conductivity values expected to be encountered at reservoir conditions (API RP-19D; ISO 13503-5, 2015). The short term fracture conductivity procedure is the one used in this study.

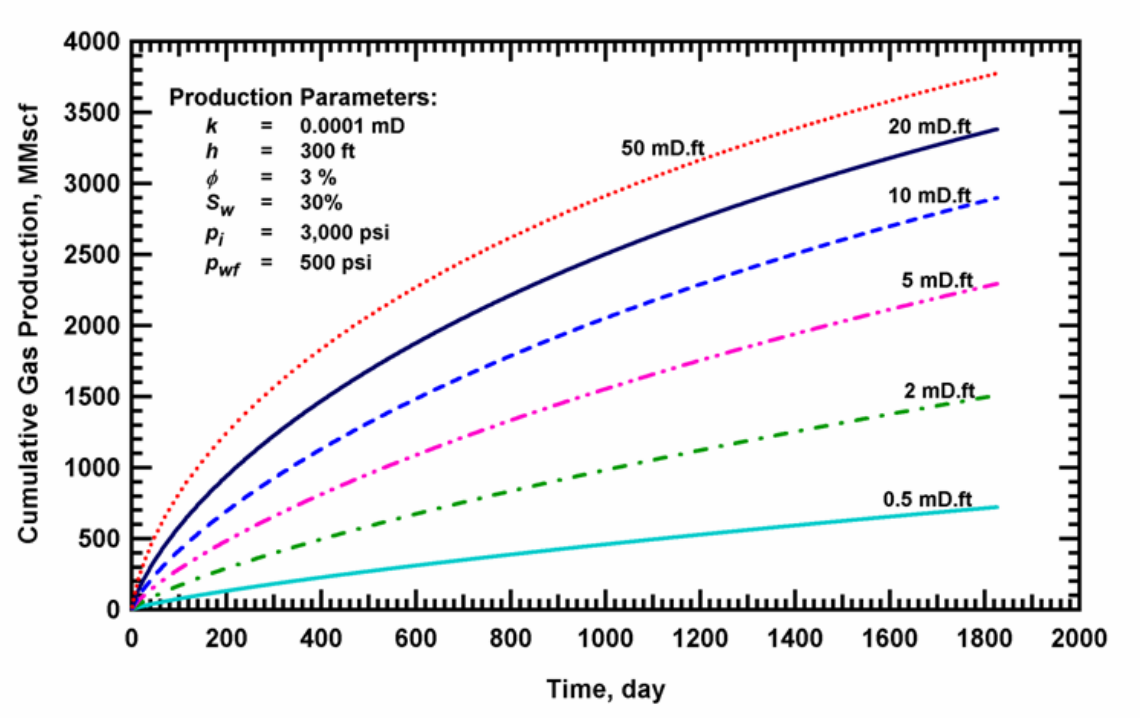

Figure 7. Plot displaying increasing cumulative production with increasing fracture conductivity (Reprinted from Mayerhofer et al., 2006).

The flow through the proppant pack in the fracture can have non-Darcy flow effects, referred to as inertial flow effects. Non-Darcy flow effects can be taken into account using the Forchheimer equation (Cooke, 1973). This study does not go into further detail on non-Darcy flow effects since the volumetric flow rate was maintained in laminar flow. According to McGinley, keeping the volumetric flow rate below 2 liters per minute prevents the onset of turbulent flow (McGinley et al., 2015).

1.1.3. Austin Chalk Overview

The Austin Chalk formation first saw activity starting with vertical wells in the 1920's close to the gulf coast (Kyte and Meehan, 1996). As can be seen in Figure 8, the Austin Chalk stretches across the southeastern United States, through parts of Mississippi, Louisiana, and Texas, then continues into Mexico.

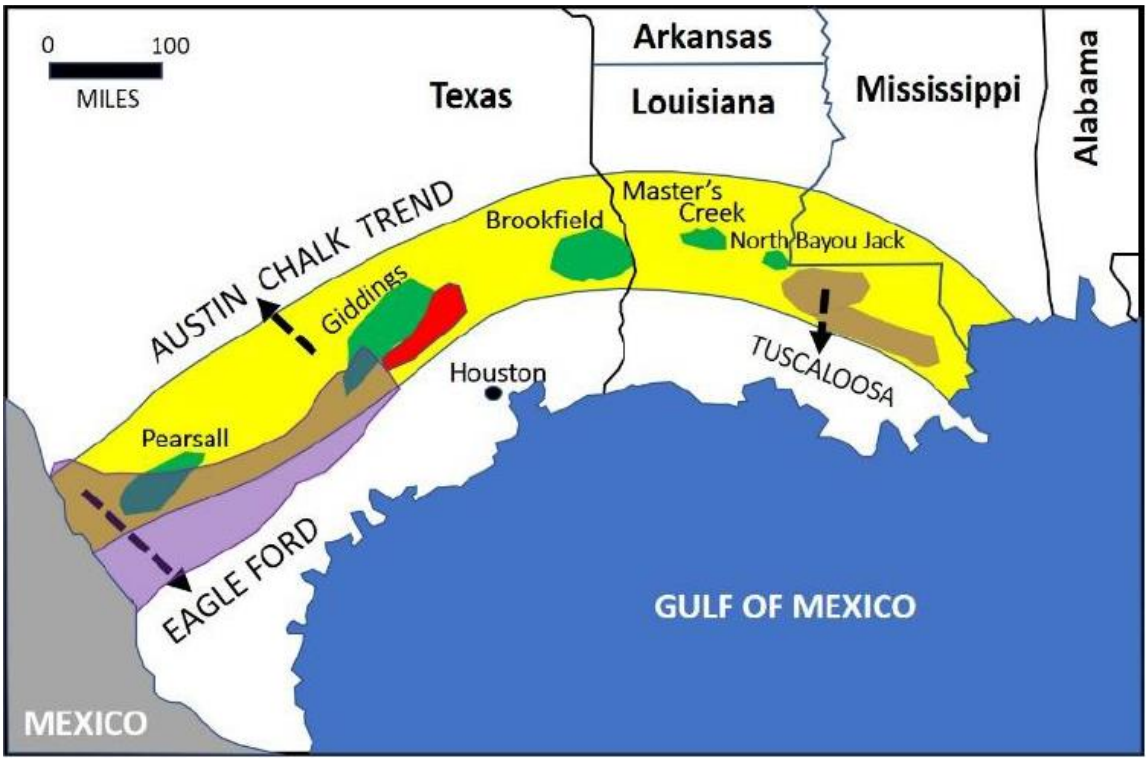

Figure 8. Austin Chalk trend across the southeastern United States (Reprinted from Panja and Sorkhabi, 2022).

After initial development in the 1920's, the next period of increased focus on the Austin Chalk occurred in the 1970's due to the U.S. oil crisis (Martin et al., 2011). The average completion design in the 1970's consisted of 200,000 gallons of borate crosslinked guar gel, with 250,000 pounds of 20/40 proppant, and were pumped between 40 and 60 bpm (Dees et al., 1990). Figure 9 is an expanded map that focuses on the Austin Chalk play in Texas.

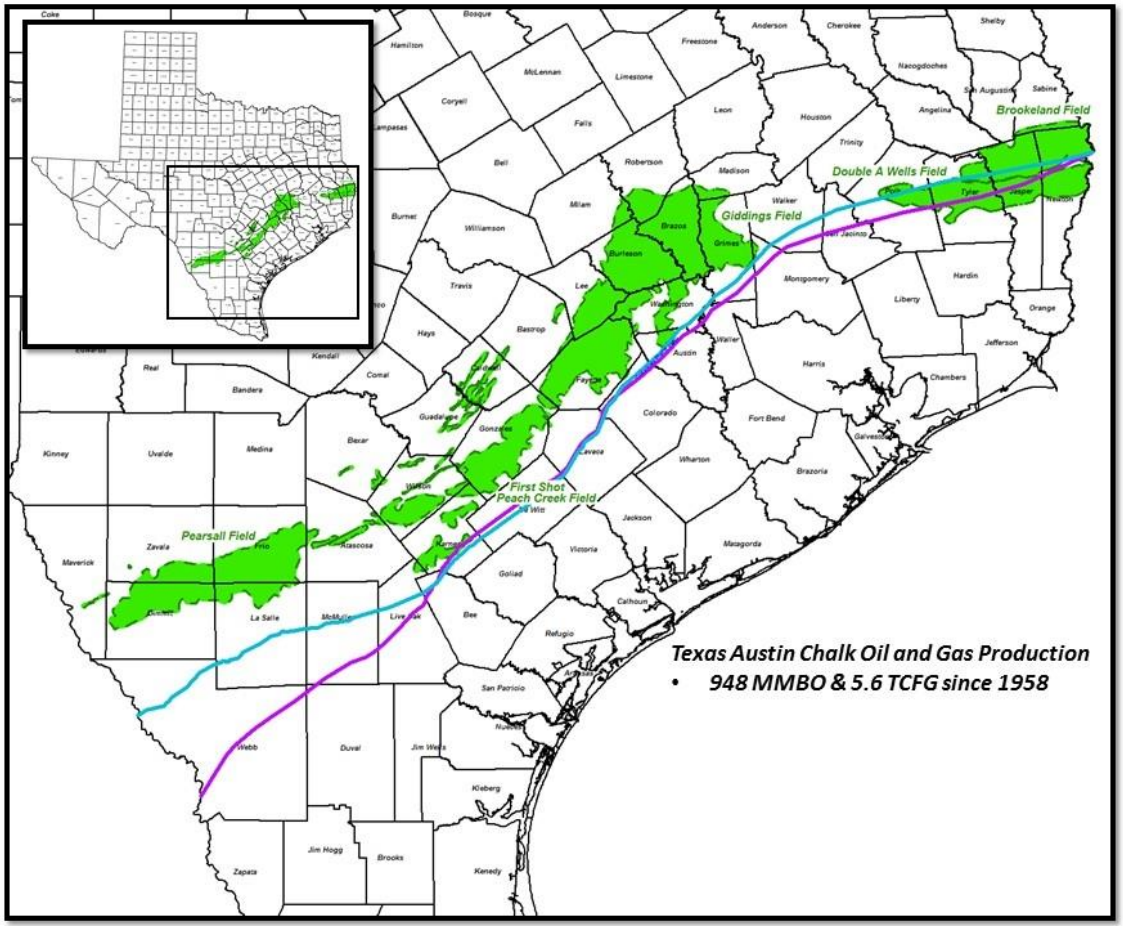

Figure 9. Austin Chalk trend across Texas (Reprinted from austinchalkoilgas.com, 2022).

This was followed with a resurgence in activity in the 1990's (Martin et al., 2011). The first deployment of horizontal drilling in the Austin Chalk occurred in the 1980's (Pope and Handren, 1990). Completion designs for horizontal wells included open hole, cased hole, and slotted liners. The stimulation designs that accompanied the horizontal wells included acid washes with coiled tubing, acid fracs up to 30 bpm, and water fracs at over 200 bpm with 8,000 - 20,000 pounds of wax beads for diversion (Hollabaugh and Dees, 1993). Over four million acres in Texas are covered by the Austin Chalk and Texas is where the majority of activity is concentrated (Austin Chalk Oil and Gas, 2022). For shallower wells in the Austin Chalk (4000-

8000 ft total vertical depth) the normalized cumulative production (NCP) is 0.44 STB/lateral ft/month and increases to 0.75 STB/lateral ft/month for the deeper wells (8000-14000 ft total vertical depth). In comparison, the Eagle Ford's NCP is 0.42 STB/lateral ft/month for shallower wells (4000-10000 ft total vertical depth) and 0.71 STB/lateral ft/month for deeper wells (10000-14000 ft total vertical depth) (Panja and Sorkhabi, 2022). As can be seen in Figure 10, the Austin Chalk and Eagle Ford unconventional plays make up about 10% of total US crude production (Panja and Sorkhabi 2022).

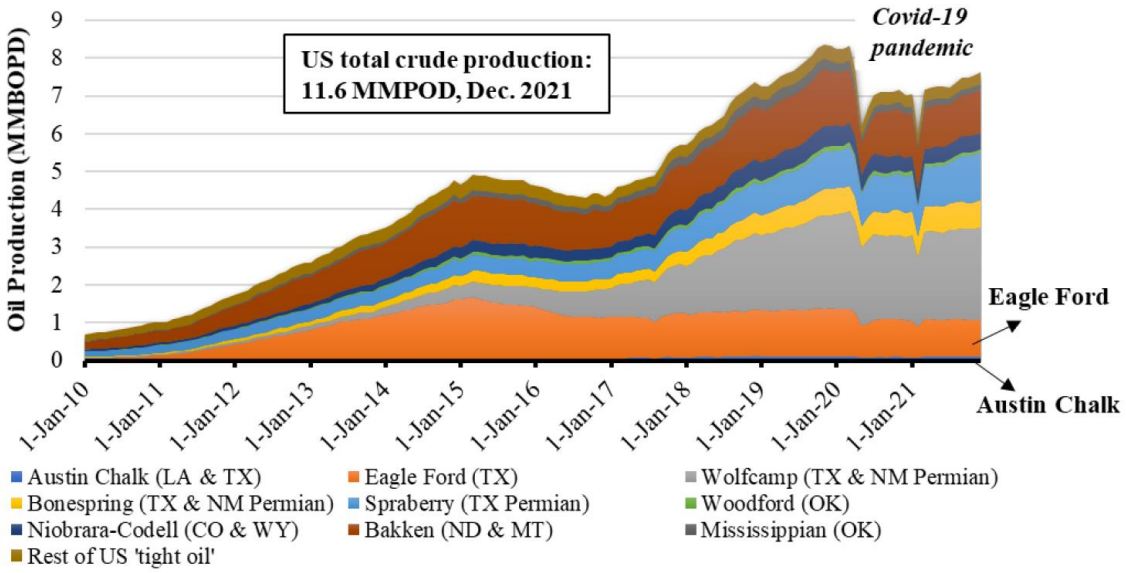

Figure 10. Total US crude production (Reprinted from Panja and Sorkhabi 2022).

The Austin Chalk formation is Upper Cretaceous in age and overlies the Eagle Ford Shale (Martin et al., 2011). The Eagle Ford shale is the source rock for the Austin Chalk. The Austin Chalk gets its name from an outcrop near Austin, Texas. The Austin Chalk consists of interbedded chalks, volcanic ash, and marls. Please see Figure 11 for a stratigraphic column of the Austin Chalk formation.

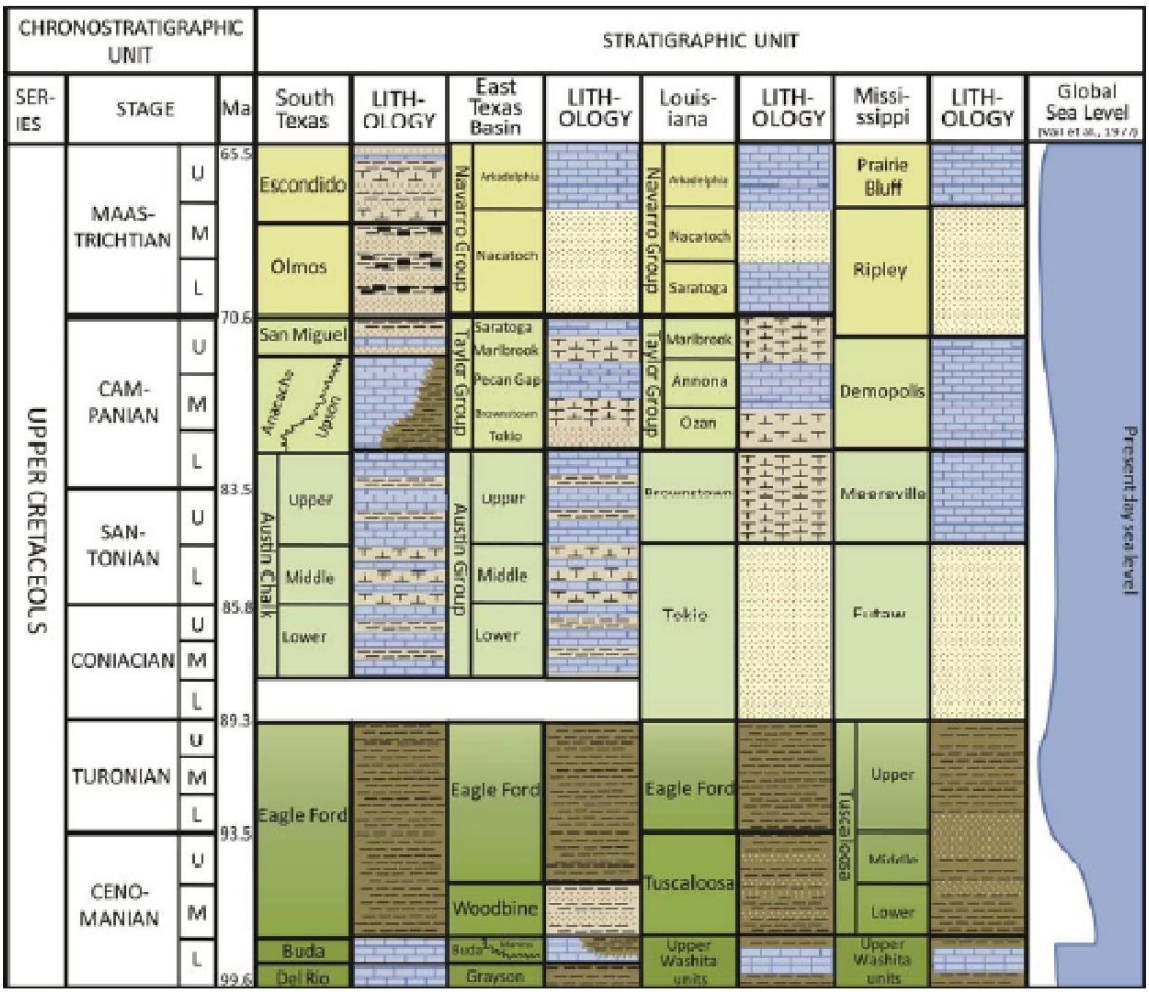

Figure 11. Stratigraphic column of the Austin Chalk formation (Reprinted from Martin et al., 2011).

1.2. Problem Description

The overwhelming majority of onshore U.S. oil and gas operations are focused in unconventional reservoirs. These unconventional reservoirs need to be hydraulically fractured to be economically viable. After the industry downturn in 2015-2016 and the most recent downturn in 2020 due to Covid-19, there has been an ever-increasing focus on refining better completion designs to create better performing wells. This study aims to improve completion designs by analyzing the fracture conductivity in the Austin Chalk. By determining the condition that yields

the optimal fracture conductivity, this study will provide the information to improve completion designs and yield better well economics.

1.3. Research Objectives

With a renewed level of drilling and completion activity in the Austin Chalk formation, it is very important to better understand fracture conductivity to help improve completion techniques. The objectives of this research include the following:

1. Develop an experimental procedure that provides a consistent means to measure fracture conductivity.
2. Determine how proppant concentration affects the fracture conductivity of Austin Chalk samples.
3. Determine if outcrop samples can be used as proxies for downhole core samples in determining fracture conductivity.
4. Compare the fracture conductivities of sawcut and fractured samples to see how they compare.

The successful completion of these objectives will provide valuable data to improve completion designs in the Austin Chalk. It will also determine if outcrop samples can be used in place of downhole core, and if sawcut samples can be used instead of fractured samples.

2. EXPERIMENTAL PROCEDURE*

2.1. Experimental Sample Collection

Both Austin Chalk outcrop and Austin Chalk downhole cores were selected for this study. Outcrop is much easier and cheaper to obtain with large supply. Downhole cores are hard to get, but they may provide the information closer to field conditions. It was planned to verify the outcrop's ability to be used as a proxy for downhole core. Austin Chalk outcrop samples were collected from a roadcut on US90, 4 miles west of Langtry, TX. Figure 12 shows the map of the location that samples were collected, and Figure 13 shows the outcrop. Downhole cores were provided by SM Energy from the coring of a south Texas well in Webb County, Texas.

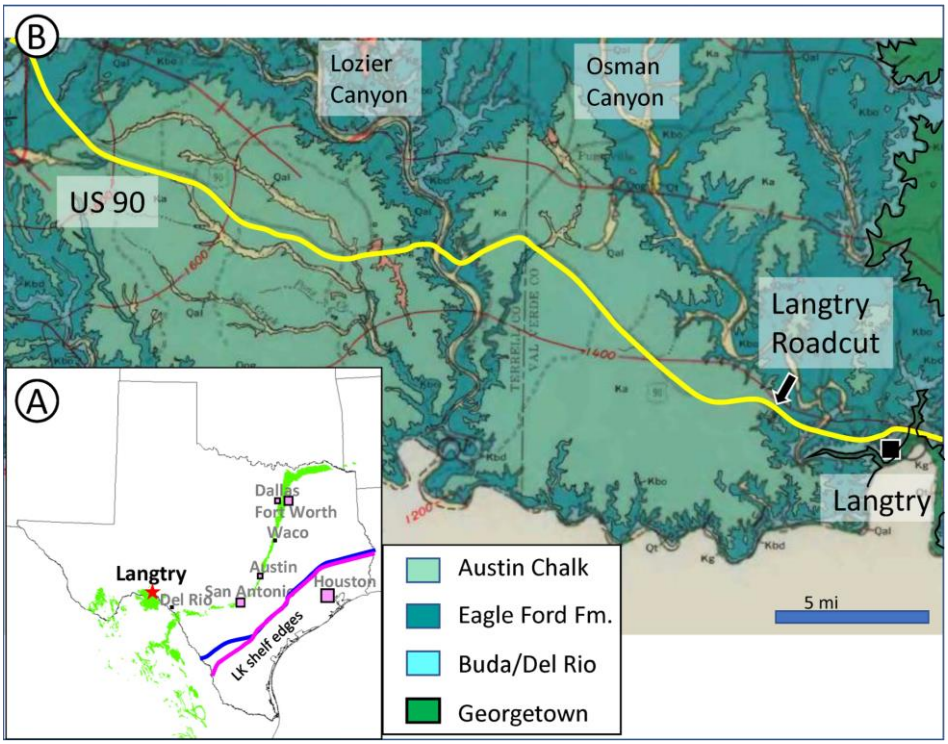

Figure 12. Map of the US90 roadcut west of Langtry, TX (Reprinted from Griffith et al., 2019).

* Used with permission of Society of Petroleum Engineers (SPE), from Fracture Conductivity Created by Proppants and Acid in the Austin Chalk Formation, A. T. Brashear; A. D. Hill; D. Zhu; E. Kerr; R. Scofield; D. Jordan; E. Estrada; T. Tajima, 2022; permission conveyed through Copyright Clearance Center, Inc.

Figure 13. Austin Chalk outcrop collection west of Langtry, TX. Blue #: Austin Chalk beds. Black #: feet above top Eagle Ford. L2: 18' above Eagle Ford. L1: 10' above top Eagle Ford Figure 12. Map of the US90 roadcut west of Langtry, TX.

There are two ways to generate fractures for conductivity tests, tensile-fracture the rock or sawcut the rock. Sawcut samples were used due to their quicker availability and cheaper manufacturing. Fractured samples were used in limited experiments to compare with sawcut samples to verify close approximate values to one another. In addition, a fractured outcrop sample was used to establish unpropped fracture baseline conductivity. Only fractured outcrop samples were used for this study. Both downhole core and outcrop Austin Chalk sawcut samples were used in this study. An example of a fractured outcrop surface can be found in Figure 14.

Figure 14. Fractured outcrop sample in progress.

2.2. Experiment Conditions

2.2.1. Proppant Concentrations

Proppant concentrations of 0.05lb/ft^2, 0.10lb/ft^2, and 0.20lb/ft^2 were chosen for this study. These values were chosen specifically to best represent the actual proppant concentrations used in fracturing unconventional reservoirs today. For each proppant concentration condition, three sawcut outcrop fracture conductivity experiments were performed to attain a more representative average response. At low concentration, it is believed the partial mono layer proppant distribution is obtained. A partial mono-layer of proppant occurs when the proppant concentration is sufficiently low that a single layer of proppant only covers part of the fracture surface, as illustrated in Figure 15. Previous studies have shown that a partial mono-layer of proppant can yield fracture conductivity values nearly 10 times higher than multiple layers of tightly packed proppant, as illustrated in Figure 16 (Brannon et al., 2004).

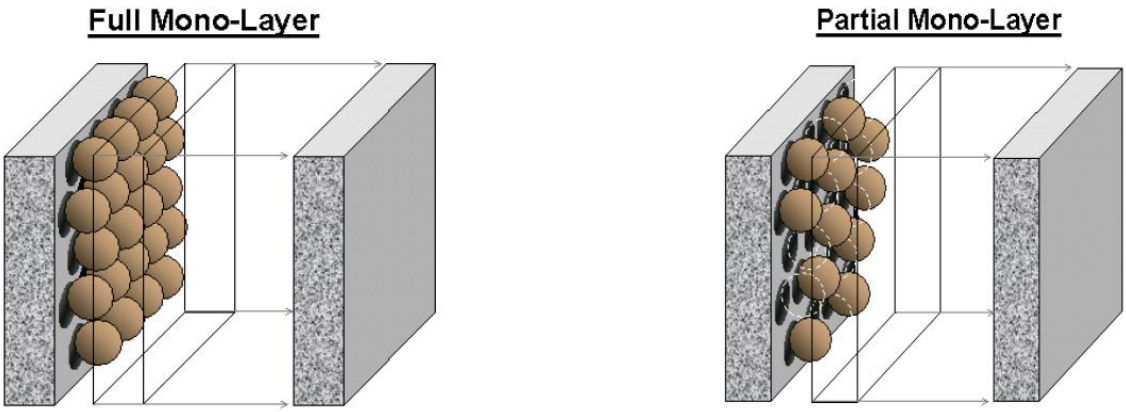

Figure 15. Representation of a full mono-layer and partial mono-layer of proppant (Modified from Brannon et al., 2004).

One way to define proppant concentration is proppant mass per unit fracture area (lbm/ft^2). This concentration is expressed as:

$$C_p = w_f \rho (1 - \phi) \quad (1)$$

where C_p is proppant concentration, w_f is the width of the fracture, ρ is the density of the proppant, and ϕ is the porosity of the proppant pack.

$$\phi = 1 - \frac{C_p}{\rho w_f} \tag{2}$$

For the case that C_p is 0.05lb/ft^2, ρ is 165lb/ft^3, and w_f is 0.012 inches (50 mesh proppant diameter), ϕ is equal to 69%. The same calculation with C_p as 0.10lb/ft^2 gives a porosity of 38%. A proppant concentration of 0.20lb/ft^2 yields greater than a mono-layer of proppant.

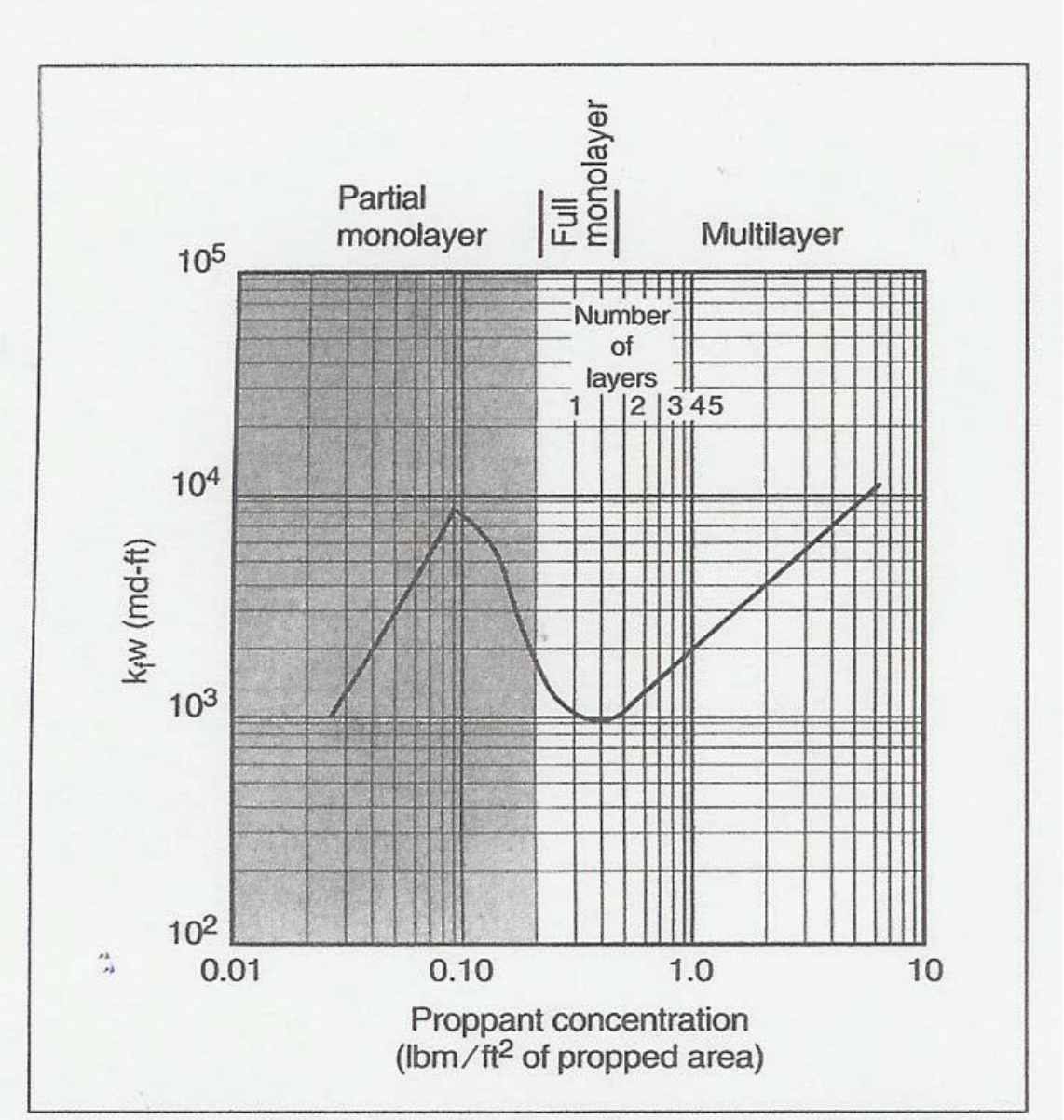

Figure 16. Variation of fracture conductivity in relation to proppant concentration (Reprinted from Brannon et al., 2004).

The design parameters include:

1. Type of rock (downhole or outcrop).
2. Method of creating fracture.
3. Proppant concentration.

The experimental design matrix can be seen in Figure 17.

Experiment #	Outcrop or Downhole Core	Sawcut or Fractured	Proppant Concentration (lb/ft^2)
1	Outcrop	Sawcut	0.20
2	Downhole Core	Sawcut	0.20
3	Outcrop	Sawcut	0.20
4	Downhole Core	Sawcut	0.20
5	Outcrop	Sawcut	0.20
6	Outcrop	Sawcut	0.10
7	Downhole Core	Sawcut	0.10
8	Outcrop	Sawcut	0.05
9	Outcrop	Sawcut	0.05
10	Outcrop	Sawcut	0.05
11	Outcrop	Sawcut	0.10
12	Outcrop	Sawcut	0.10
13	Outcrop	Fractured	0.00
14	Outcrop	Fractured	0.20
15	Outcrop	Fractured	0.05
16	Outcrop	Fractured	0.10

Figure 17. Experimental design matrix.

All tests are run at room temperature. Injection rate varies from 0.1 L/min to 1 L/min to generate conductivity at each closure stress. The details will be discussed later in this chapter.

2.3. Description of Experimental Apparatus

Figure 18 is a schematic depicting the laboratory apparatus. The main components that make up the laboratory apparatus are the following:

- Hydraulic pump
- GCTS hydraulic load frame
- Cylinder of nitrogen
- Flow lines
- Volumetric flowmeter

- Gauge and differential pressure transducers
- Modified API conductivity cell
- GCTS load frame control box
- Data acquisition system

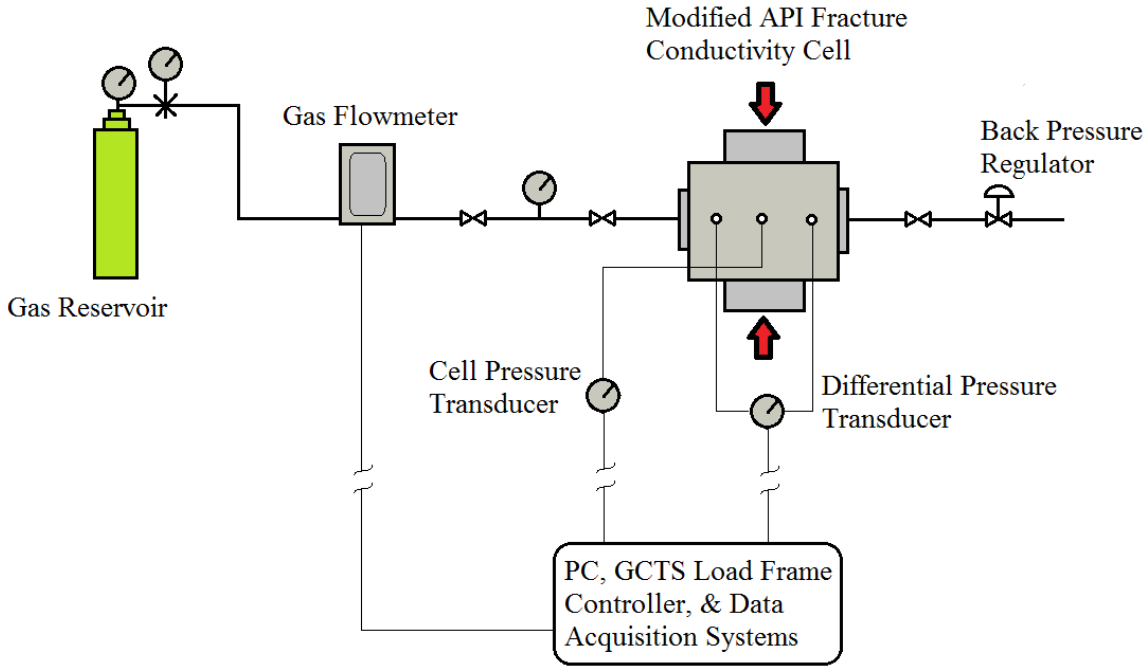

Figure 18. Graphical representation of the laboratory apparatus (Reprinted from Guerra, 2019).

Figure 19 shows the actual experimental apparatus in the laboratory. A needle valve was added after the mass flowmeter and before the modified API conductivity cell. This was done to decrease the transition time between closure stresses and to act as an inline choke. Figure 20 shows the back side of the apparatus. There are two differential pressure transducers, one with a range of 0-2 psi differential pressure and the other with a range of 0-0.2 psi differential pressure. This is done to more accurately measure the very low differential pressure measurements

associated with very high fracture conductivity values. The cell pressure transducer has a gauge pressure range from 0-30 psi.

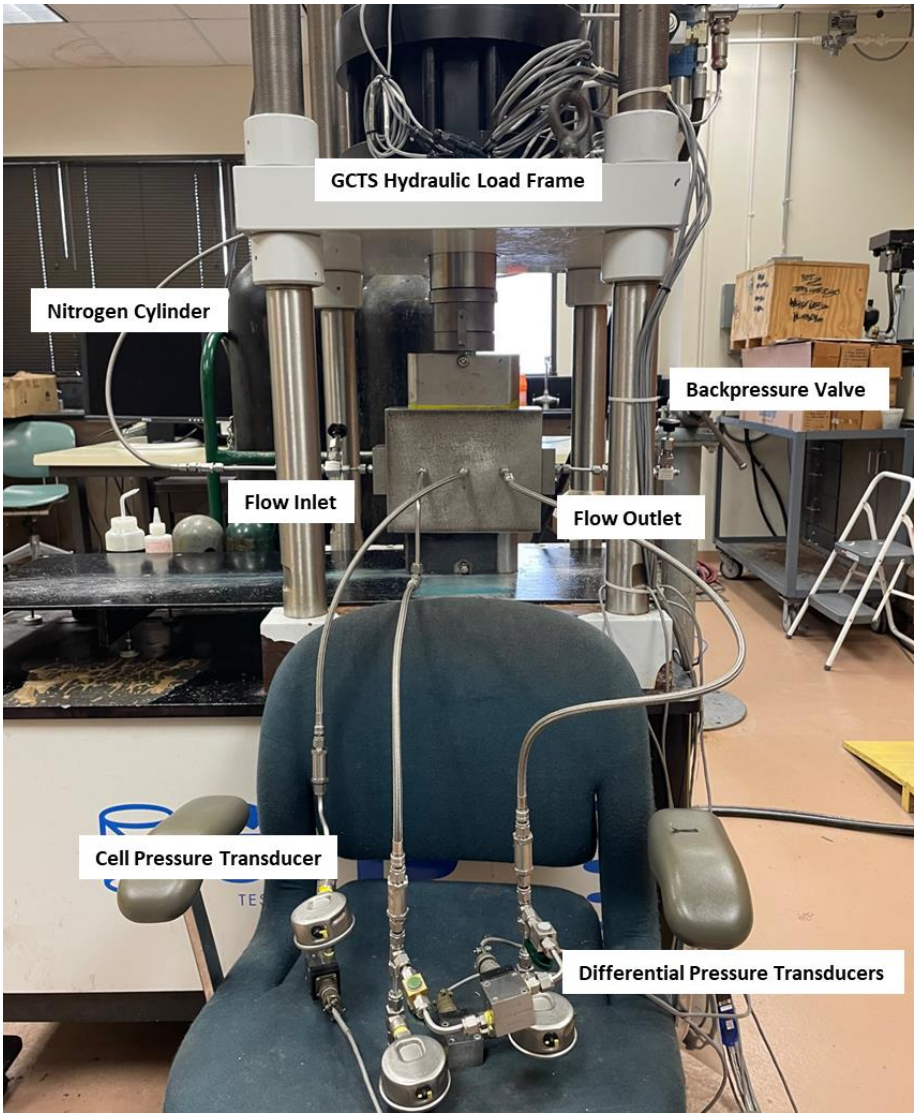

Figure 19. Front side of experimental apparatus.

The GCTS load cell can apply a maximum force of 208,000 lbs and has a maximum loading rate of 1,215 lbf/min.

Figure 20. Backside of the experimental apparatus displaying the volumetric flowmeter and spring valve.

Figure 21shows the GCTS control box and software used to control the loading in the load cell frame.

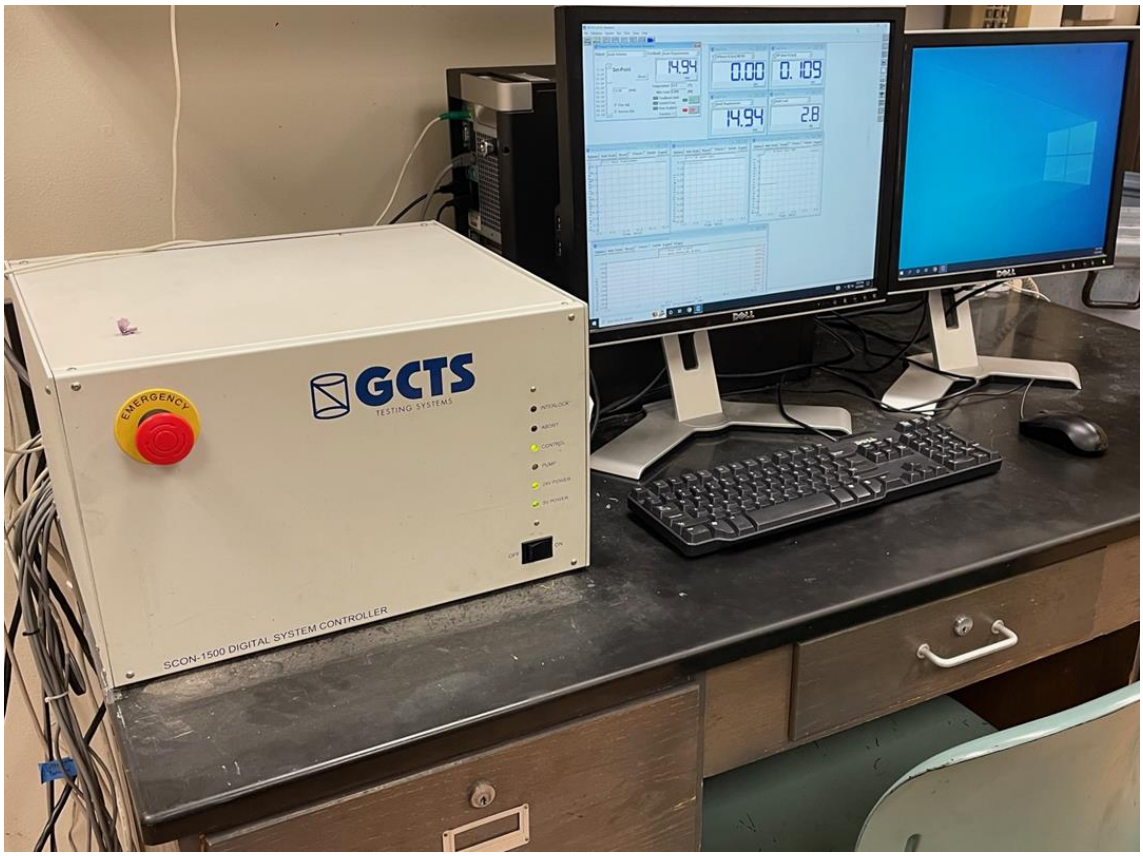

Figure 21. GCTS control box and software displayed.

The API conductivity cell is shown in Figure 22. The conductivity test samples have dimensions of 7 inches in length, 1.65 inches in width, and the thickness depends on the availability of the rock sample (Figure 23). Each piece of a pair of a fracture conductivity sample is nominally 3 inches thick when having enough rock.

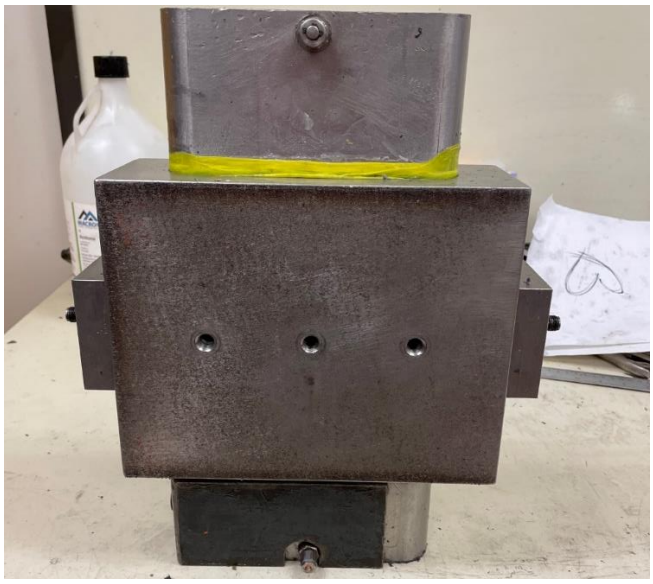

Figure 22. Modified API conductivity cell.

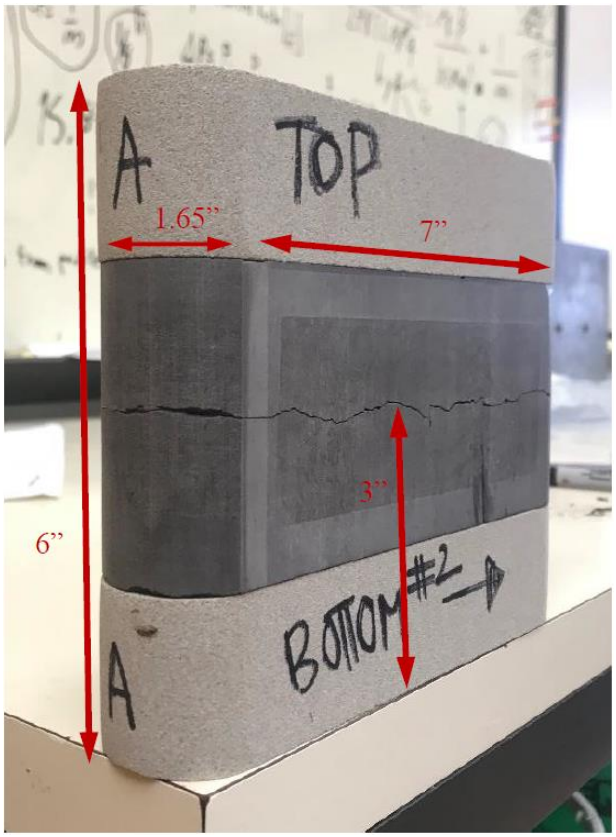

Figure 23. Fracture conductivity sample dimensions (Reprinted from Copeland, 2020).

2.4. Experimental Procedure

The workflow for this study is presented in Figure 24. There are 6 steps in each experiment; sample collection, preparation, proppant placement, sample assembly, pressure/flow measurement, and conductivity generation. Details are discussed below.

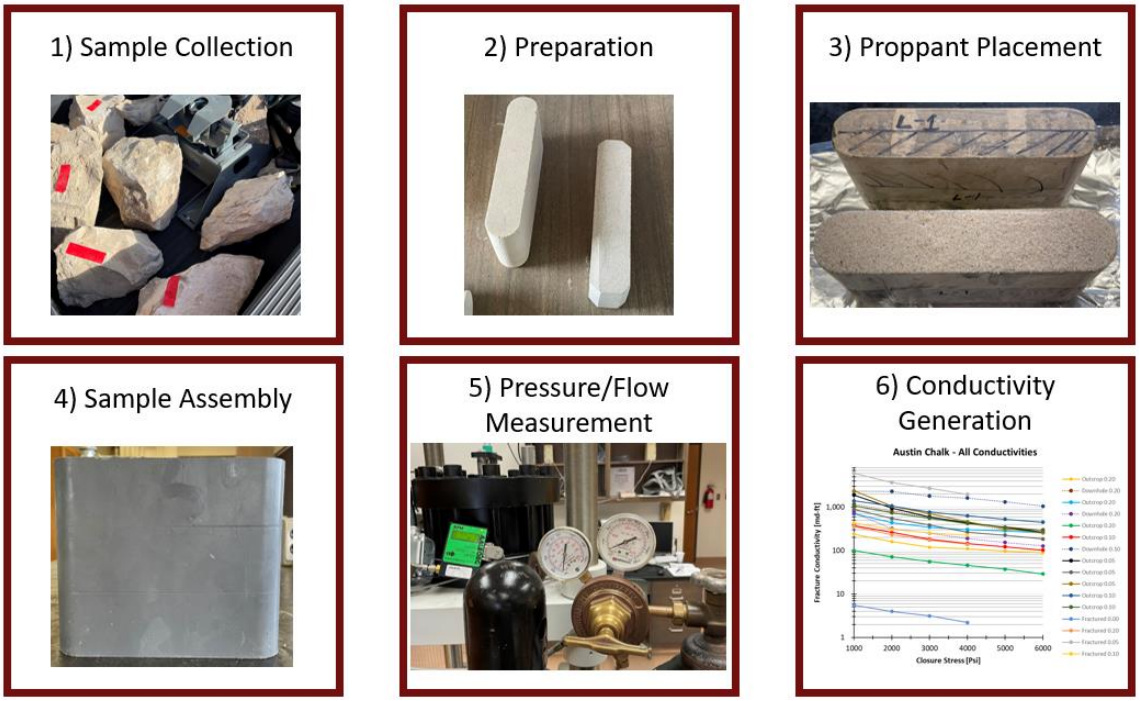

Figure 24. Experimental workflow.

2.4.1. Sample Preparation

The fracture conductivities were obtained using nitrogen as the working fluid and a modified API conductivity test cell. The most important part of the procedure is a consistent process for proppant application for each sample. This allows consistency from one test to another. One of the biggest errors in testing fracture conductivity is in the application of the procedure for preparing the samples for testing, especially the proppant application. The collected rocks are first cut into the correct geometry for the modified API conductivity test cell by Kocurek Industries in Caldwell, TX. Some of these steps are shown in Figure 25 - Figure 29. Figure 25

shows raw pieces of collected Austin Chalk outcrop after sections have been cut off to be made into samples.

Figure 25. Raw Austin Chalk outcrop before preparation.

Figure 26 shows a finished sample on the left side and a sample after the preliminary shaping cuts on the right side.

Figure 26. A finished sample on the left and a sample in progress on the right.

Figure 27 shows the jig used to create the radiused ends of the finished sample.

Figure 27. A jig used to create the end radii of the samples.

Figure 28 shows the jig post hole the jig is inserted into, and belt sander used to shape the radii of the samples.

Figure 28. The jig post is inserted into the post hole and a belt sander is used to finish the end radii of the samples.

Figure 29 shows the finished product of six pairs of fracture conductivity samples ready for testing.

Figure 29. Six finished samples ready for fracture conductivity test preparation.

2.4.2. Proppant Placement and Sample Assembly

After the sample has been formed into the correct geometry, it is finished for fracture conductivity testing through the following steps:

1. Place the bottom piece of the sample on a sheet of aluminum foil with three sides folded up to catch any proppant that falls off the fracture surface of the sample, Figure 30.

Figure 30. Aluminum foil folded on 3 sides to catch any proppant that falls off the sample.

2. Fill a cup with proppant that is over the amount of proppant to be used (~100 grams). See Table 1 for the required mass for each proppant concentration. The values in Table 1 were developed by taking the sample geometry to be two semi circles connected by a rectangle in the middle. Using a width of 1.65 inches and a length of 7 inches yields an area of 0.0761ft^2. Multiplying this area by the proppant concentration of 0.20lb/ft^2 gives 0.015lbm. Now multiply by 454g/lbm to arrive at the required mass of proppant in grams.

Table 1. Proppant mass to be used for the corresponding proppant concentration.

Proppant Concentration	Proppant Mass to be used
Unpropped	0.00g
0.20lb/ft^2	6.81g
0.10lb/ft^2	3.40g
0.05lb/ft^2	1.70g

3. Place the cup with proppant inside of it on a scale and tare the scale. The scale needs to have a resolution of 0.01 grams. Figure 31. By taring the scale, it prevents having to do subtraction to determine how much proppant has left the cup. Slowly pour proppant out of the cup onto the fracture surface of the sample until the desired amount of proppant is achieved. Frequently put the cup back on the scale to check how much proppant has left the cup. The scale will read a negative value, but this value is how much proppant has left the cup, Figure 32.

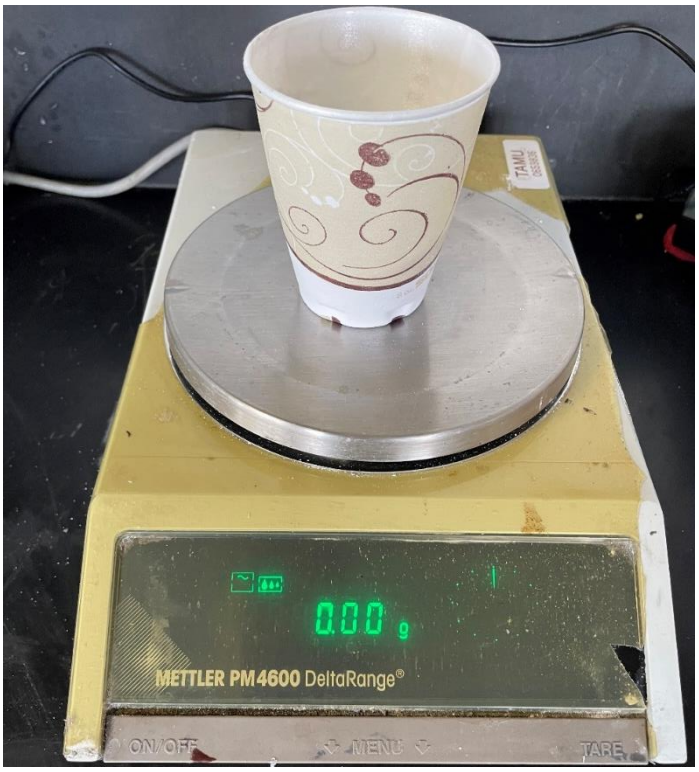

Figure 31. Cup with proppant on the scale, after the scale has been tared.

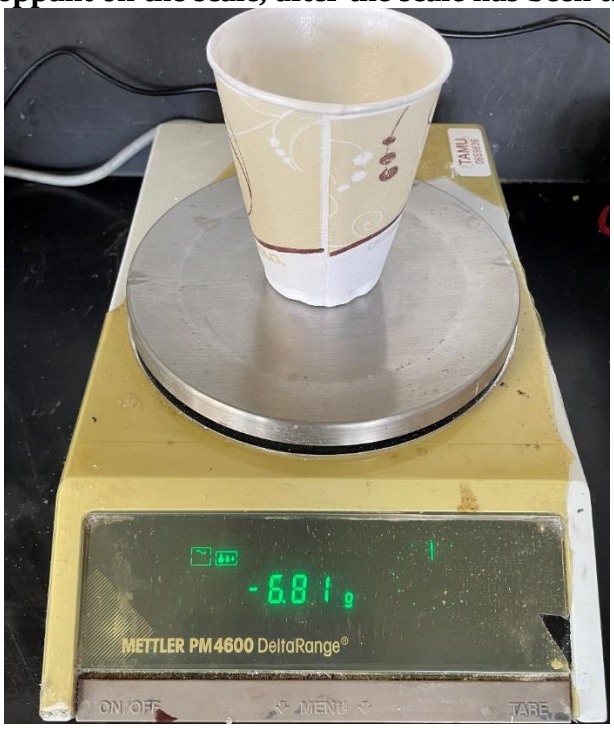

Figure 32. Scale showing 6.81g have left the cup and is on the sample fracture surface.

4. After the desired amount of proppant has left the cup, verify none of the proppant has fallen off the sample onto the aluminum foil. If any has, carefully take the bottom half of the sample off the aluminum foil, place it on the countertop, pick up the aluminum foil, and pour the proppant from the aluminum foil back onto the sample. See Figure 33.

Figure 33. Sample after proppant has been poured on but before smoothing.

5. Next place the top of the sample onto the bottom of the sample, moving the top of the sample in small circles to even out the proppant in both the length and width directions. See Figure 34.

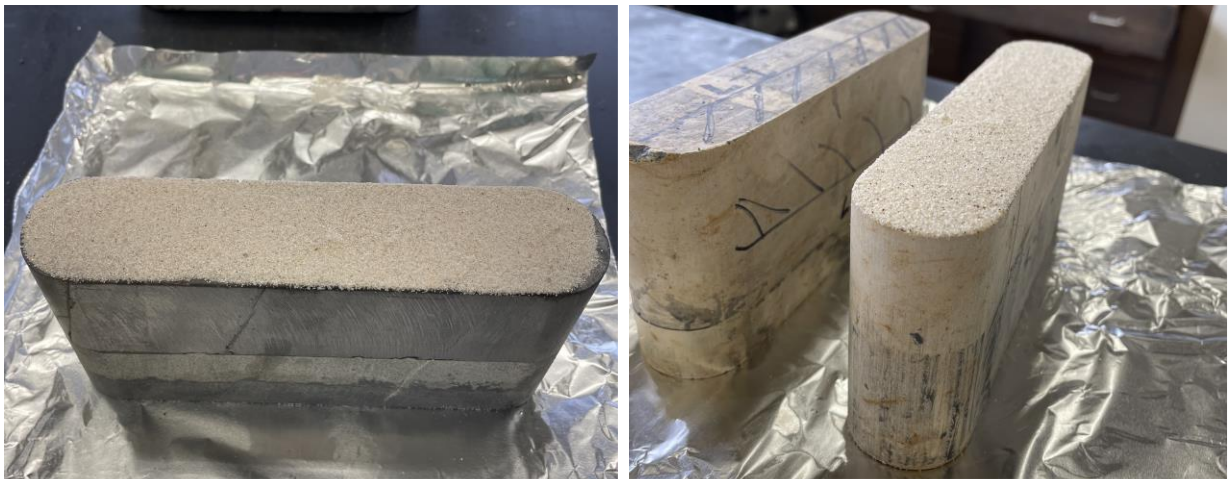

Figure 34. Sample with proppant applied, left - downhole core, right - outcrop.

6. Apply super glue around the perimeter of each half of the sample, above and below the fractured surface. Apply painters' tape around the sample, covering the fracture to prevent epoxy from entering the fracture, see Figure 35.

Figure 35. Application of super glue and painter's tape (Modified from Copeland, 2020).

7. Coat the sample with Momentive SS4155 epoxy primer three times allowing the primer to dry for 15 minutes between coats, see Figure 36.

Figure 36. Left - Momentive SS4155. Right - sample with dried primer coating (Modified from Fojtasek, 2022).

8. Mix about 75 grams total of Momentive RTV627 parts A and B in a 1:1 ratio. Parts A and B come in separate buckets and are labeled with an “A” and a “B”. Allow the mixed epoxy to stand for 15 minutes to release trapped air bubbles from the mixing process, Figure 37. No more air bubbles will be visible on the surface of the epoxy. It is very important to thoroughly mix both parts of the epoxy in their individual containers to stir the settled particles back into solution. Neglecting to do this will result in poor epoxy quality from the last 1/3 of the buckets.

Figure 37. Momentive RTV627 parts A and B.

9. Clean the aluminum mold with acetone, then coat three times with silicon mold release spray, waiting 15 minutes between each application. Silicone mold release is of paramount importance in achieving a high-quality fracture conductivity sample by preventing the epoxy from sticking to the aluminum mold and tearing away from the fracture conductivity sample. See Figure 38.

Figure 38. Aluminum mold cleaned with acetone (Reprinted from Copeland, 2020) and coated with silicone mold release spray.

10. After the epoxy primer has dried, place the sample in the mold, then slowly apply the epoxy around the sample in a circular fashion to allow air bubbles to escape, Figure 39.

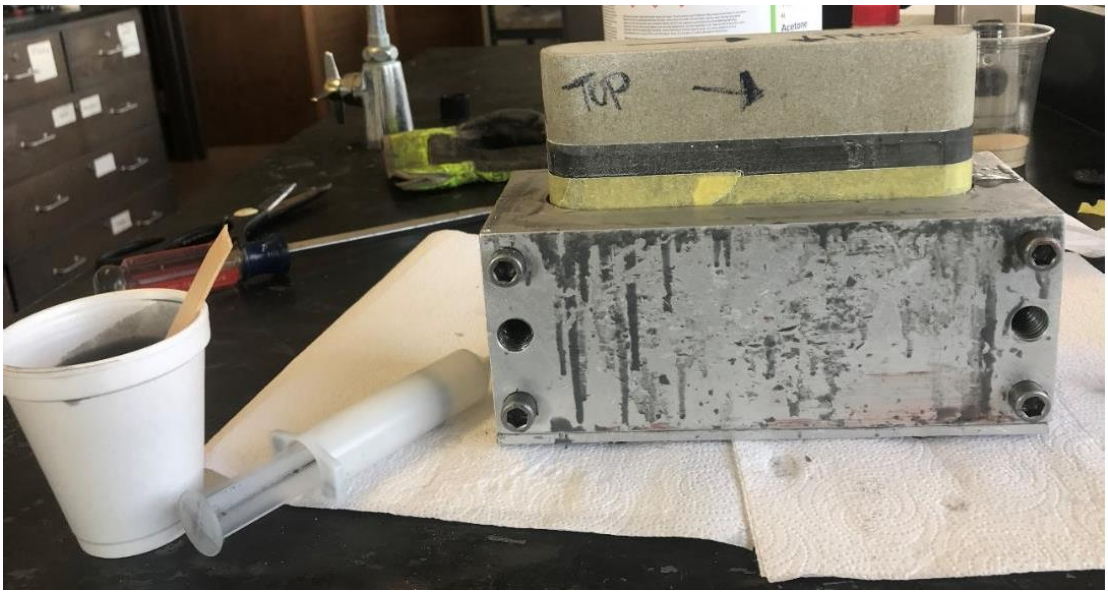

Figure 39. Sample in the mold surrounded by epoxy, ready to be cured in the oven (Reprinted from Copeland, 2020).

11. Place the sample in the oven to cure. The small electric oven with the number dial set at a “4” for 2 hours was the process used for this study.

12. Remove the sample from the oven and carefully remove the sample from the mold. Remember to keep the sample oriented the same way it went into the oven to not accidentally shift the proppant inside the sample, see Figure 40.

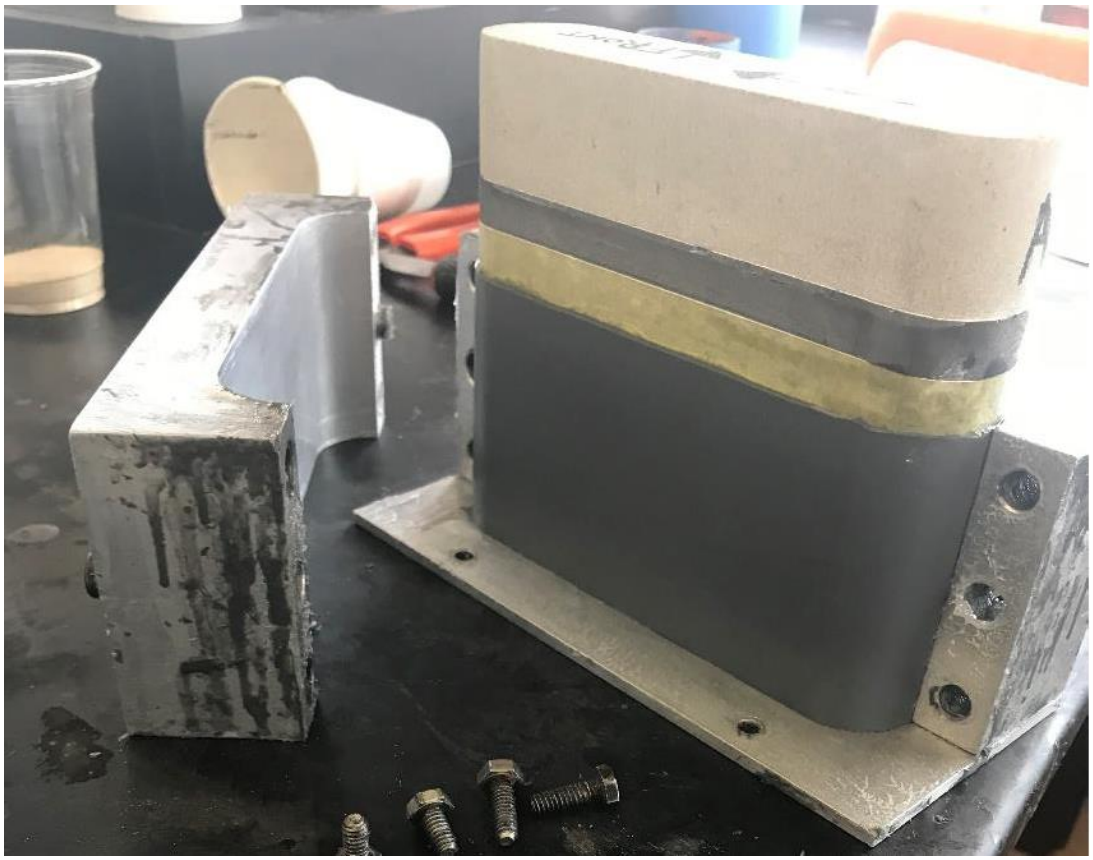

Figure 40. Mold deconstruction after the epoxy has cured in the oven (Reprinted from Copeland, 2020).

13. After the bottom half of the sample is coated in epoxy, steps 7-12 are repeated. A tall mold (about 10 inches in total height) is used to coat the top half of the sample. This was found to save time and prevent other issues associated with reusing the short

mold, only placed higher on the sample. Figure 41 shows a finished sample that is ready for conductivity testing.

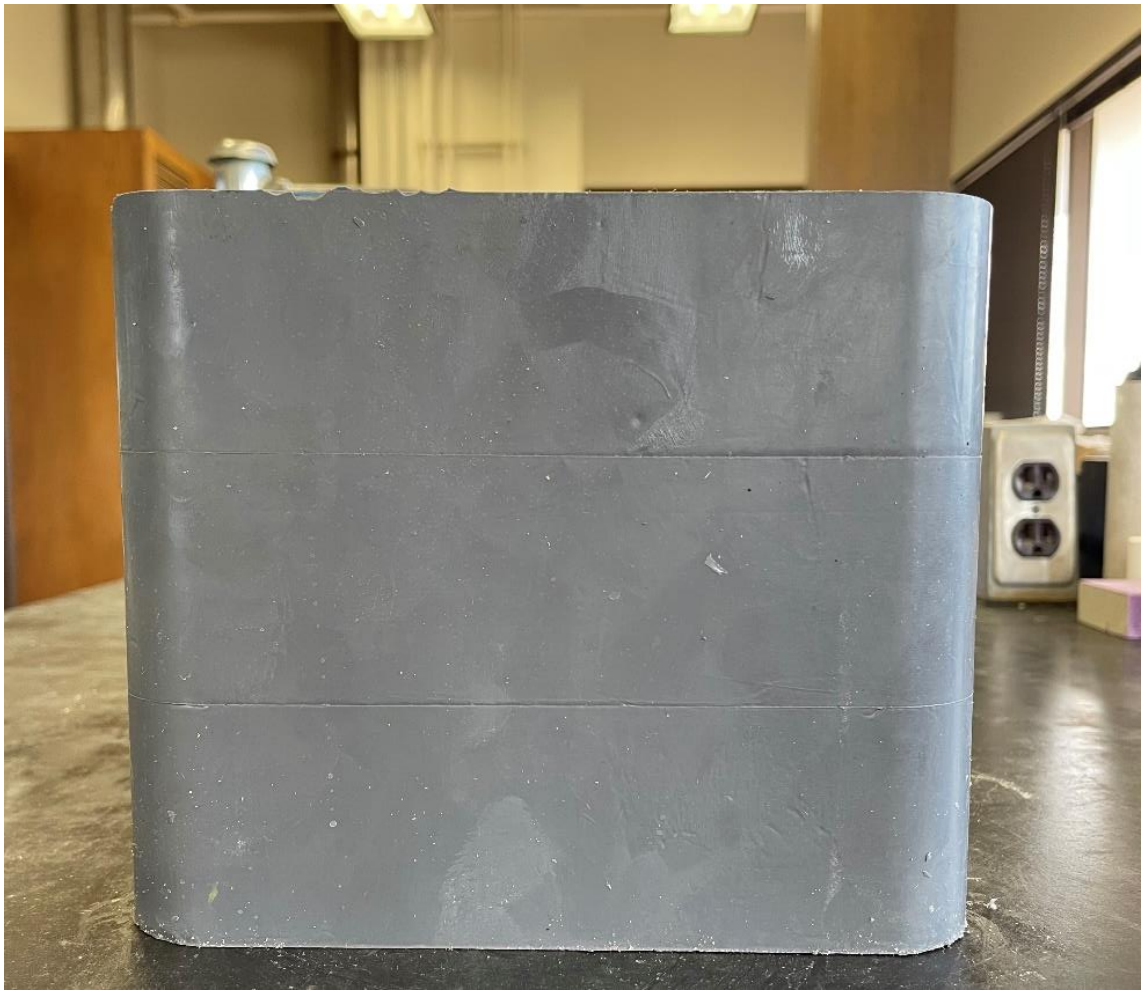

Figure 41. Completed sample preparation, ready for fracture conductivity testing.

2.4.3. Sample Reuse Additional Considerations

In the author's experience, it added an average of 2 hours of additional preparation time to each sample, when having to reuse a sample, for a total of 8 hours. The average new sample preparation time was 6 hours (1 hour for proppant placement, super glue, tape, epoxy, etc. 2 hours oven. 1 hour remove sample from mold, clean, prime, re-epoxy. 2 hours oven.). Reusing a

sample added 2 hours by requiring removal of all the old epoxy. Large groupings of epoxy are first removed using a putty knife as seen in Figure 42.

Figure 42. Representative putty knife used to remove epoxy.

Next, steel wool is used to remove the trace amounts of epoxy that are left over from using the putty knife. Worth noting, it appears that the primer loses its effect on priming the sample with each additional sample use. This requires additional priming and waiting time for the primer to cure before applying the next coat.

During the final three experiments conducted, an incredible time saving procedure was discovered when using previously used samples. If the bottom inch of epoxy on the bottom half of the sample from the last experiment is left intact, this acts as a seal and allows a one epoxy pour sample to be created. Completely removing the top half of the sample of epoxy is still required but only one preparation and oven cycle is required. This saves roughly 3 hours of preparation time.

2.5. Fracture Conductivity Measurement

Now that the fracture conductivity sample has been properly prepped, the actual collection of data can occur. The steps to do so are outlined below:

1. After the sample has cured, the first step is to wrap the sample with Teflon tape, separating the pressure ports horizontally and vertically from the top and bottom of the sample, see Figure 43.

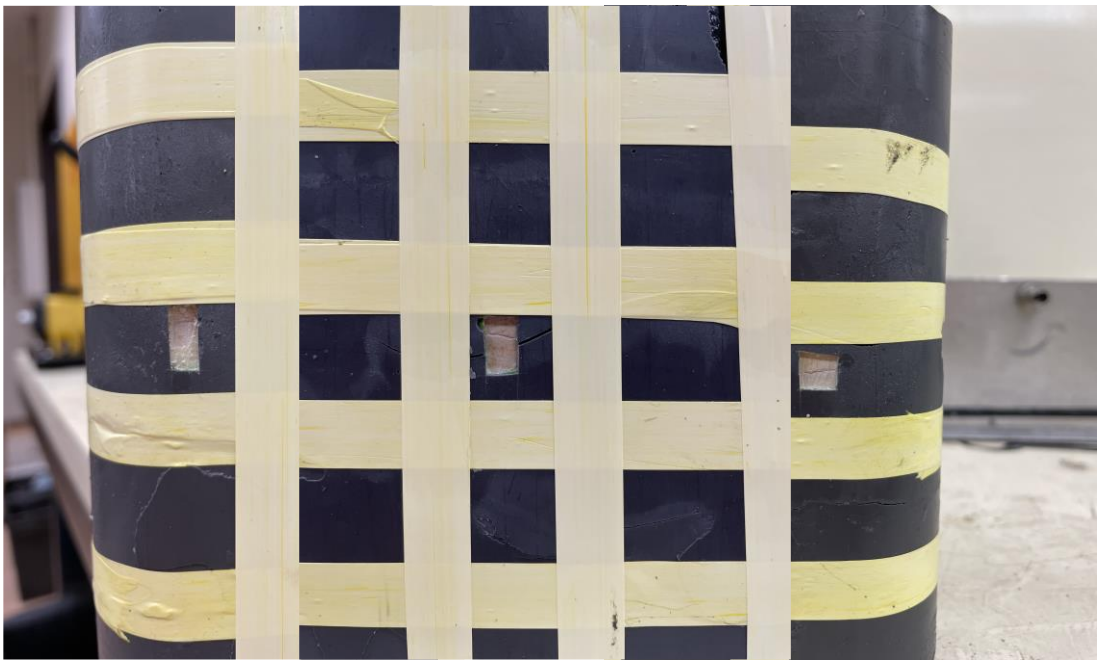

Figure 43. Three pictures put together to display the copious amount of Teflon tape applied to the sample.

2. Cut away the epoxy in the fracture plane only where the flow lines and pressure ports will meet the sample, see Figure 44. The outside most pressure ports are separated by 5.25 inches, with the middle pressure port directly in the middle between the first two pressure ports. The fracture plane is nominally 3 inches from the bottom of the sample but can vary depending on the original sample geometry. Spacers can be used during the sample preparation phase to closely place the fracture plane at or near 3 inches.

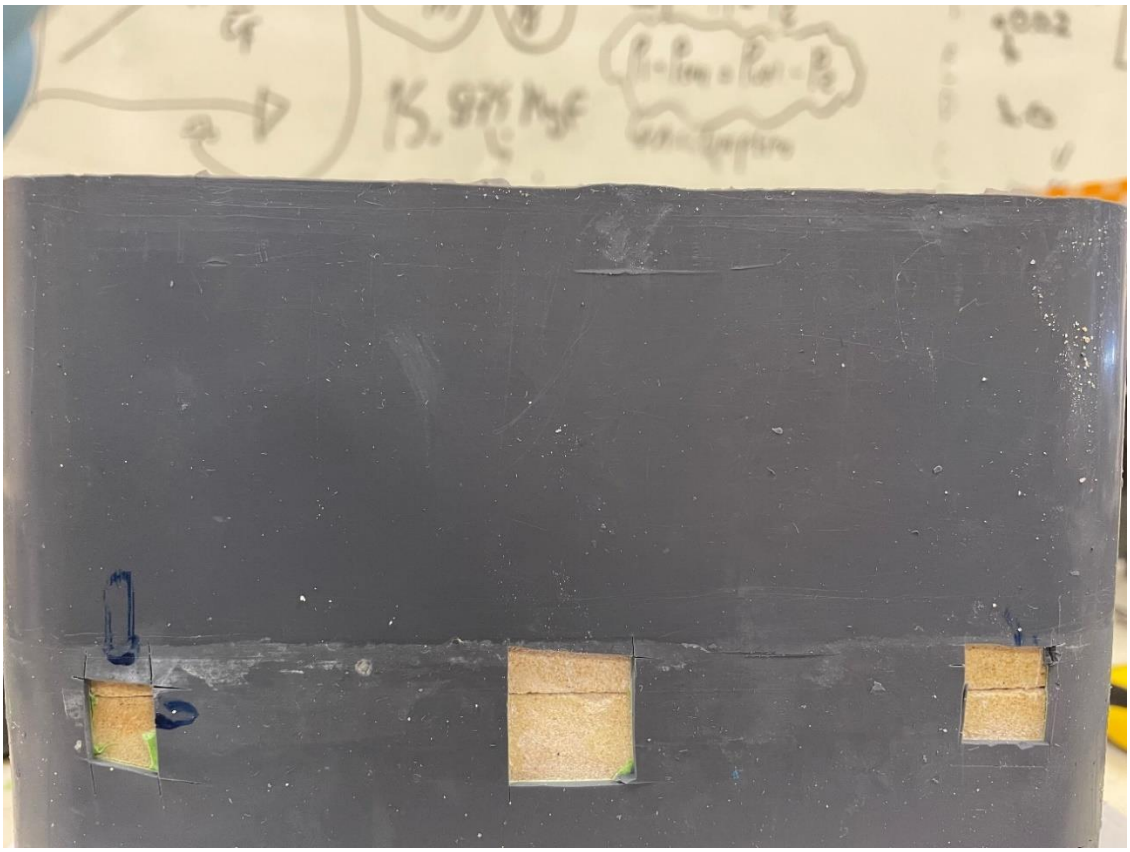

Figure 44. Fracture plane exposed to pressure ports.

3. Place the conductivity cell on top of the bottom piston, making sure the metal stop is installed around the bottom piston. This locates the conductivity cell.
4. Coat the sample in a thin film of grease to aid installation into the conductivity cell, see Figure 45. Use caution around the openings cut into the epoxy so that grease will not enter the exposed fracture when the sample is installed in the conductivity cell. Insert the sample into the modified conductivity test cell, verifying line of sight from the flow lines and pressure ports to the fracture plane.

Figure 45. Molykote vacuum grease used during sample installation into the conductivity cell.

5. Install the top piston into the conductivity cell using a hydraulic press.
6. Load the conductivity test cell into the GCTS load frame.
7. Log into the laboratory computer, turn on the GCTS controller box, and start the data acquisition system.
8. Calibrate the pressure transducers.
9. Install the flow inserts, connect the flow lines, back pressure valve, and pressure transducers.
10. Increase the closure stress on the sample to 500psi to take up any gaps in the sample. Then install the top and bottom piston caps to seal the system.
11. Slowly pressurize the system with nitrogen to just under 30psi, checking for leaks. Record the leak off value. It should be very low, 0.03L/min or less.

12. Increase the closure stress on the sample to 1000psi. Most experiments took measurements at 1000, 2000, 3000, 4000, 5000, and 6000 psi closure stress. If the experimental conditions are changed, start at the smallest closure stress first.
13. At each closure stress, take readings at 4 different flowrates and the resulting axial displacement, differential pressure, and cell pressure waiting at least 5 minutes between each reading, or until there is no change in data with time, which ever takes longer. It is recommended to start with the highest flowrate first.
14. Numerous individuals have determined the flowrate should be kept below 1 liter per minute and others decided on 2 liters per minute. The author has found at very low closure stresses that a flowrate of 2 liters per minute can cause the proppant in the fracture to shift, see Figure 46.

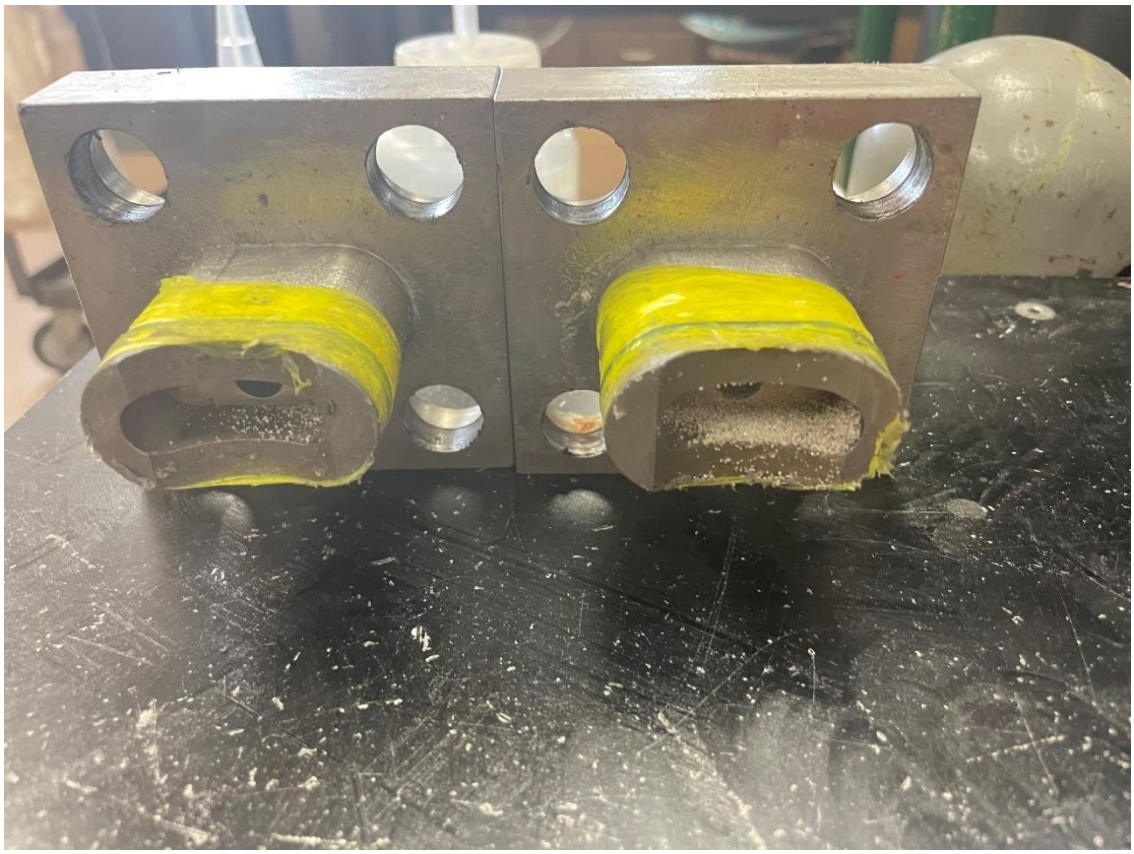

Figure 46. Evidence of proppant movement due to high flowrates through the sample fracture.

15. Readings are taken at 1000, 2000, 3000, 4000, 5000, and 6000 psi closure stresses if it is an outcrop sample and at 1000, 2000, 3000, and 4000psi if it is a fractured sample.
16. Unload the GCTS load cell and depressurize the sample, making sure to slowly bleed pressure off using the back pressure needle valve. If the flow lines are loosened while the conductivity cell is still pressurized, the nitrogen can rush out of the fracture, shifting the proppant in the sample fracture.
17. Remove all flowlines and flow inserts.

18. Carefully press out the sample from the modified API conductivity cell using a hydraulic jack, cut the epoxy away from the fracture, and open the fracture.

19. Collect the proppant on a clean sheet of paper, remove obvious crushed pieces of the sample from the proppant, see Figure 47.

20. Transfer the proppant for a sand sieve analysis.

Figure 47. Crushed proppant collection after a fracture conductivity experiment with crushed sample contamination (the dark pieces are crushed pieces of the downhole core sample.

2.6. Fracture Conductivity Equation Development

As is common in petroleum engineering, Darcy's Law in equation 3 was the foundation used to arrive at an expression for fracture conductivity using the recorded experimental data,

$$-\frac{\boldsymbol{dP}}{\boldsymbol{dL}} = \frac{\boldsymbol{\mu v}}{\boldsymbol{k_f}} \tag{3}$$

where $-\frac{dP}{dL}$ is the change in pressure per unit length (psi/in) with the negative due to the pressure decreasing over the length, μ is viscosity (cP), v is velocity (ft/s), and k_f is permeability (md). Gas flux, given by equation 4, is the mass flow rate per cross sectional area per unit of time,

$$\frac{\dot{m}}{A} = \rho v \tag{4}$$

where $\dot{m}$ is mass flow rate (kg/s), A is the cross-sectional area (m^2), ρ is the density (kg/m^3), and v is velocity in (m/s). The next step is to multiply both sides of equation 3 by ρ to yield equation 5.

$$\rho\left(-\frac{dP}{dL}\right) = \rho\left(\frac{\mu v}{k_f}\right) \tag{5}$$

Next, we introduce the real gas law in equation 6 due to nitrogen being the working fluid of investigation,

$$\rho = \frac{PM_g}{ZRT} \tag{6}$$

where P is the absolute pressure (psi), M_g is the molar mass of the gas in question - nitrogen (kg/mol), Z is the compressibility factor (dimensionless), R is the universal gas constant (J/mol-K), and T is absolute temperature (degrees kelvin). Equation 4 is solved for density and replaces the density term on the right side of equation 5, canceling out the velocity term. Equation 6 replaces the density term on the left side of equation 5, yielding equation 7.

$$-\frac{PM_g}{ZRT}\left(\frac{dP}{dL}\right)=\frac{\dot{m}\mu}{Ak_f} \tag{7}$$

Equation 8 is generated by bringing the dL term to the right side and integrating equation 7.

$$-\frac{M_g}{ZRT}\left(\frac{{P_2}^2-{P_1}^2}{2}\right)=\frac{\dot{m}\mu}{Ak_f}L \tag{8}$$

Distributing the negative sign on the left side of equation 8 to the difference of squared pressures term and rearranging those terms gives equation 9.

$$\frac{M_g}{ZRT}\left(\frac{{P_1}^2-{P_2}^2}{2}\right)=\frac{\dot{m}\mu}{Ak_f}L \tag{9}$$

Equation 10 gives the velocity of nitrogen in the test sample fracture as,

$$v=\frac{Q}{h_f w_f} \tag{10}$$

Where Q is volumetric flow rate (m^3/s), h_f is the height of the sample fracture (in) (width in the test sample ~1.75in), and $w_f$is the width of the sample fracture (in) (the separation distance in the test sample, height of proppant). Substituting equation 10 into equation 4 for v, replacing the $\frac{\dot{m}}{A}$ term in equation 9 with the resultant, and moving the L term to the left side develops equation 11.

$$\frac{M_g\left({P_1}^2-{P_2}^2\right)}{2ZRTL}=\frac{Q\rho\mu}{h_f}*\frac{1}{w_f k_f} \tag{11}$$

Equation 12 and 13 relate the three pressure ports in the modified conductivity cell as seen in Figure 48.

$$P_1-P_2=\Delta P \tag{12}$$

$$P_{cell} \tag{13}$$

Equating the constants on both sides of equation 11 to C_1 and C_2, then simplifying yields equations 14-17.

$$C_1\left({P_1}^2 - {P_2}^2\right) = C_2 \frac{1}{w_f k_f} \tag{14}$$

$$C_1(P_1 - P_2)(P_1 + P_2) = C_2 \frac{1}{w_f k_f} \tag{15}$$

$$C_1(\Delta P) = \frac{C_2}{P_1 + P_2} \frac{1}{w_f k_f} \tag{16}$$

$$P_{cell} = \frac{P_1 + P_2}{2} = \bar{P} \tag{17}$$

Notice on the right side of equation 11 that the right most term is the inverse of the fracture conductivity, as seen in equation 18.

$$\frac{1}{C_f} = \frac{1}{w_f k_f} \tag{18}$$

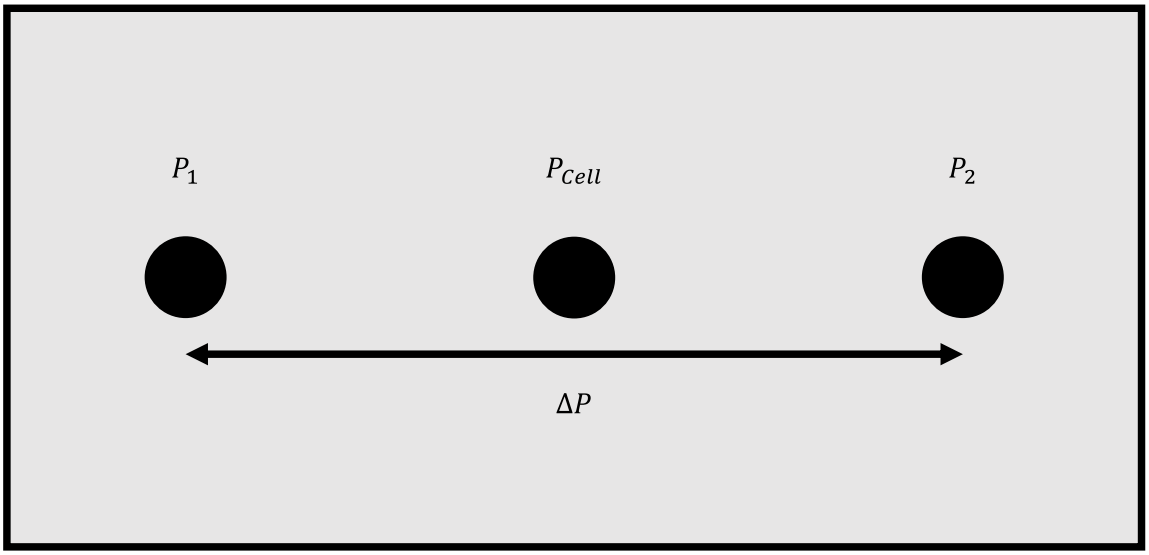

Figure 48. Schematic of pressure port configuration.

This successfully achieves the goal of an expression for fracture conductivity using the recorded experimental data. Please note that careful consideration should be given to conversion factors used in converting from imperial to SI units. The constant values used to determine the different fracture conductivities for this study can be found in Table 2.

Table 2. Constants used to determine fracture conductivity.

N2 Molecular Weight (MW) [kg/mol]	0.0280134
Fracture Width (h_f) [in]	1.75
Z factor (Z)	1
(R) [J/mol K]	8.3144
Temp (T) [K]	295.93
Fracture Length (L) [in]	5.25
N2 Viscosity (μ) [Pa*s]	1.75923E-05
N2 Density (ρ_f) [kg/m^3]	1.16085
Atmospheric Pressure [psi]	14.7

Plotting the $\frac{Q\rho\mu}{h_f}$ values on the x axis and the $\frac{M_g\left({P_1}^2-{P_2}^2\right)}{2ZRTL}$ values on the y axis, then taking the inverse of the slope of the best fit line segment through four measurements will yield the fracture conductivity. An example of the described plot can be found in Figure 49.

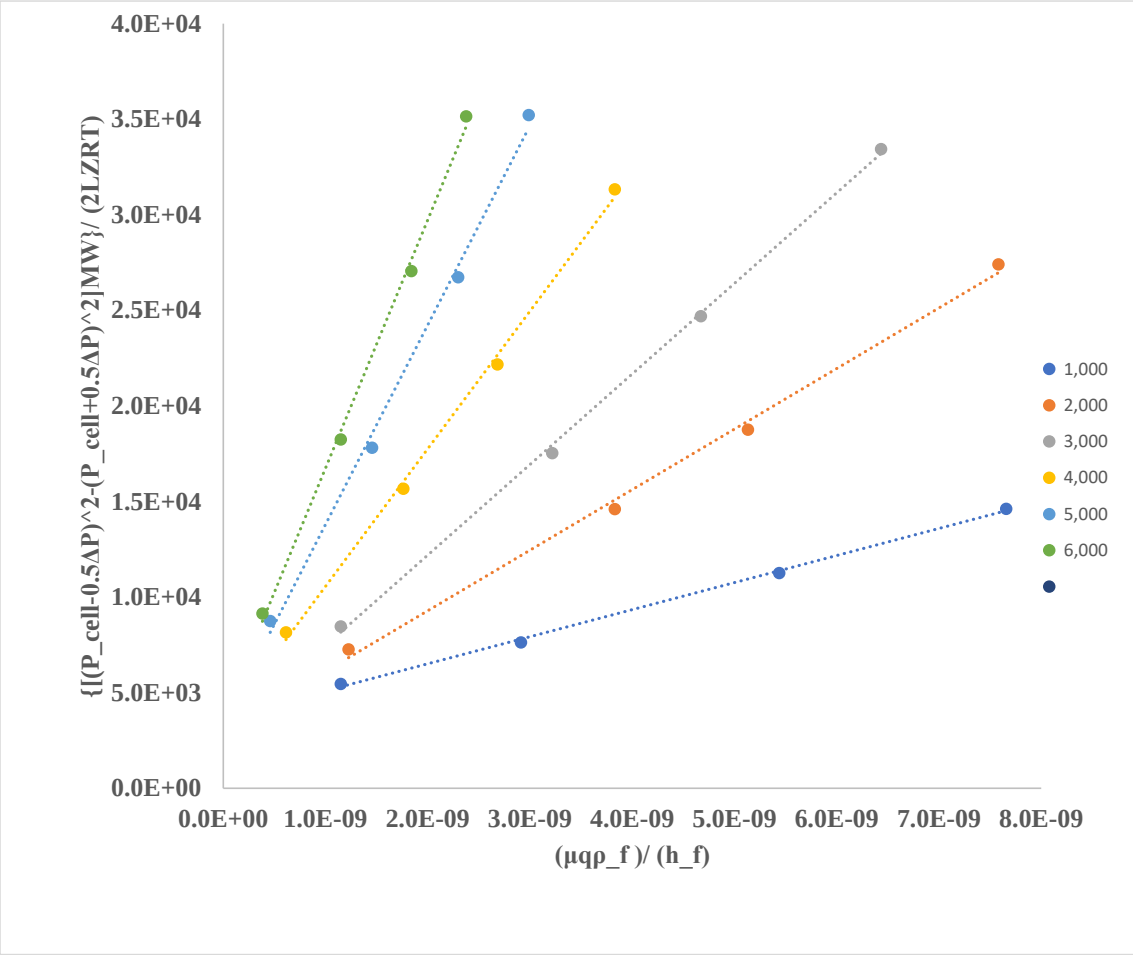

Figure 49. Representative plot where the inverse of the slope of each line segment represents the fracture conductivity at different closure stresses.

2.7. Proppant Sieve Analysis

After the fracture conductivity experiment is completed, the proppant is collected to perform proppant sieve analysis to quantify the amount of proppant crushing. Sieve analysis is performed as described by the American Society for Testing and Materials procedure ASTM C 136–01. A Ro-Tap machine with mesh sizes of 40, 50, 70, 80, 100, 120, 140, and pan is used for the proppant sieve analysis, see Figure 50. The collected proppant from the fracture conductivity

experiment is poured into the top sieve, the lid is put on, and the Ro-Tap machine is run for 15 minutes.

Figure 50. Ro-Tap machine used for proppant sieve analysis.

The proppant is then carefully collected into cups using a brush to be weighed, see Figure 51.

Figure 51. Cups used for proppant sieve analysis in the corresponding sieve mesh sizes used for this study: 40, 50, 70, 80, 100, 120, 140, and pan.

After the sieved proppant is collected, and the scale is tared to zero, each cup's starting weight is recorded, see Figure 52 and Figure 53. Then after each cup is thoroughly cleaned, each cup is again weighed, see Figure 54. This is necessary as a large discrepancy between seemingly identical cups was discovered to exist. After both weights are recorded for each mesh size cup, the proppant mass can be determined. A percent of mass breakdown per mesh size can then be graphed. A pre-experiment baseline is also graphed to see the quantified change from before and after the experiment.

Figure 52. Scale tared to zero, used to weigh proppant for sample preparation and sieve analysis.

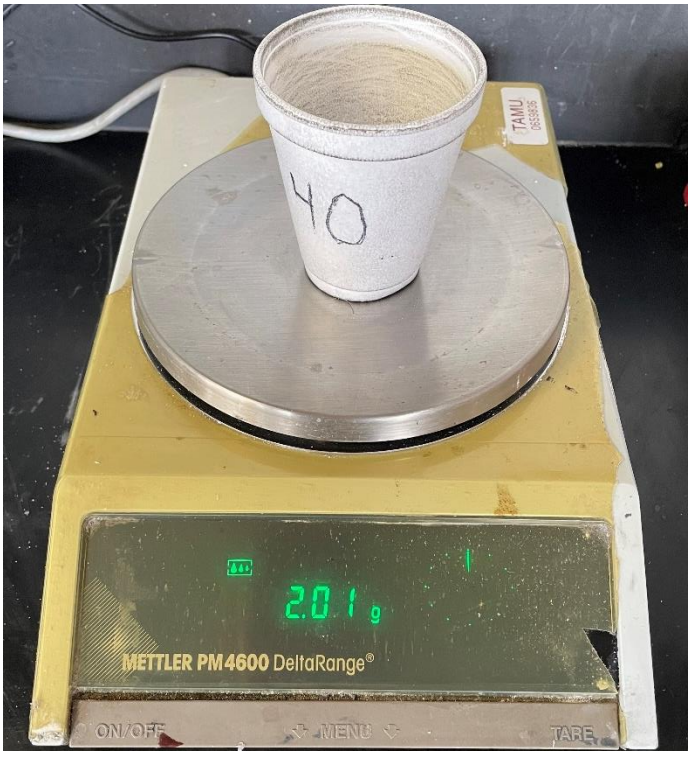

Figure 53. Scale weighing the mass of proppant and the sieve analysis cup.

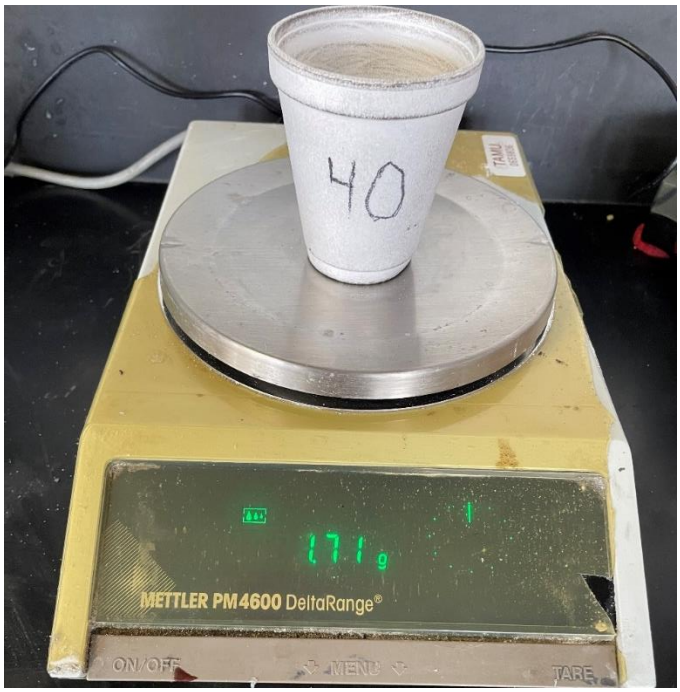

Figure 54. Scale weighing the mass of only the cup after being thoroughly brushed cleaned.

2.8. Experimental Trouble Shooting

Whenever experimental work is performed, there will always be unexpected setbacks. Below are just a few examples of setbacks encountered and how they were overcome. When checking for a very low leak off value, many times leaks were discovered, see Figure 55. At first, the connector leaks were fixed by tightening the connections. This was found to expedite wearing out of the connectors, ultimately preventing them from sealing at all. At this point, connectors incorporating O-rings were used which all but eliminated connector leaks. It was discovered the O-ring for the top piston was damaged requiring a new O-ring, see Figure 56.

Figure 55. Left - A leak detected on a pressure port. Right - A leak detected on the top piston.

Figure 56. Left - New O-rings for the top and bottom pistons. Right - A new O-ring for a flow insert.

Figure 56 also displays the correct replacement O-ring for the flow inserts. Both flow inserts had damaged O-rings which can be seen detached in pieces in Figure 57 and Figure 58.

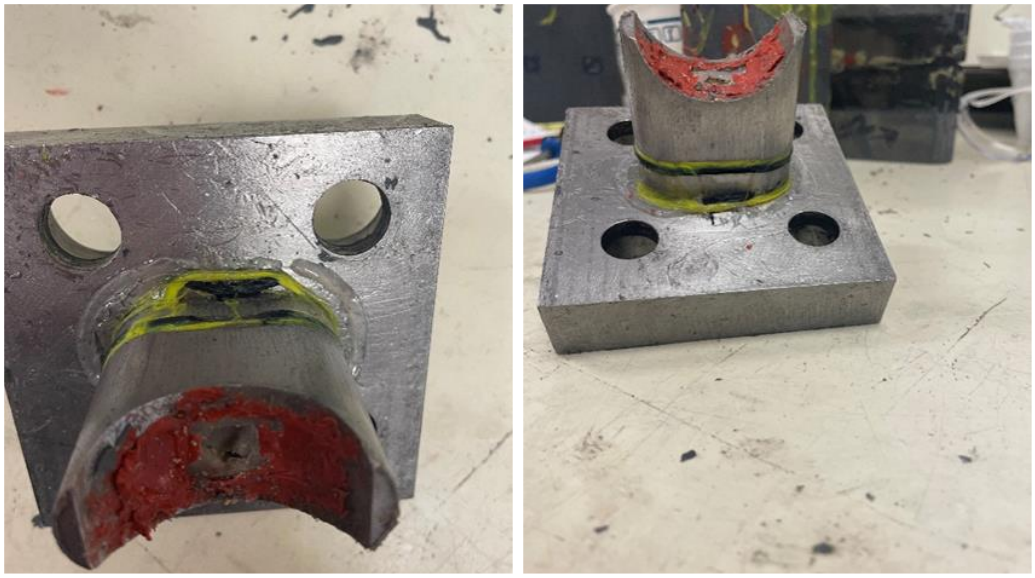

Figure 57. Failed O-ring on the entry flow insert.

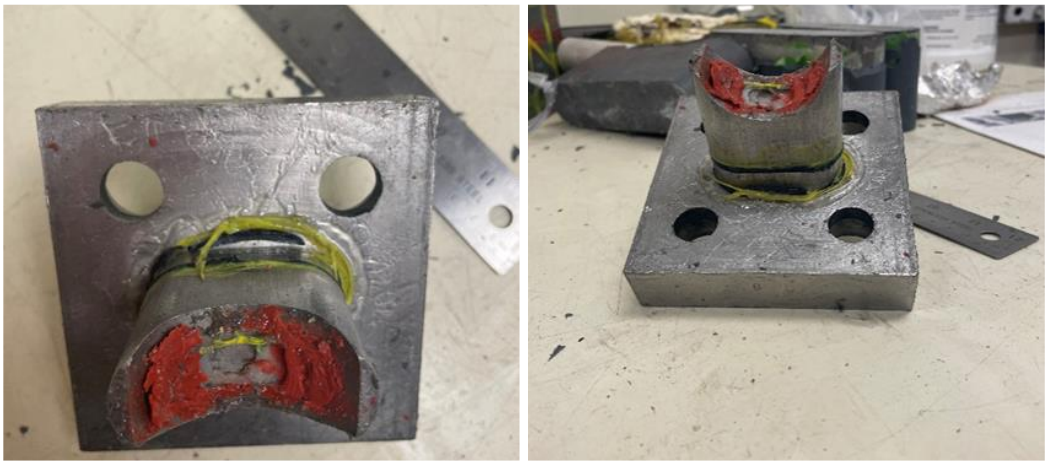

Figure 58. Failed O-ring on the exit flow insert.

Things as simple as a bolt shearing off in the aluminum mold also occurred, see Figure 59. This was fixed by Mr. John Maldonado using an extractor bit to remove the sheared bolt.

While trouble shooting the pressure transducers, rust was discovered inside of one requiring cleaning.

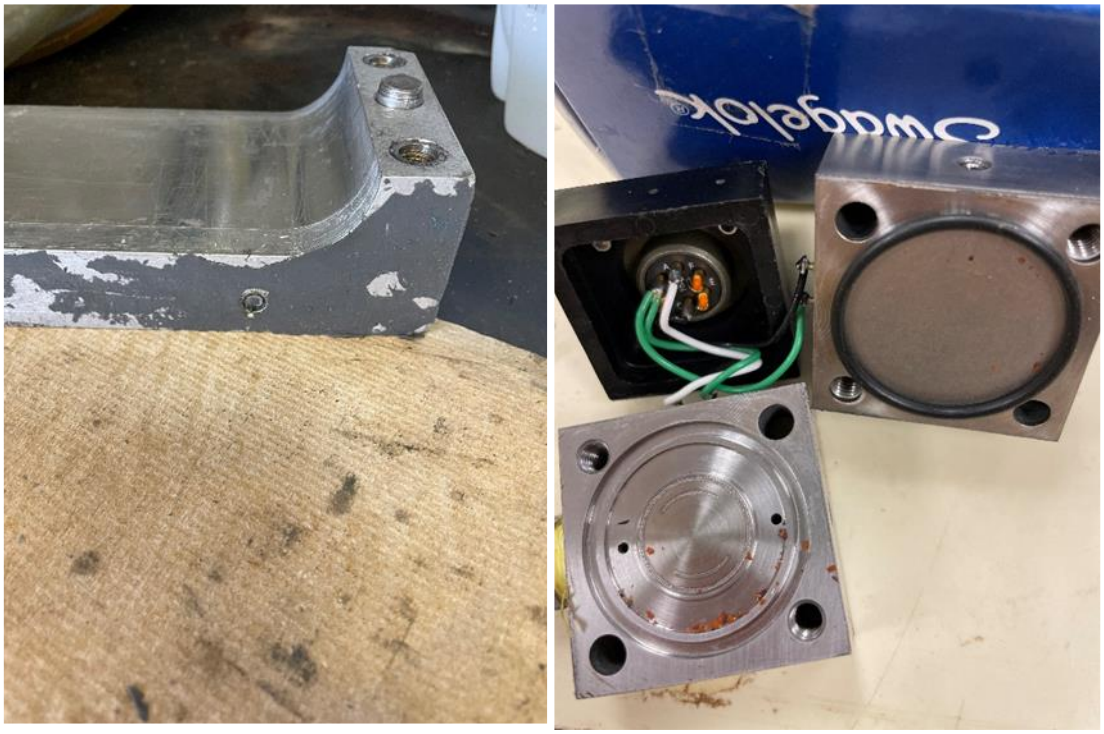

Figure 59. Left - Sheared bolt from the aluminum epoxy mold. Right - Rust and debris inside a pressure transducer.

After the second differential pressure transducer was added, it was discovered the hardlines did not line up with the pressure ports anymore. The fix for this was installing flex hoses which completely eliminated the sealing dependency on hardline geometry, see Figure 60.

Figure 60. Change from hard lines to flex lines to reduce connection wear.

Additionally, when the flex lines were first installed, the flex lines connected directly to the pressure port connectors. This means a connection event occurred every time a fracture conductivity test was performed. A short hard line was then added to the flex line so that the hardline can wear out and be easily replaced, preserving the flex line connection. One day the hydraulic pump would not turn on requiring investigation of the fuse box feeding power to the hydraulic pump, see Figure 61. It is very beneficial to be mechanically inclined when performing experimental work.

Figure 61. Left - Hydraulic pump that powers the load frame. Right - Fuse box that controls the hydraulic pump.

3. EXPERIMENTAL RESULTS AND DISCUSSION*

3.1. Fracture Conductivity

The below sections present the fracture conductivity values grouped into divisions of interest. In total, 16 experiments were performed. Table 3 summarizes the fracture conductivity values from the experiments performed. Figure 62 through Figure 77 show the experiments in the order in which they were performed.

Table 3. Summary of fracture conductivity from experimental data.

Experiment #	Outcrop or Downhole Core	Proppant Concentration (lb/ft^2)	Closure Stress (psi)					
			1000	2000	3000	4000	5000	6000
1	Outcrop	0.20	238	160	119	110	97	89
2	Downhole Core	0.20	1166	816	587	432	300	301
3	Outcrop	0.20	700	441	344	306	285	256
4	Downhole Core	0.20	724	321	252	190	154	127
5	Outcrop	0.20	100	72	56	46	37	29
6	Outcrop	0.10	378	263	181	146	122	102
7	Downhole Core	0.10	2321	2303	1789	1612	1324	1047
8	Outcrop	0.05	1890	945	595	438	343	266
9	Outcrop	0.05	891	547	388	266	226	185
10	Outcrop	0.05	2349	1050	702	462	319	256
11	Outcrop	0.10	1396	1064	767	629	527	448
12	Outcrop	0.10	1065	740	551	418	348	294
13	Fractured	0.00	5.5	4.0	3.2	2.2		
14	Fractured	0.20	357	233	174	140		
15	Fractured	0.05	6007	3676	2710	1967		
16	Fractured	0.10	433	307	255	227		
			Fracture Conductivity (md*ft)					

* Used with permission of Society of Petroleum Engineers (SPE), from Fracture Conductivity Created by Proppants and Acid in the Austin Chalk Formation, A. T. Brashear; A. D. Hill; D. Zhu; E. Kerr; R. Scofield; D. Jordan; E. Estrada; T. Tajima, 2022; permission conveyed through Copyright Clearance Center, Inc.

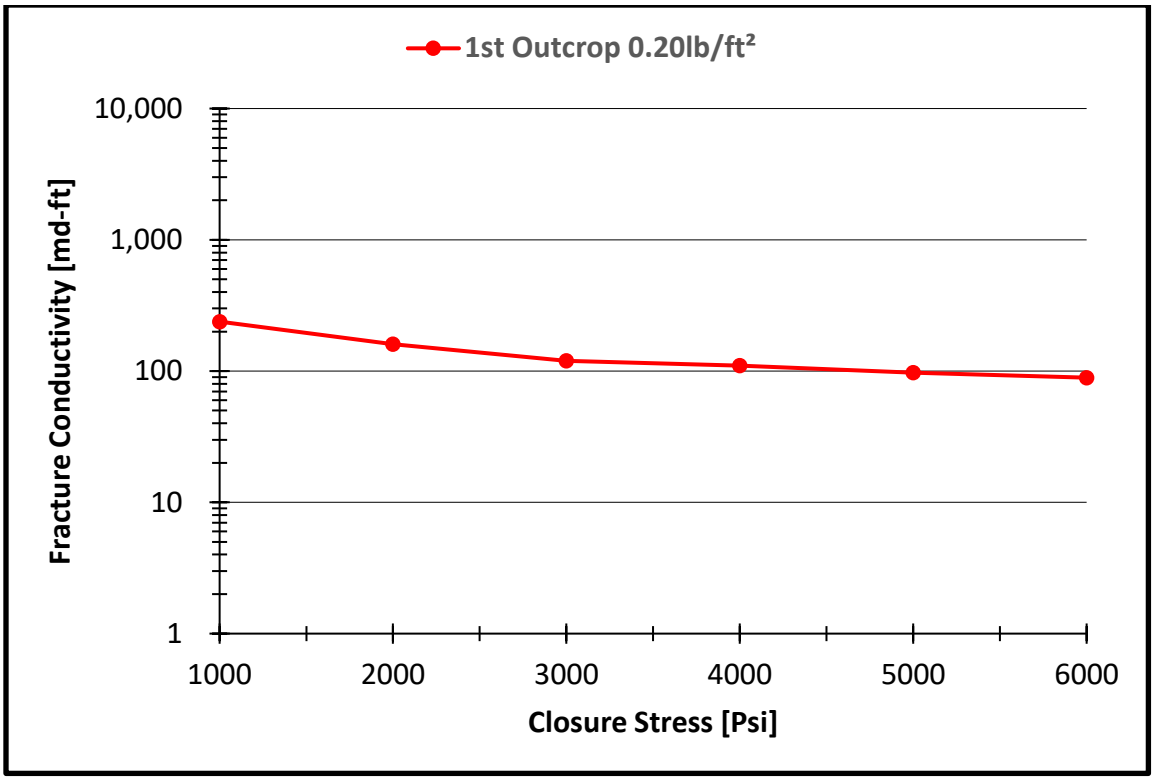

Figure 62. 1st experiment fracture conductivity of 1st Outcrop 0.20lb/ft^2

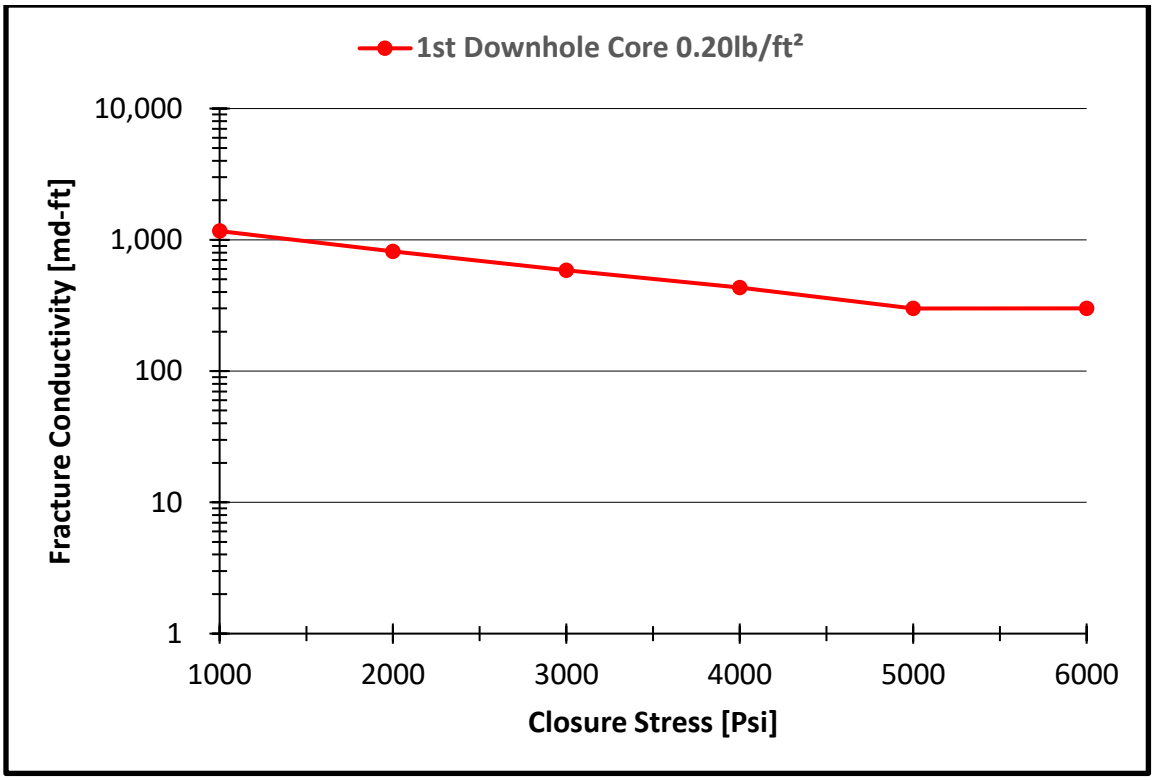

Figure 63. 2nd experiment fracture conductivity of 1st Downhole Core 0.20lb/ft^2

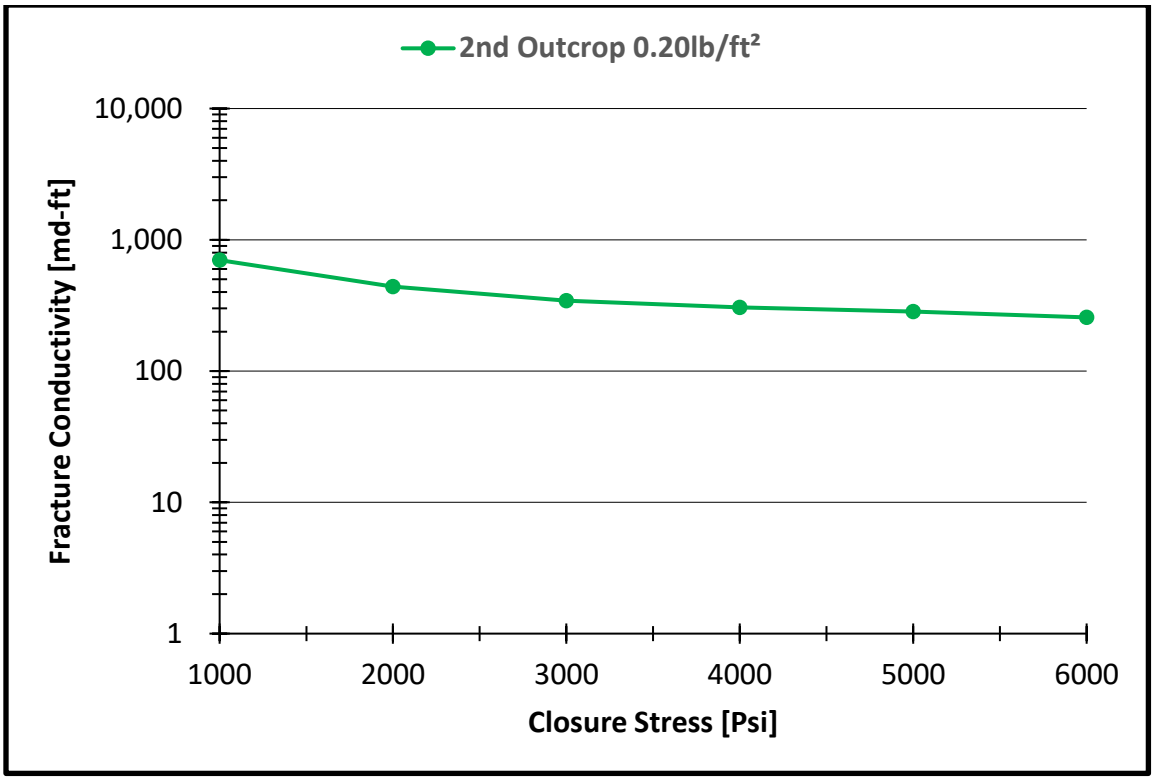

Figure 64. 3rd experiment fracture conductivity of 2nd Outcrop 0.20lb/ft^2

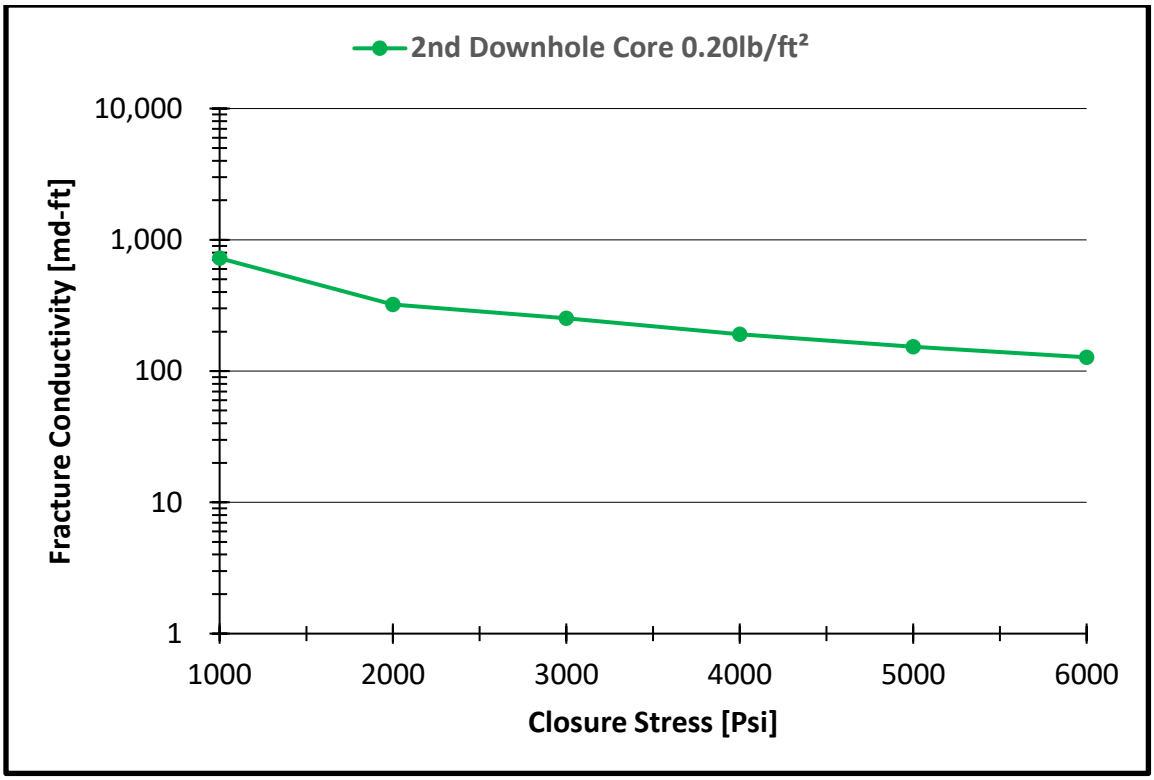

Figure 65. 4th experiment fracture conductivity of 2nd Downhole Core 0.20lb/ft^2

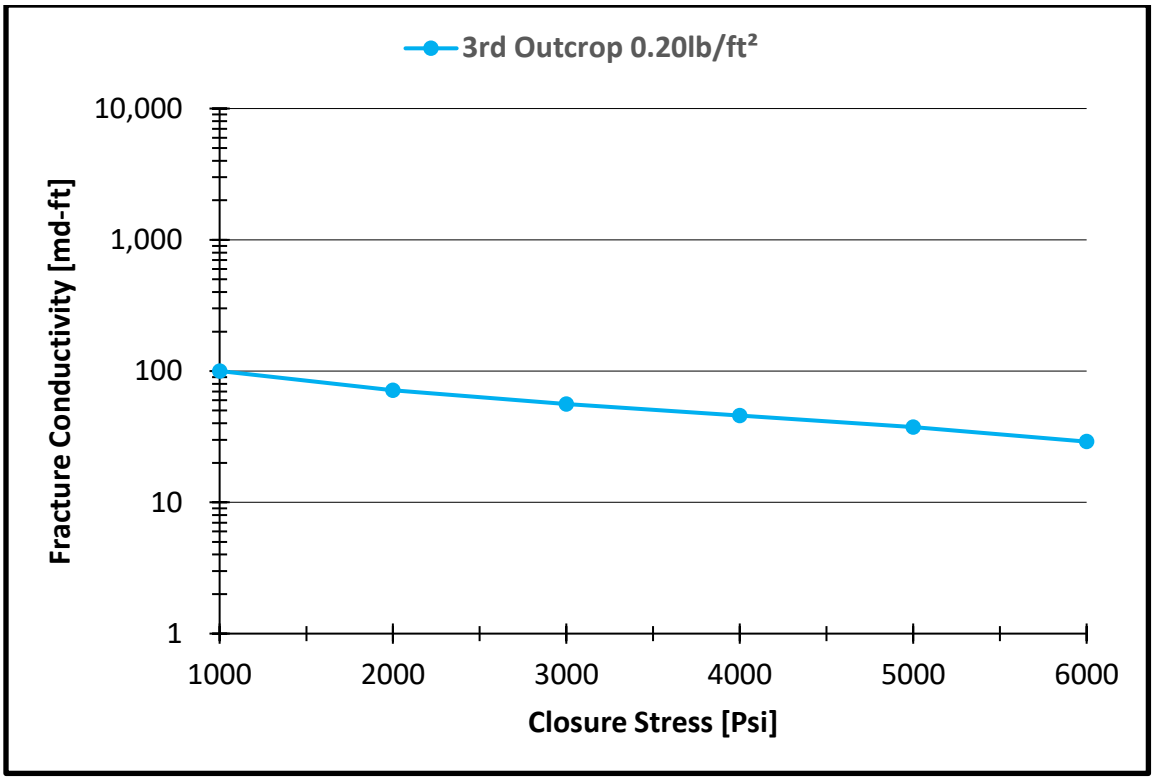

Figure 66. 5th experiment fracture conductivity of 3rd Outcrop 0.20lb/ft^2

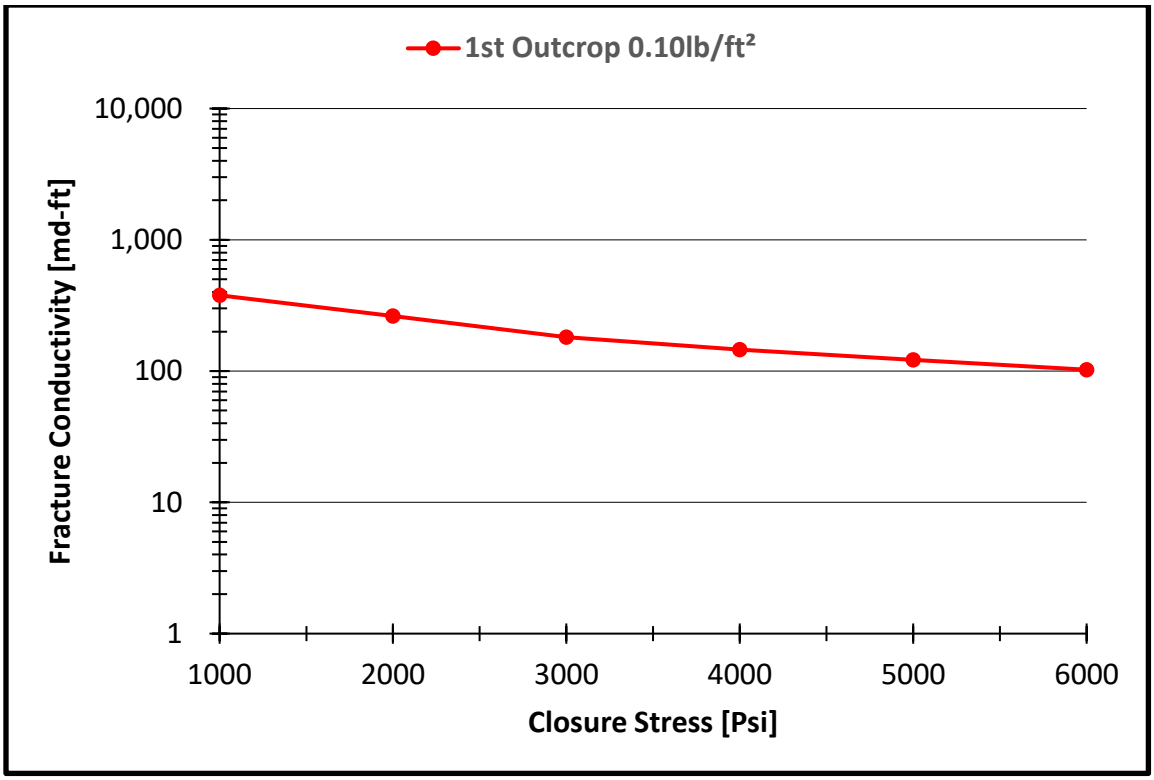

Figure 67. 6th experiment fracture conductivity of 1st Outcrop 0.10lb/ft^2

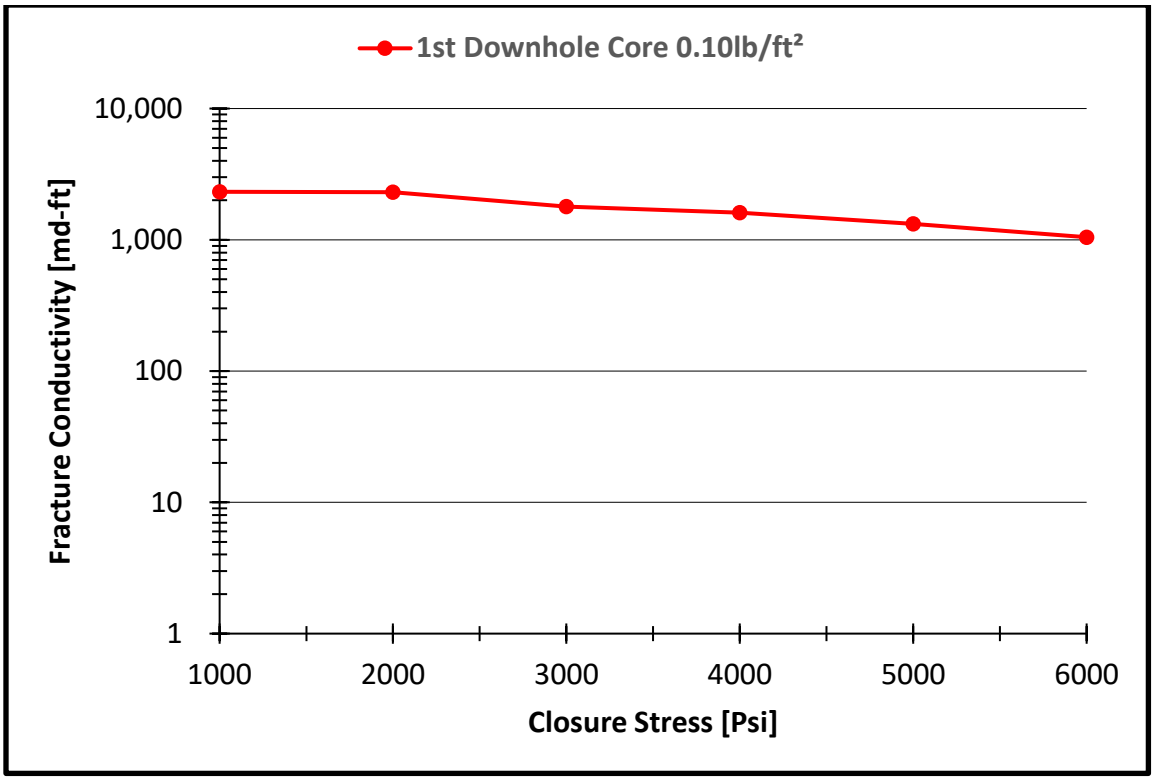

Figure 68. 7th experiment fracture conductivity of 1st Downhole Core 0.10lb/ft^2

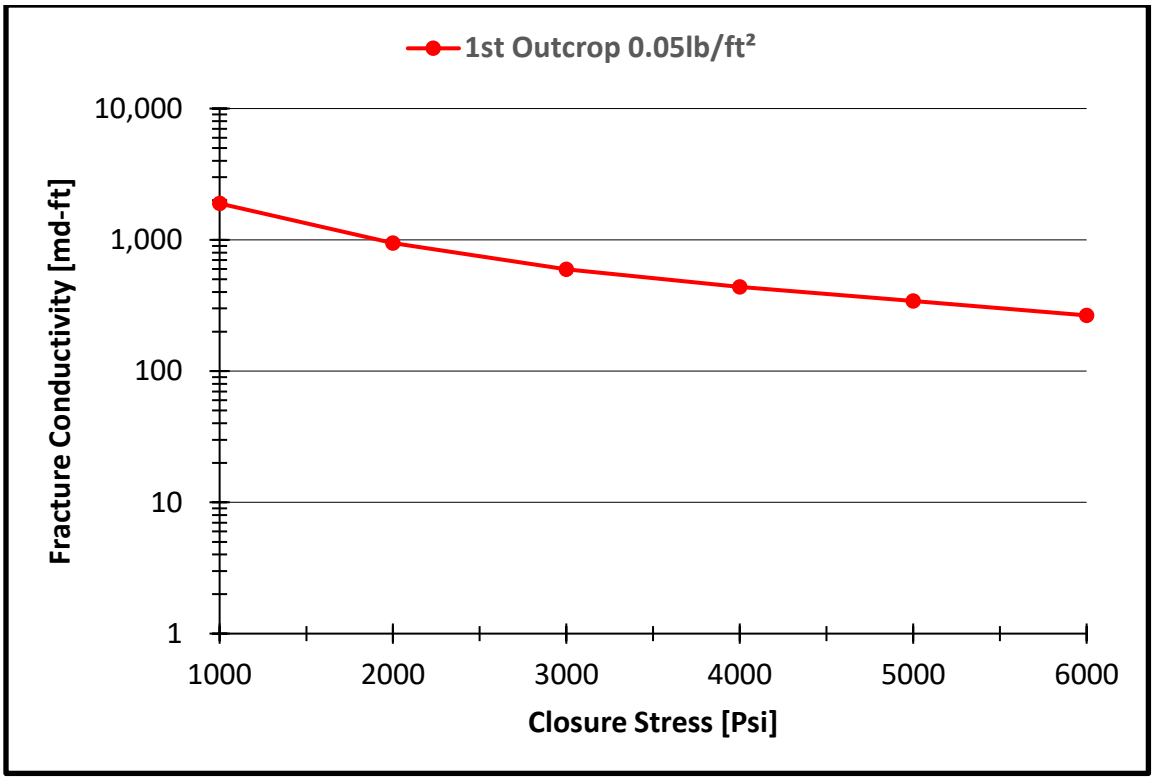

Figure 69. 8th experiment fracture conductivity of 1st Outcrop 0.05lb/ft^2

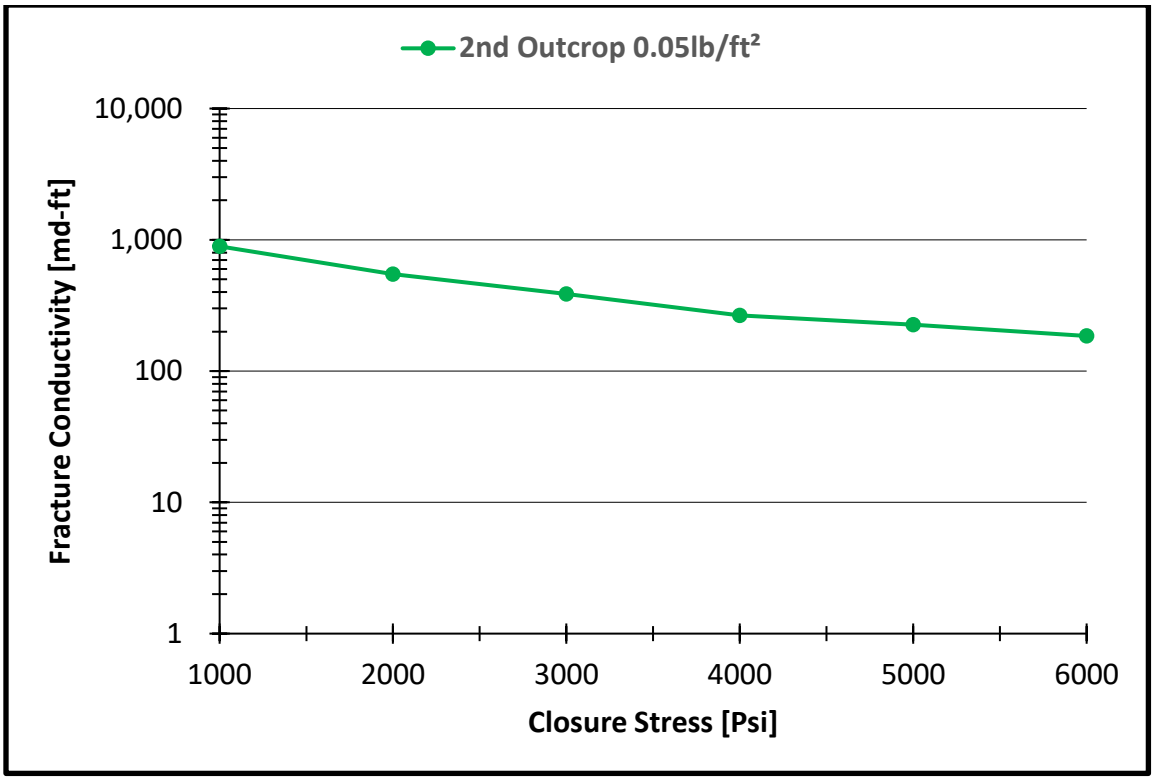

Figure 70. 9th experiment fracture conductivity of 2nd Outcrop 0.05lb/ft^2

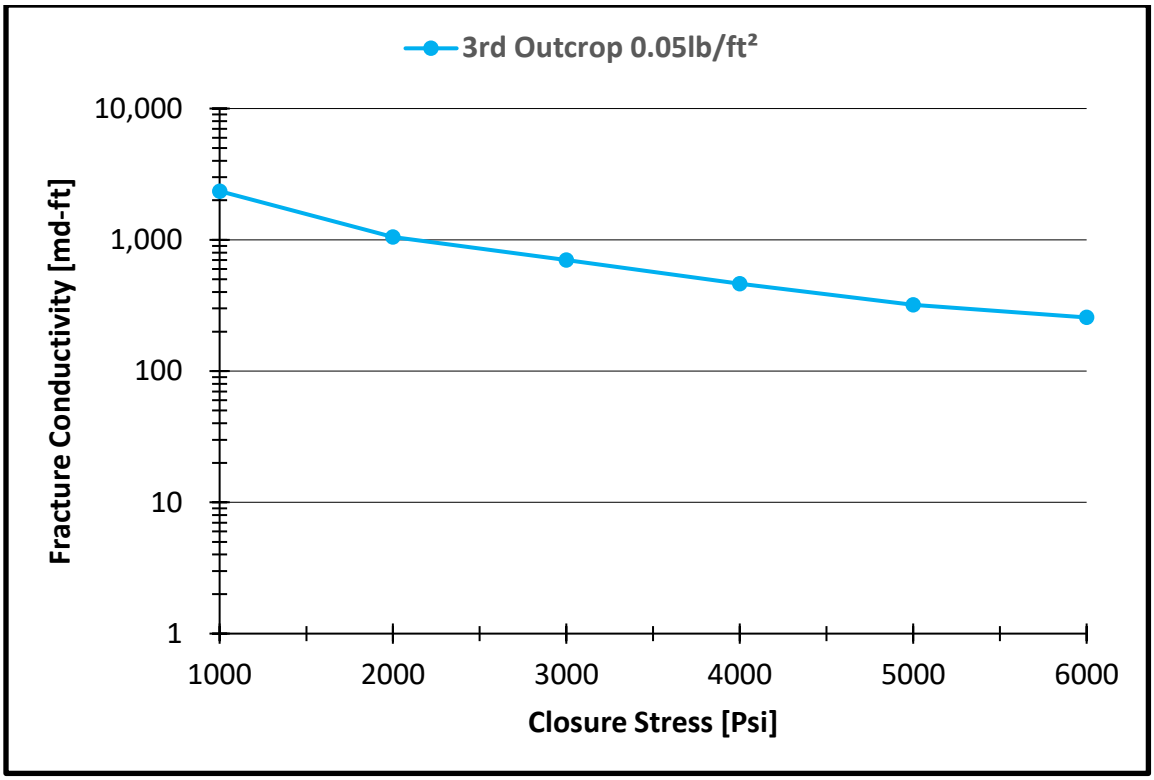

Figure 71. 10th experiment fracture conductivity of 3rd Outcrop 0.05lb/ft^2

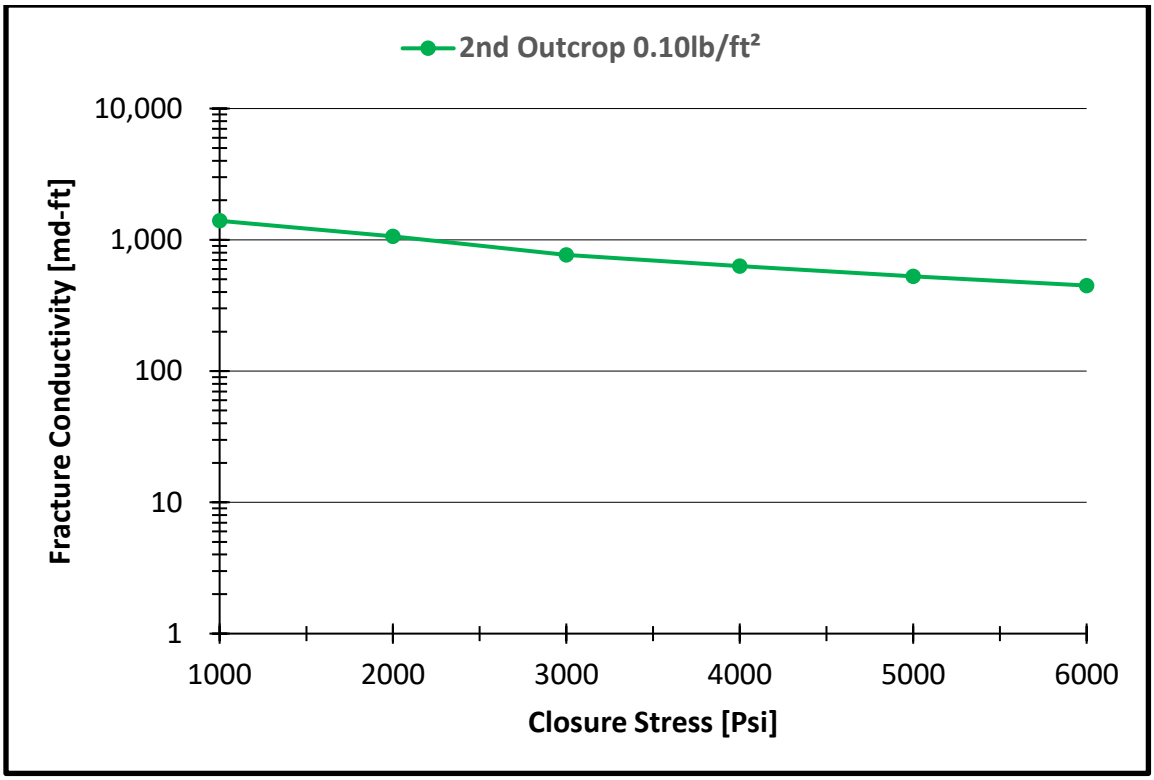

Figure 72. 11th experiment fracture conductivity of 2nd Outcrop 0.10lb/ft^2

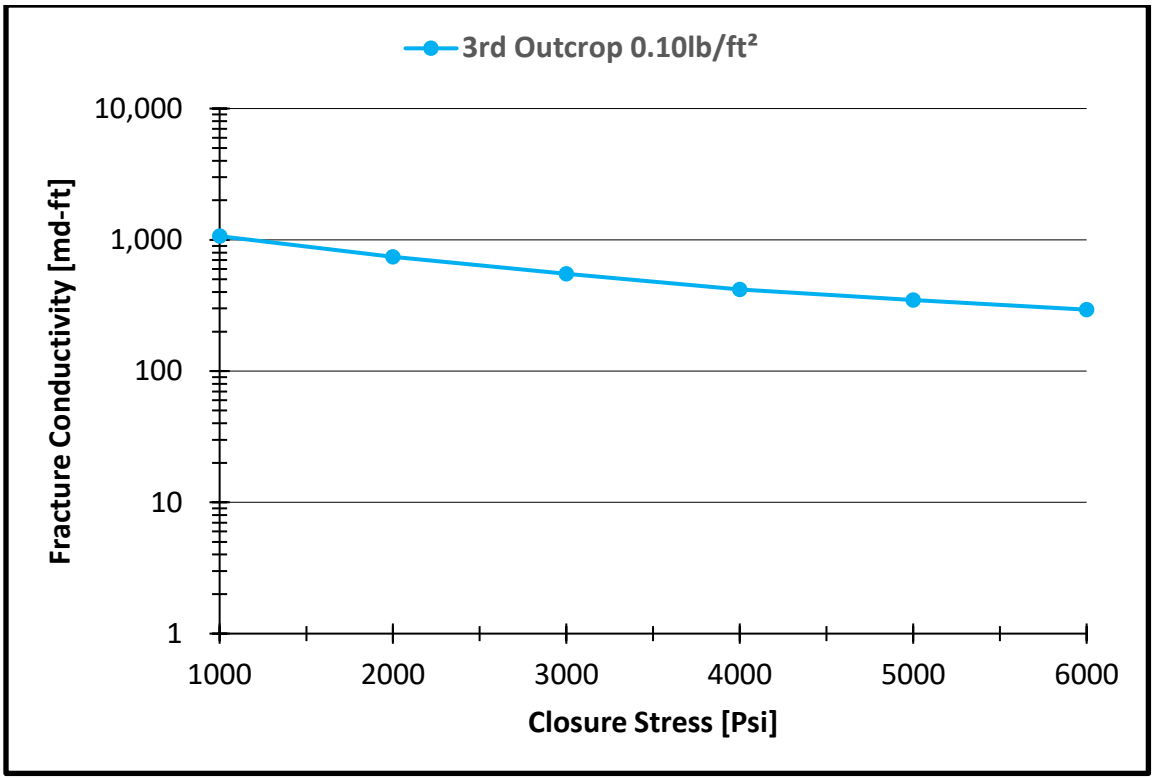

Figure 73. 12th experiment fracture conductivity of 3rd Outcrop 0.10lb/ft^2

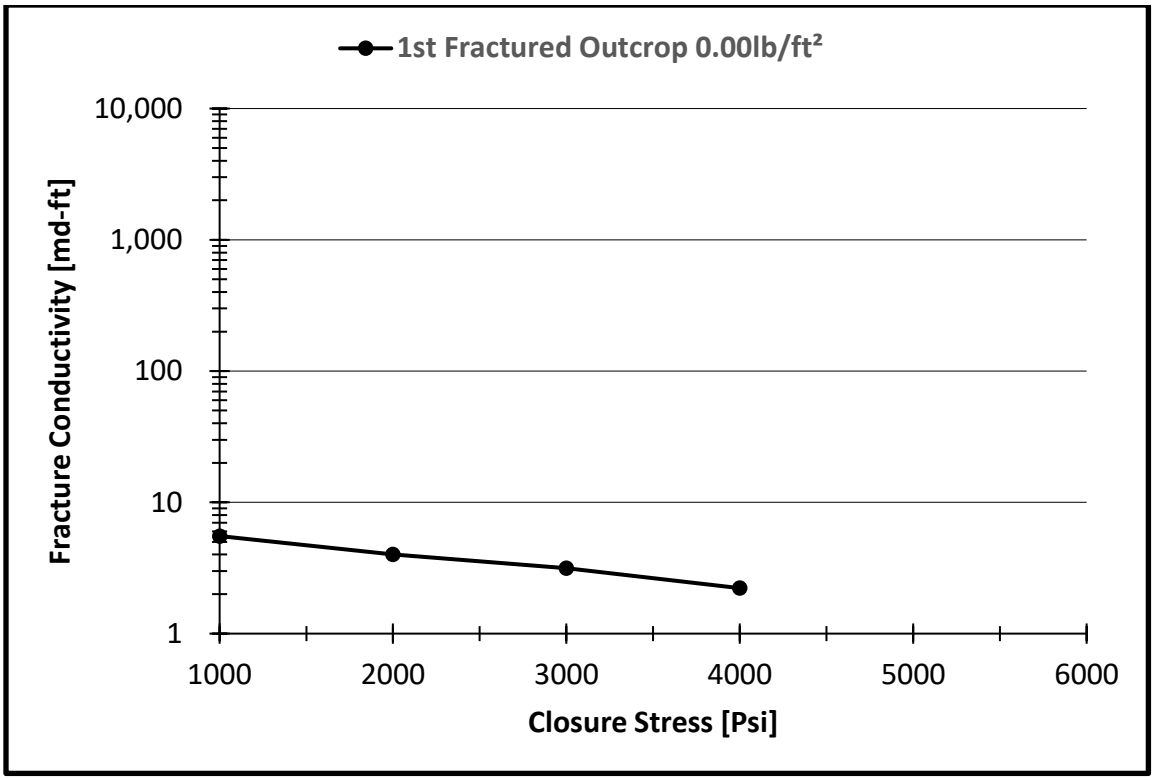

Figure 74. 13th experiment fracture conductivity of 1st Fractured Outcrop 0.00lb/ft^2

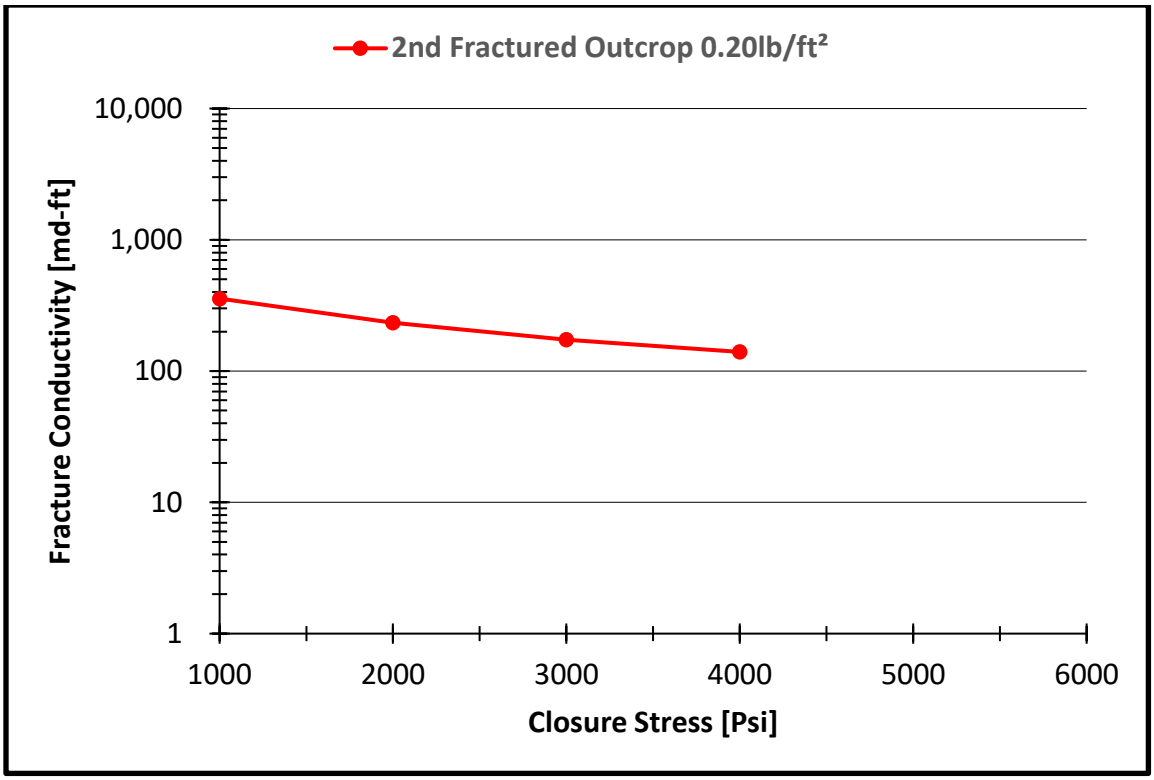

Figure 75. 14th experiment fracture conductivity of 2nd Fractured Outcrop 0.20lb/ft^2

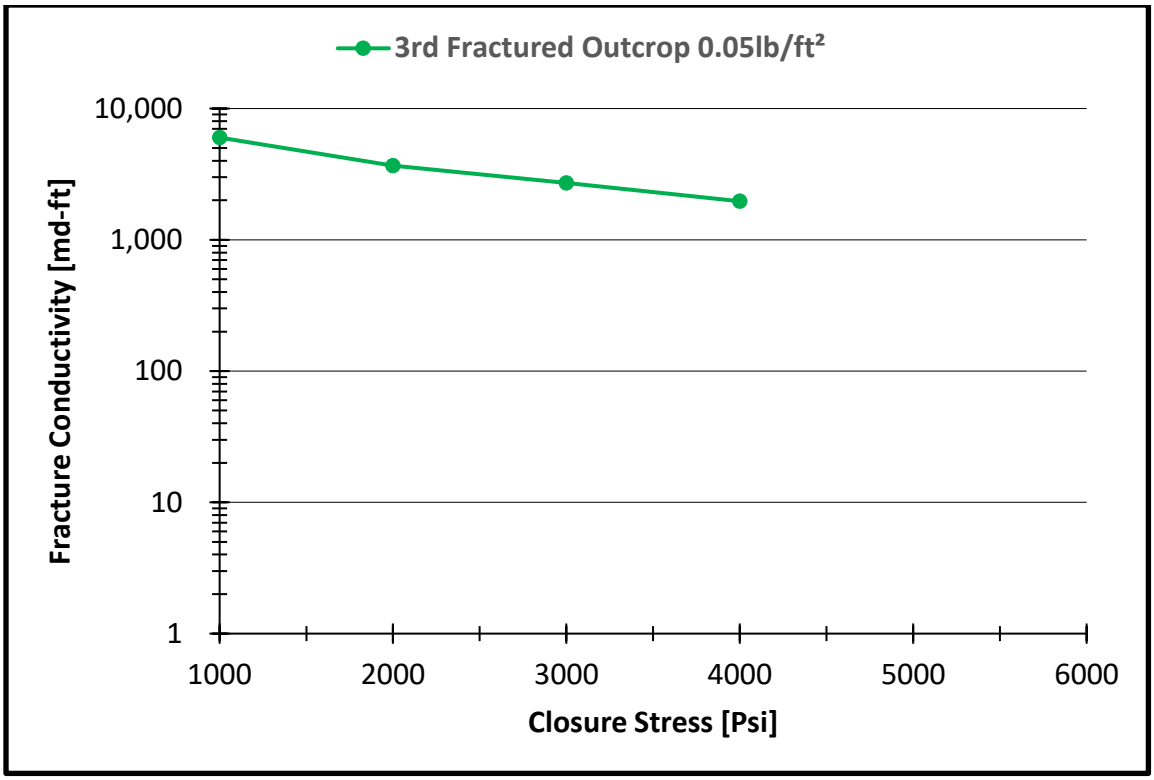

Figure 76. 14th experiment fracture conductivity of 3rd Fractured Outcrop 0.05lb/ft^2

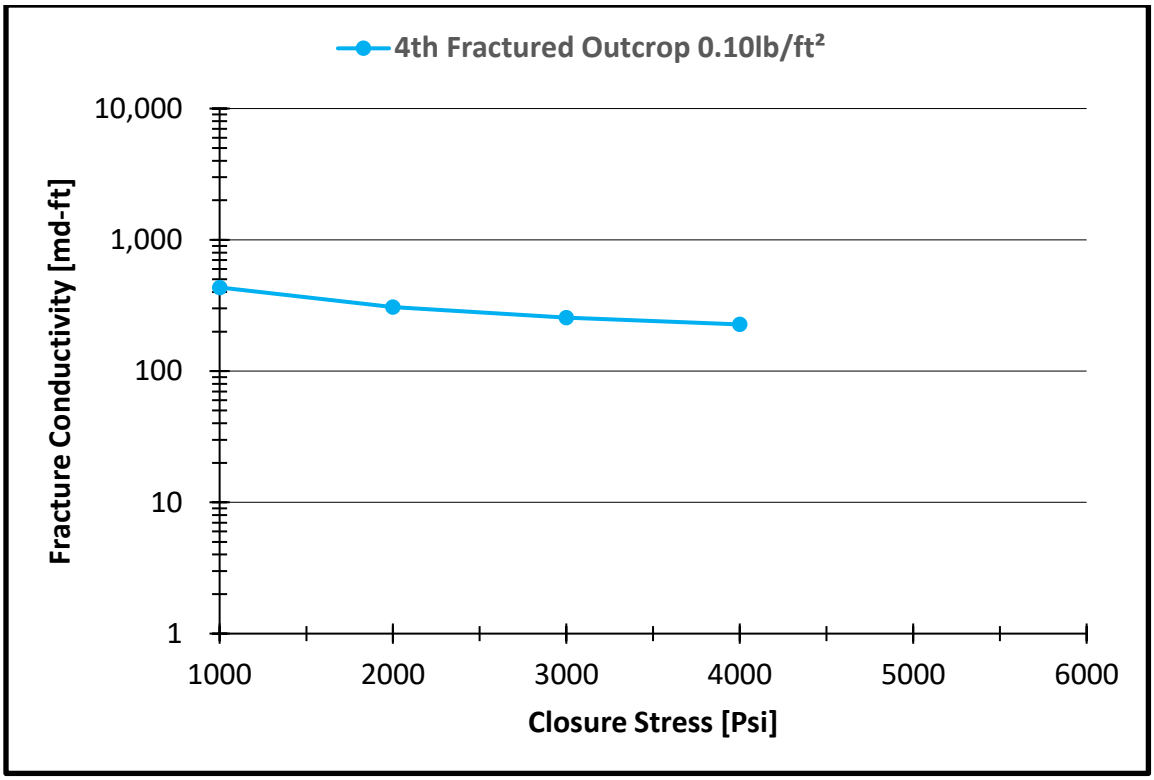

Figure 77. 16th experiment fracture conductivity of 4th Fractured Outcrop 0.10lb/ft^2

3.2. Comparison of Downhole Core with Outcrop Samples

As mentioned before, downhole core is limited in supply, but provides more accurate conductivity results to field conditions. Outcrop supplies are much easier to obtain with sufficient source. The question is if outcrop samples can be representative of downhole core. In this study, we tested downhole core against outcrop samples to validate that outcrop samples can be used for conductivity study. The comparison is done with sawcut samples at the same testing condition. The sawcut Austin Chalk outcrop samples' fracture conductivity responses were averaged together by proppant concentration and are displayed below in Figure 78. The average conductivity response with error bars is shown in Figure 79. The error bars were developed by first finding the average of the three sawcut outcrop fracture conductivity responses, then finding the standard deviation. Next, the standard deviation was divided by the square root of the number of samples. This yielded the standard error at each closure stress for each proppant concentration. The fracture conductivity response is the highest for the proppant concentration of 0.05lbs/ft^2, followed closely by 0.10lbs/ft^2. Notice this lasts until a closure stress of about 4,000 psi when the fracture conductivity for those proppant concentrations become nearly identical. The proppant loading of 0.20lbs/ft^2 starts off lower and stays lower at all closure stresses, but does have a flatter decline. Higher fracture conductivity at lower proppant concentrations is attributed to a partial mono-layer of proppant.

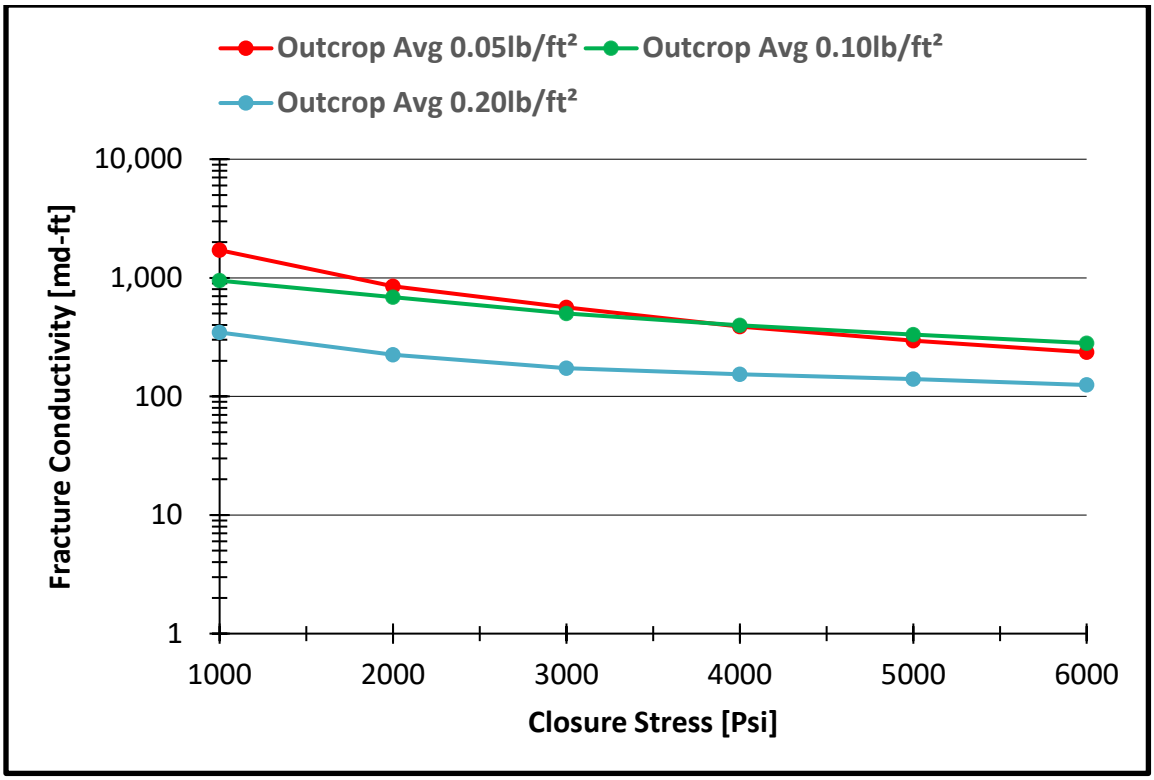

Figure 78. Outcrop fracture conductivity response averaged by proppant concentration.

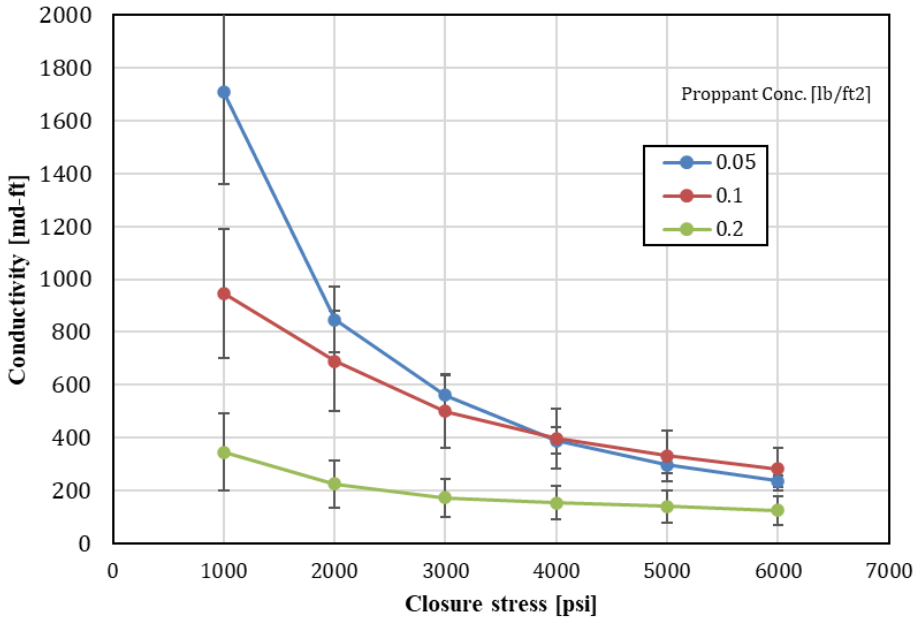

Figure 79. Average fracture conductivity response for each proppant concentration.

Only three downhole core tests were conducted, two tests at a proppant concentration of 0.20lbs/ft^2, and one at 0.10lbs/ft^2. The results are shown in Figure 81. The averaged outcrop conductivity and the conductivity for downhole core are all plotted on Figure 81. The same trend holds true that higher fracture conductivity values occur at lower proppant concentrations. However, the downhole core values are consistently higher than the averaged outcrop values. This might be due to some of the downhole core samples themselves breaking away during experimentation, and the debris is trapped in the conductivity cell leading to artificially high fracture conductivity values. Figure 47 shows such an example. Notice that the sample base for downhole core tests is small (only three tests), and this conclusion may not be general.

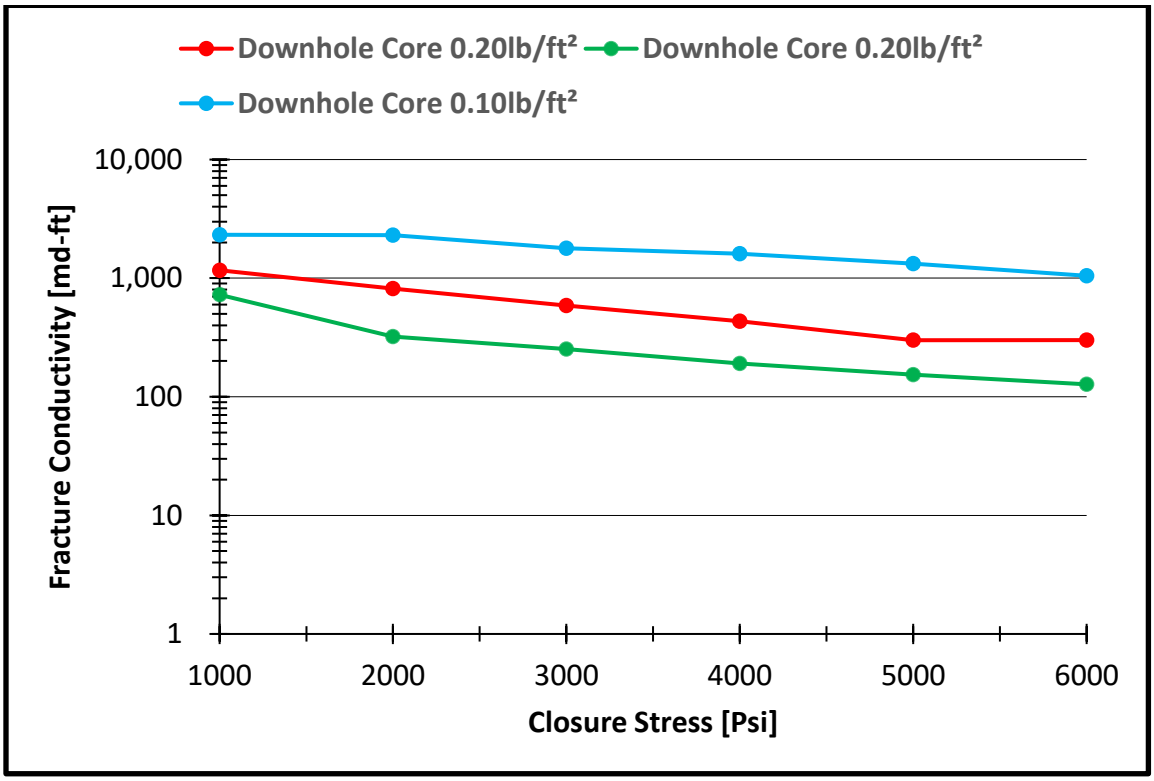

Figure 80. Downhole core fracture conductivity response.

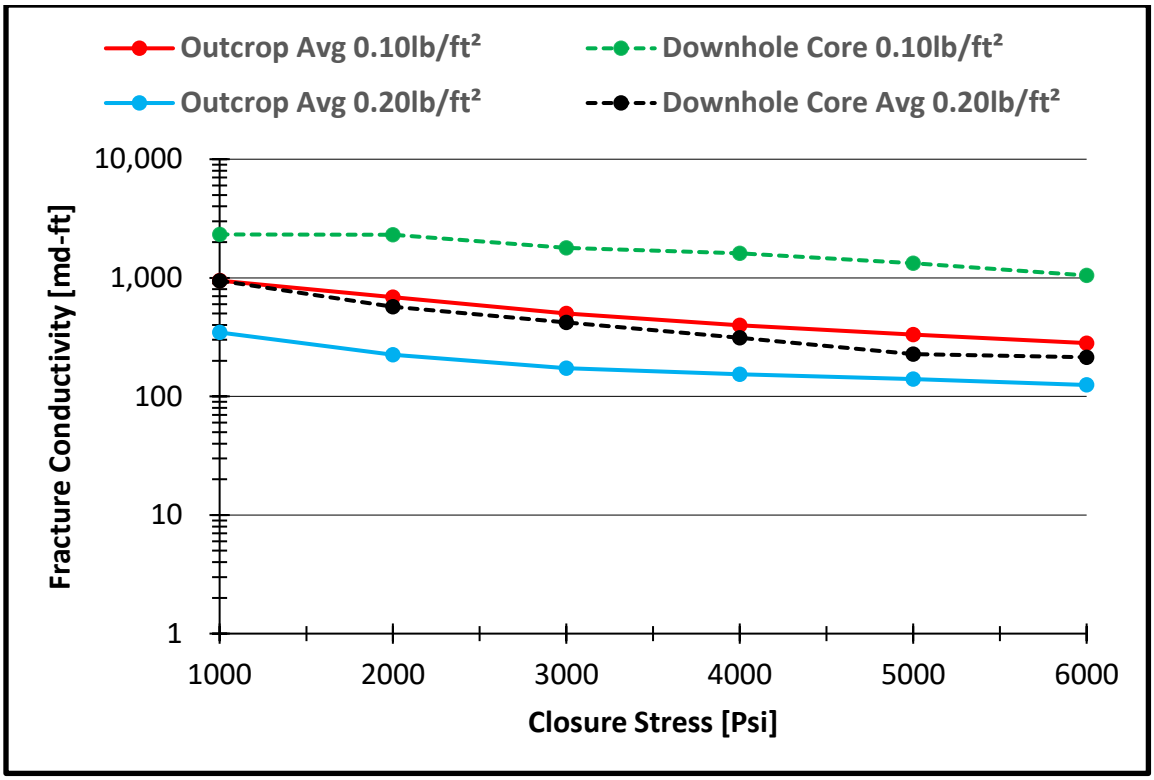

Figure 81. Outcrop and downhole core fracture conductivity response averaged by proppant concentration.

3.3. Fractured Austin Chalk Outcrop and Comparison with Sawcut Samples

The Fractured Austin Chalk outcrop experiments were only conducted from 1000 to 4000 psi, in 1000 psi increments, in an attempt to preserve the sample. Only one fractured sample was available for testing and great care was used to maintain the sample to last for all four experiments. Figure 82 shows the conductivity results for these four tests. The fracture conductivity response is the highest for the proppant concentration of 0.05lbs/ft^2, followed by 0.10lbs/ft^2, and the lowest is 0.20lbs/ft^2. Notice that all conductivity curves are nearly parallel, indicating a similar decline rate. An unpropped condition was tested and served as a baseline for propped fracture conductivity. The result indicates that having a propped fracture greatly benefits the fracture conductivity. Figure 83 compared conductivity of the outcrop fractured sample with

the averaged sawcut outcrop test results at a proppant concentration of 0.20lb/ft^2. The results overlay each other. However, Figure 84 and Figure 85 show the data for 0.10lb/ft^2 and 0.05lb/ft^2 concentration. The results are in less agreement. Notice again, the fractured results are only from one set of tests because of the limited source of one fractured sample, and the results may not be completely representative. For 0.10lb/ft^2 concentration, with the sawcut outcrop sample conductivity is higher than the one fractured sample, but for 0.05lb/ft^2, the observation is the opposite, where the fractured sample has higher conductivity. More tests are needed to draw a conclusion.

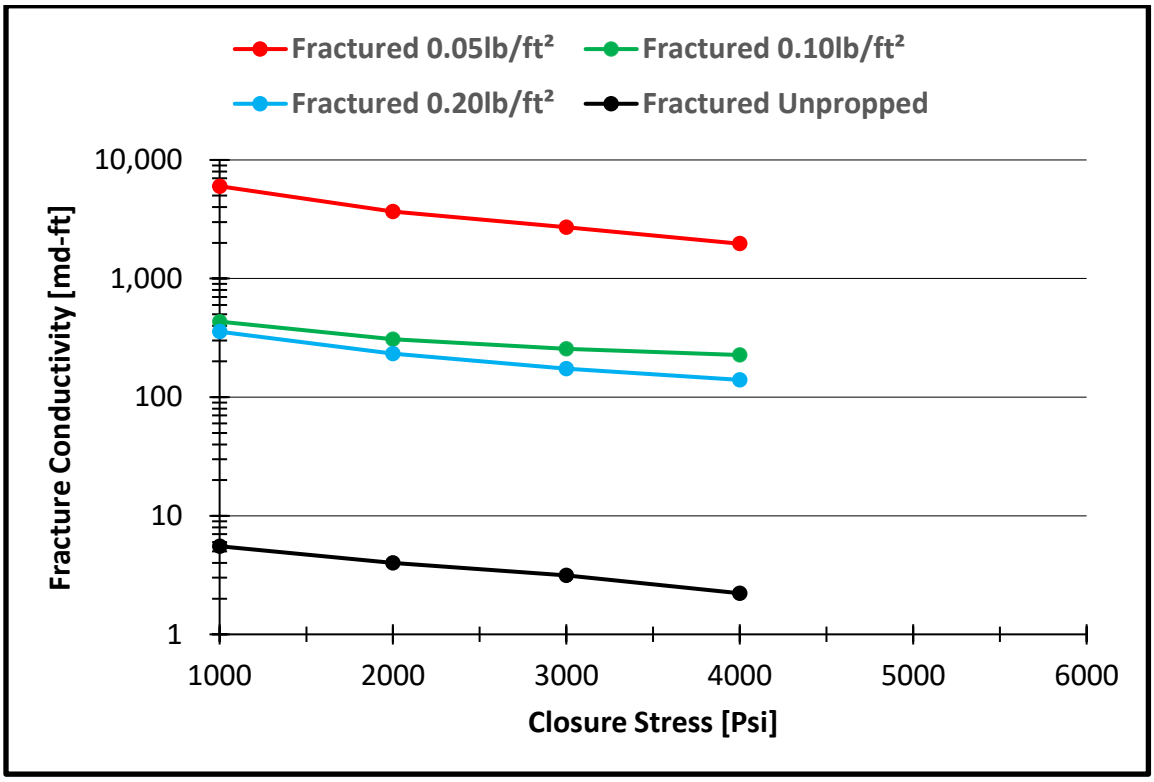

Figure 82. Fracture conductivity values of all fractured samples.

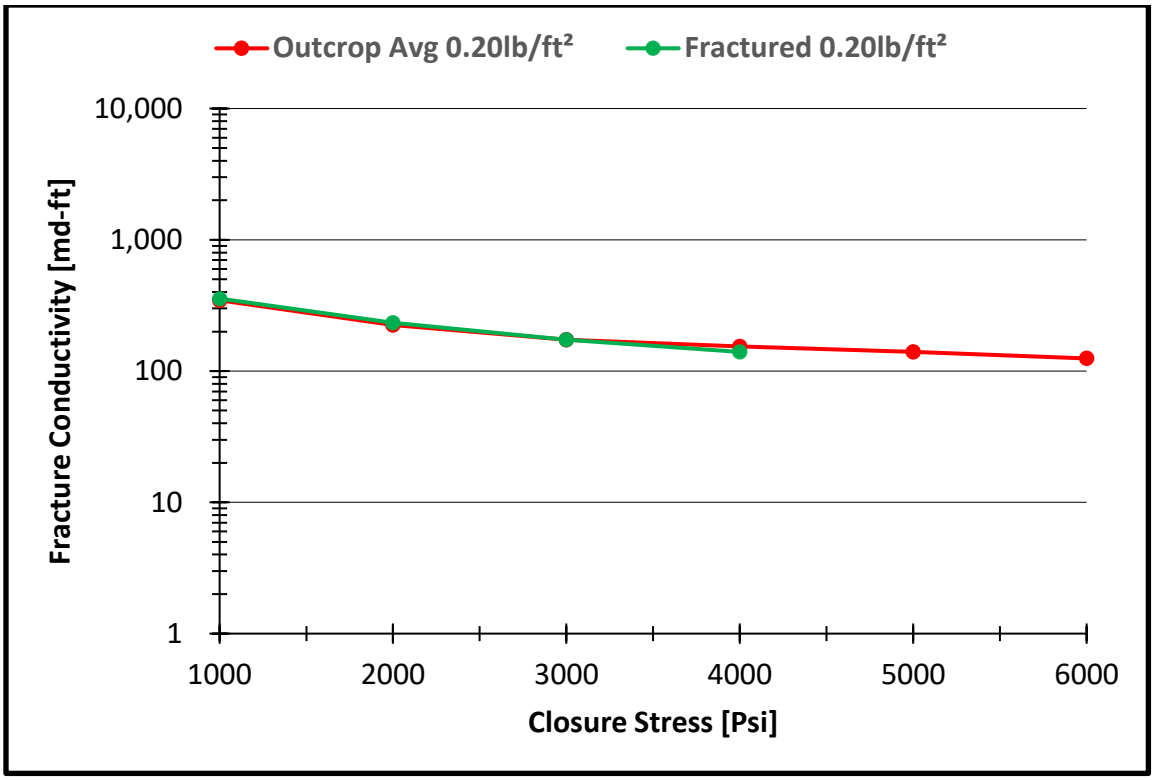

Figure 83. Fracture conductivity of outcrop average 0.20lbs/ft^2 and fractured 0.20lbs/ft^2.

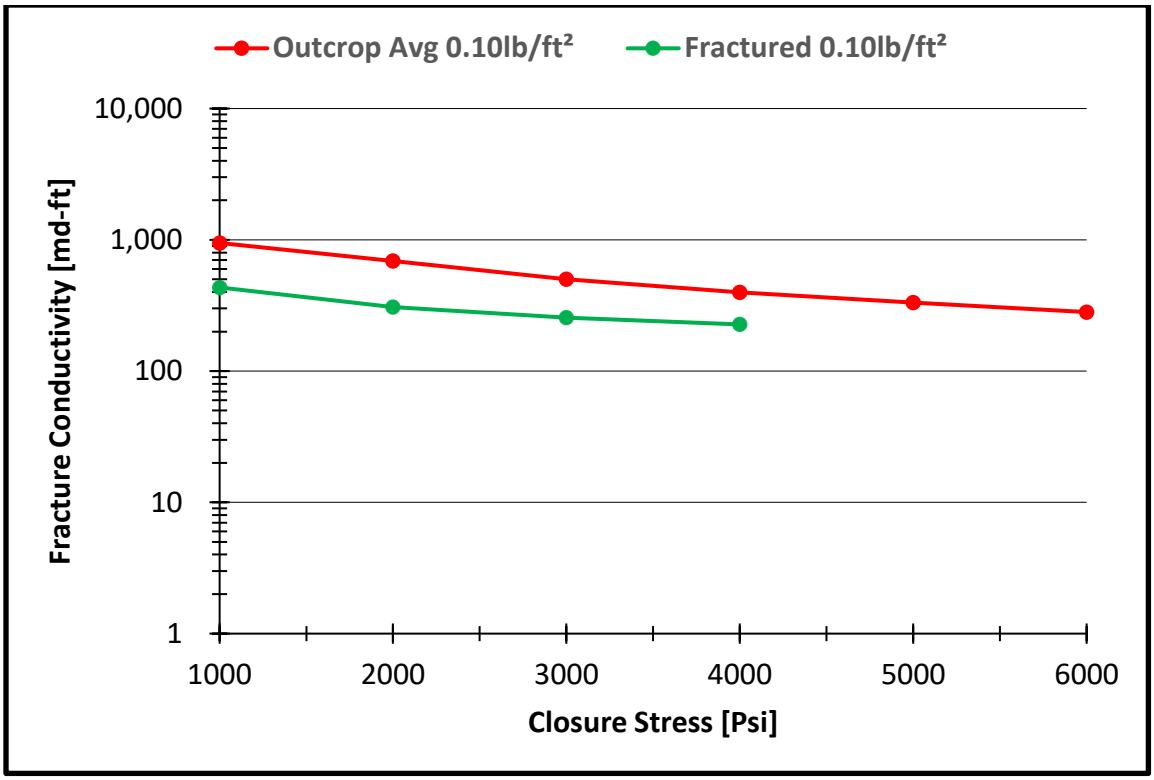

Figure 84. Fracture conductivity of outcrop average 0.10lbs/ft^2 and fractured 0.10lbs/ft^2.

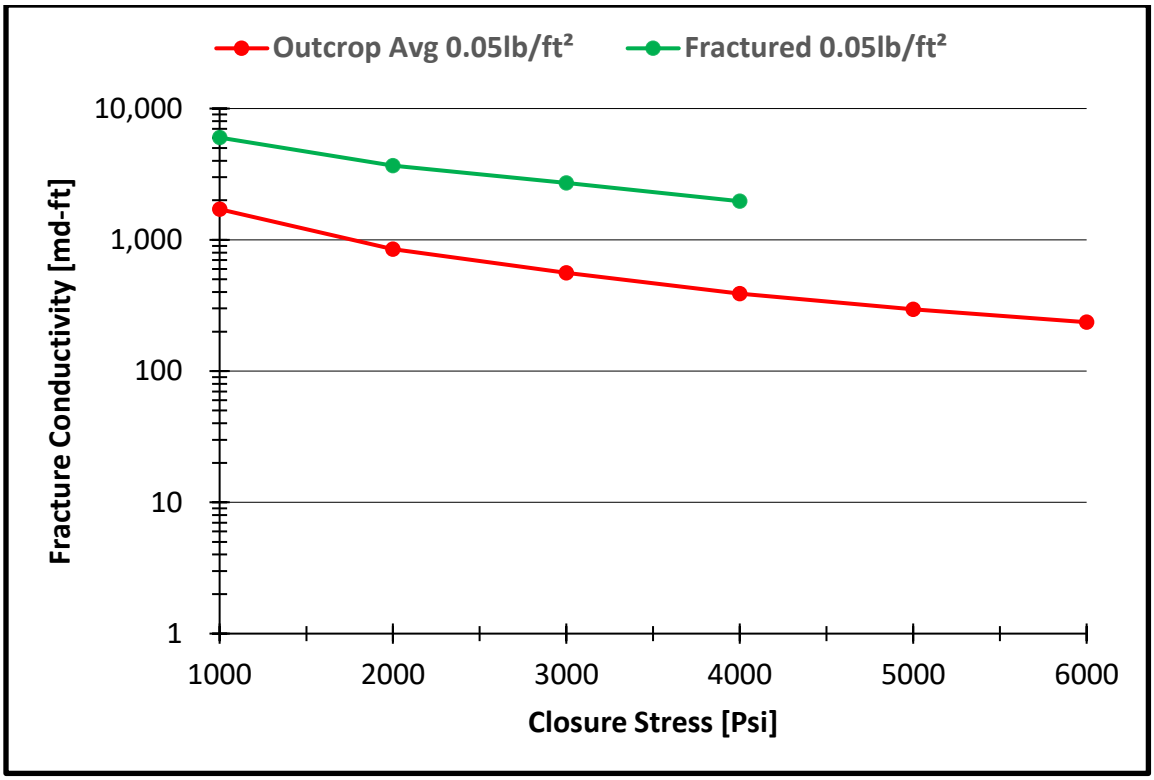

Figure 85. Fracture conductivity of outcrop average 0.05lbs/ft^2 and fractured 0.05lbs/ft^2.

3.4. Proppant Concentration

Proppant concentration is one of the more influential parameters on fracture conductivity, and also, important to fracture treatment design. For various test conditions (sawcut versus fractured, downhole core versus outcrop, etc.), we tested the fracture conductivity at three different concentrations, 0.05lb/ft^2 0.10lb/ft^2, and 0.20lb/ft^2. Figure 86 displays all the fracture conductivity values for all 16 experiments, only filtered by the proppant concentration. Data is only displayed from 1,000 to 4,000 psi to prevent inflections in the plot since all sixteen tests have data from 1,000 to 4,000 psi. Congruent in all previous subsections, the lower the proppant concentration the higher the fracture conductivity response we observed, excluding the unpropped condition. The unpropped condition yields fracture conductivity values two orders of

magnitude lower than the worst propped case. The observations of this study indicate that increasing proppant concentration does not necessarily benefit fracture conductivity. At the lowest concentration tested (0.05lb/ft^2) partial mono-layer proppant distribution occurred, resulting in higher conductivity. This observation can help optimize fracture design with better conductivity and less cost of the fracture treatment. Figure 87 shows the fracture conductivity response for all the experiments.

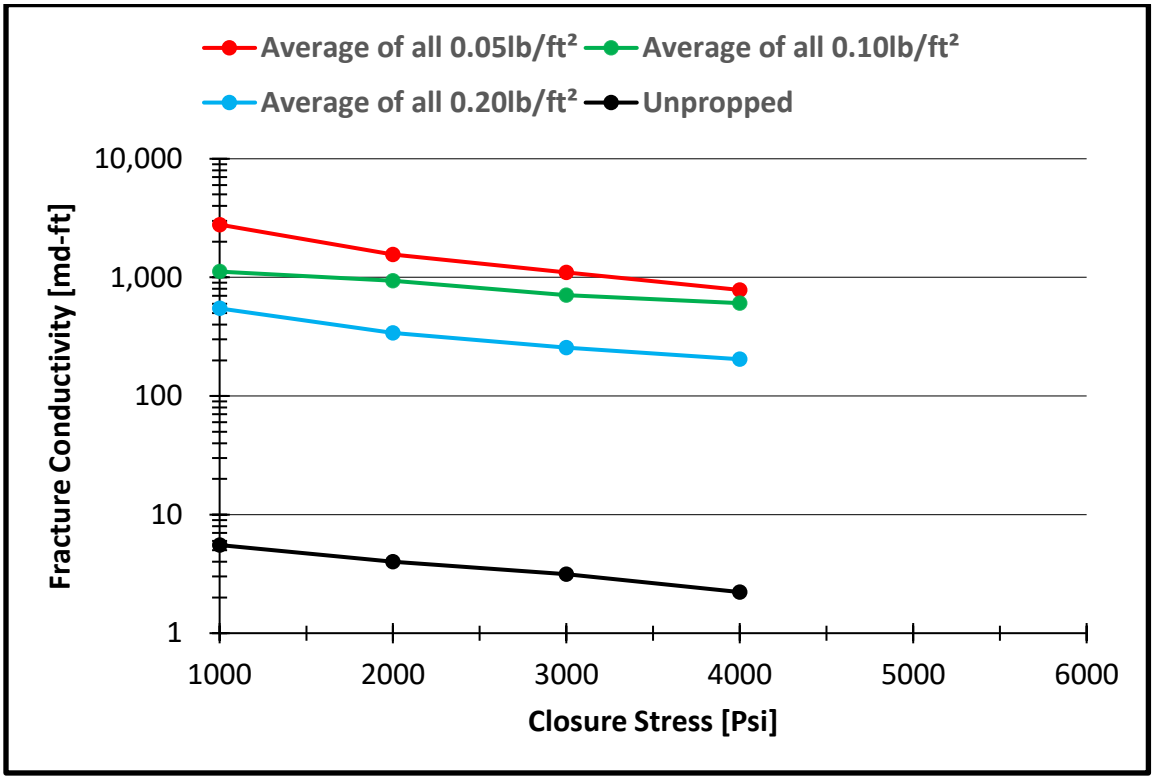

Figure 86. Fracture conductivity of all samples only filtered by proppant concentration.

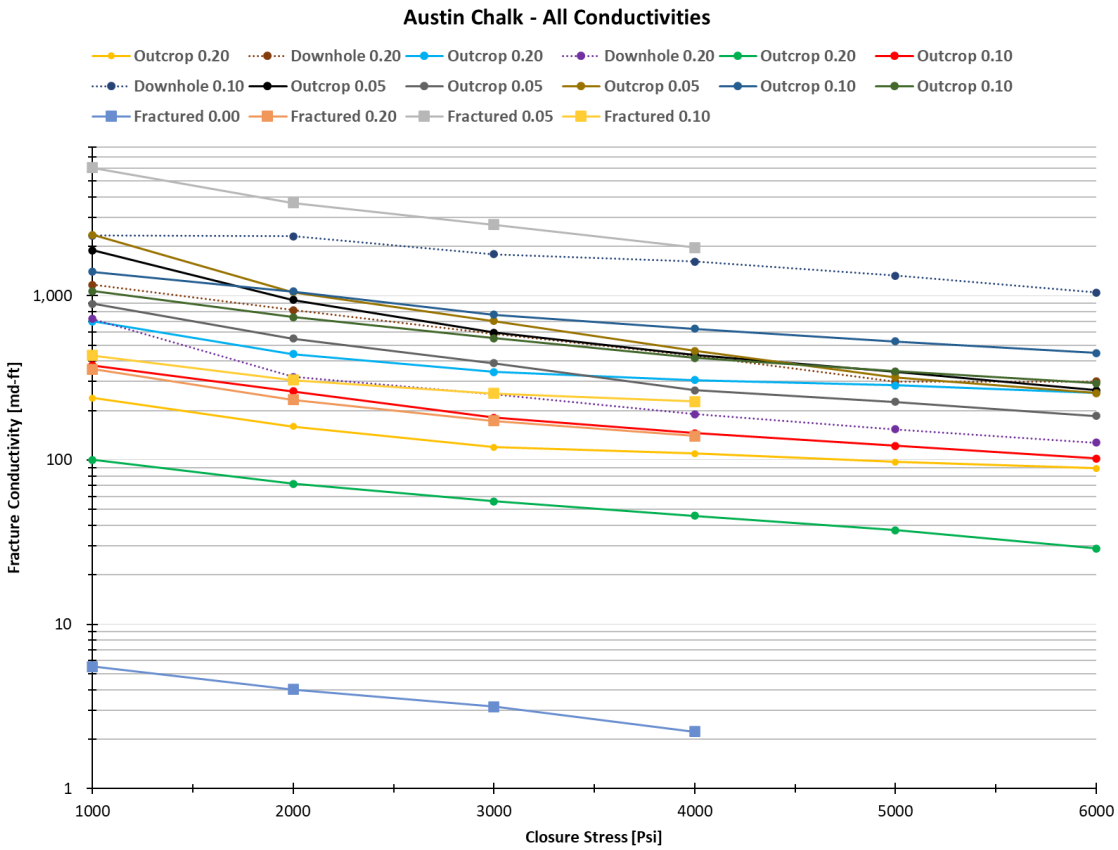

Figure 87. Fracture conductivity of all samples.

3.5. Proppant Sieve Analysis for Proppant Crushing

Proppant sieve analyses were performed to quantify the extent of proppant crushing encountered. Figure 88 through Figure 108 display the proppant sieve analyses performed for this study. The numerical data for all 21 proppant sieve analyses data can be found in Appendix A. The 40-mesh size is the largest and retains the largest size proppant particles. The 140-mesh size is the smallest and retains the smallest size proppant particles. All proppant particles smaller than a 140-mesh fall into the pan. Proppant crushing can be identified by a decrease in percent mass from the larger size meshes and an increase in the smaller size meshes. This is seen in the plots as taller blue bars on the left side of the plots and taller orange bars on the right side, paying

particular attention to the percent of mass that lands in the pan. When quality checking the proppant sieve data, it appears that an old previously provided 100 mesh proppant was used for the first 3 experiments which yielded impossible data compared to the pre-experiment baseline. Only the sieve analysis conducted on the SM Energy sourced proppant will be included for analysis. Table 4 displays the size of each mesh size used in this study.

Table 4. Sieve opening size for U.S. standard mesh sizes used in this study.

	Sieve Opening	
U.S. Standard Mesh Size	Inches	millimeters
40	0.0165	0.420
50	0.0117	0.297
70	0.0083	0.210
80	0.0070	0.177
100	0.0059	0.149
120	0.0049	0.124
140	0.0041	0.104
Pan	<0.0041	<0.104

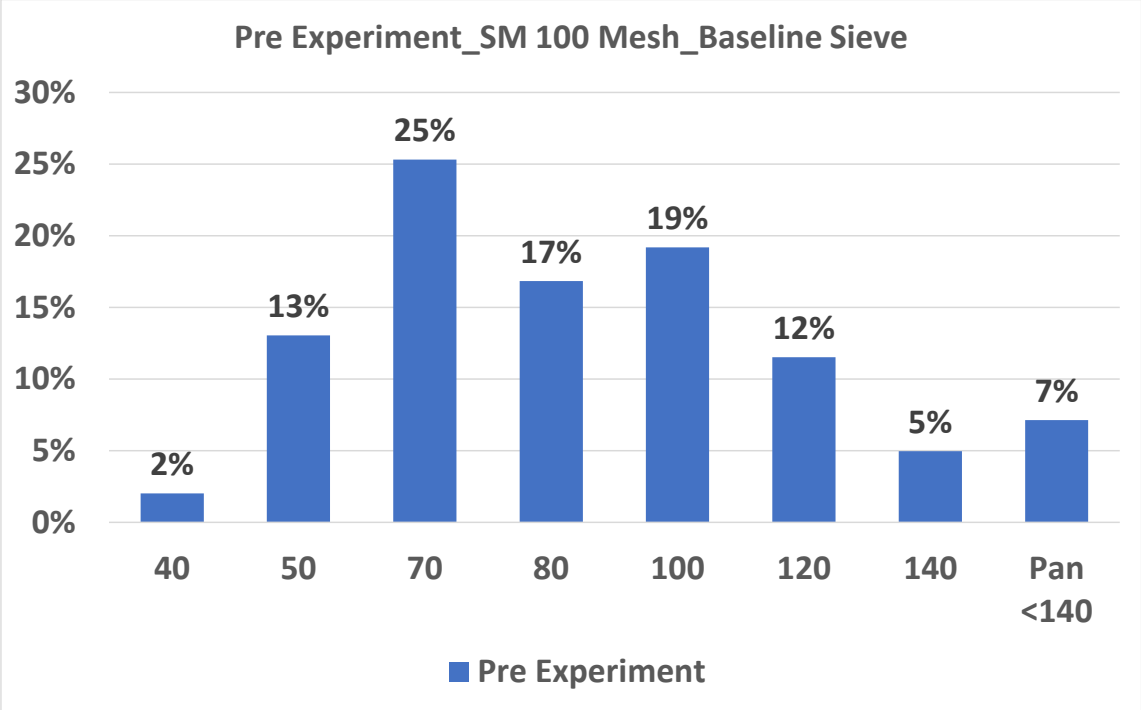

Figure 88. Sieve analysis for pre-experiment SM 100 mesh baseline.

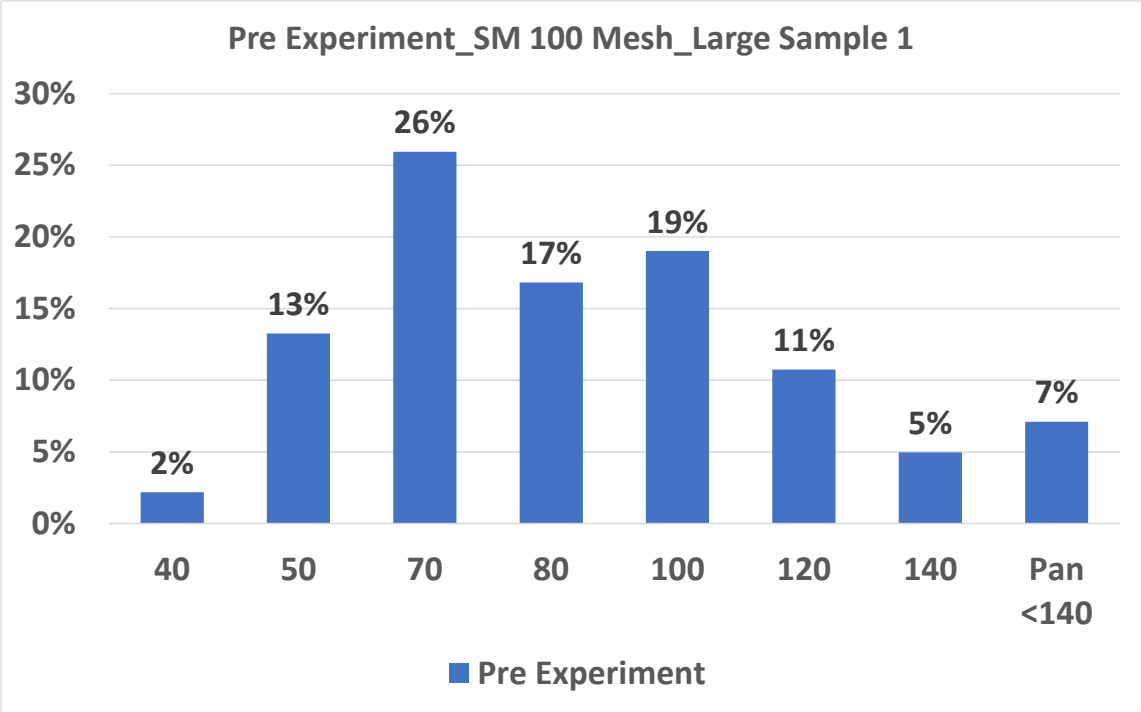

Figure 89. Sieve analysis for pre-experiment SM 100 mesh large sample 1.

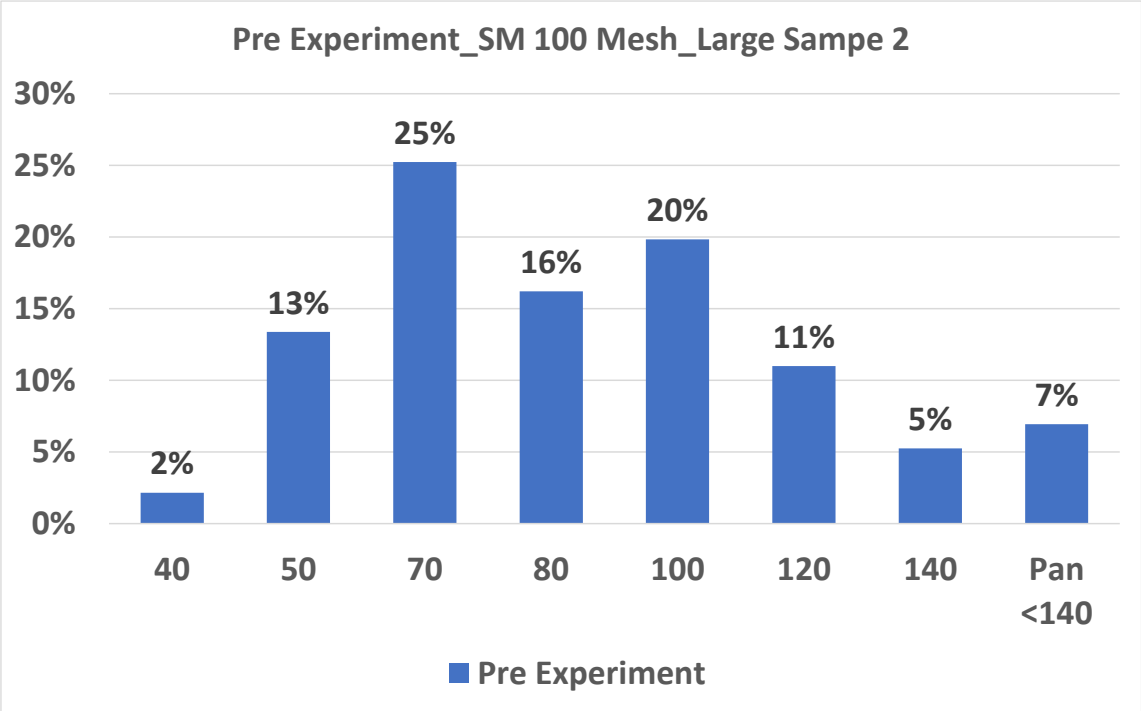

Figure 90. Sieve analysis for pre-experiment SM 100 mesh large sample 2.

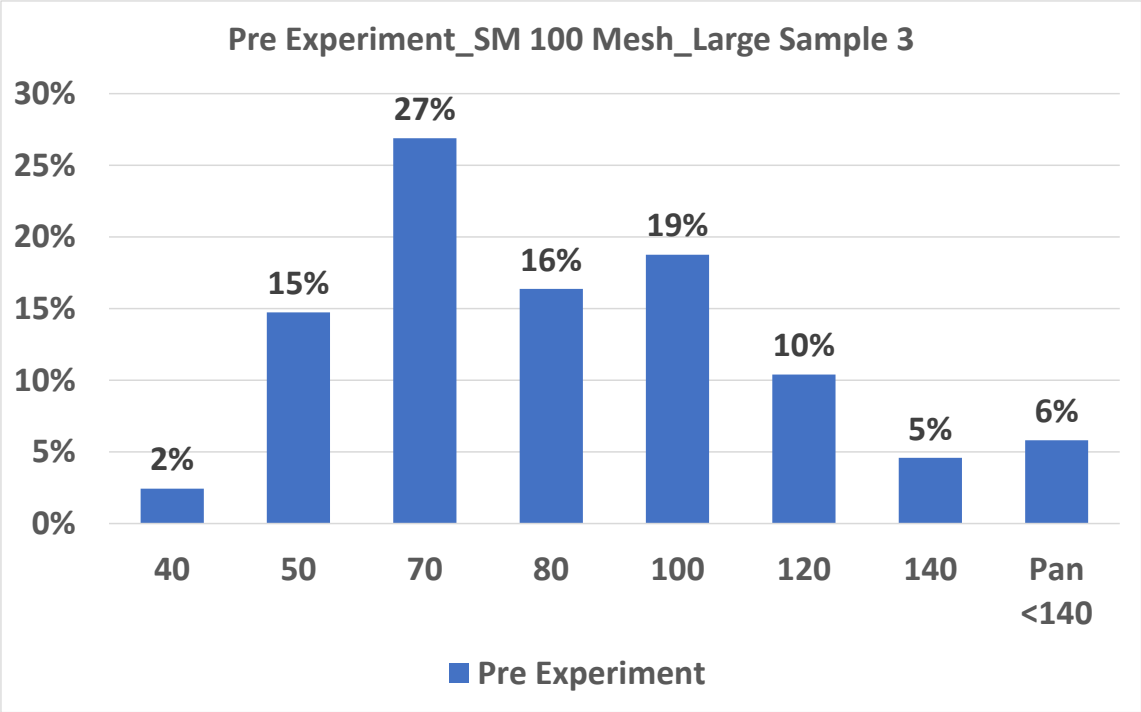

Figure 91. Sieve analysis for pre-experiment SM 100 mesh large sample 3.

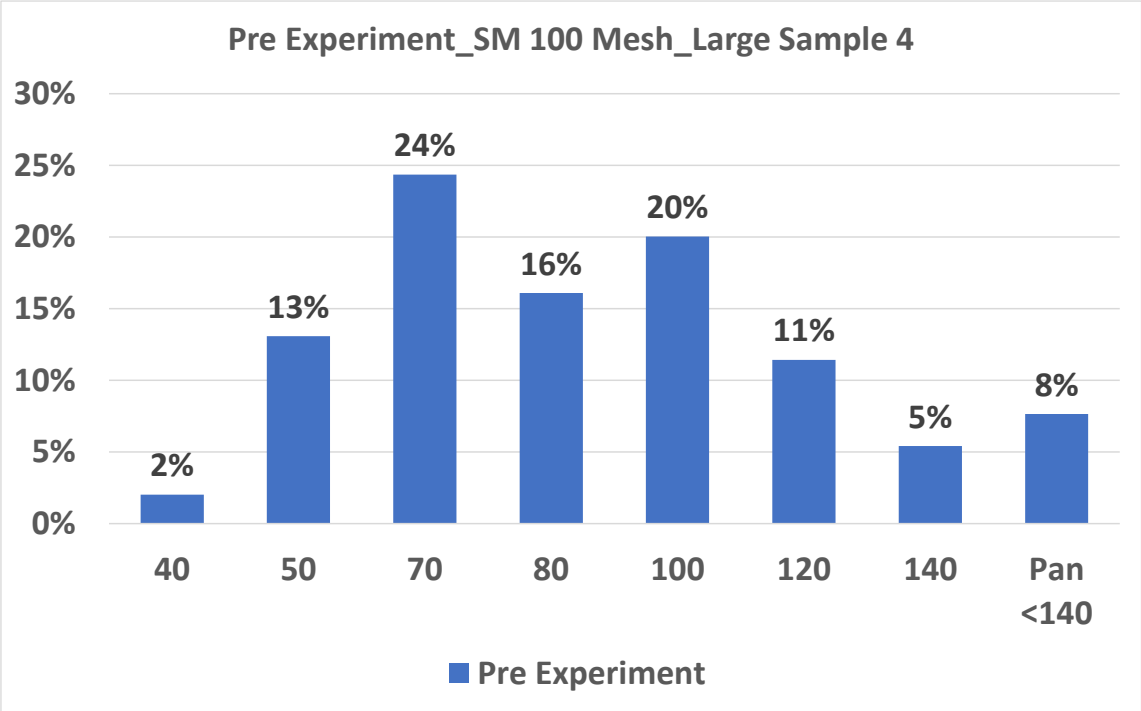

Figure 92. Sieve analysis for pre-experiment SM 100 mesh large sample 4.

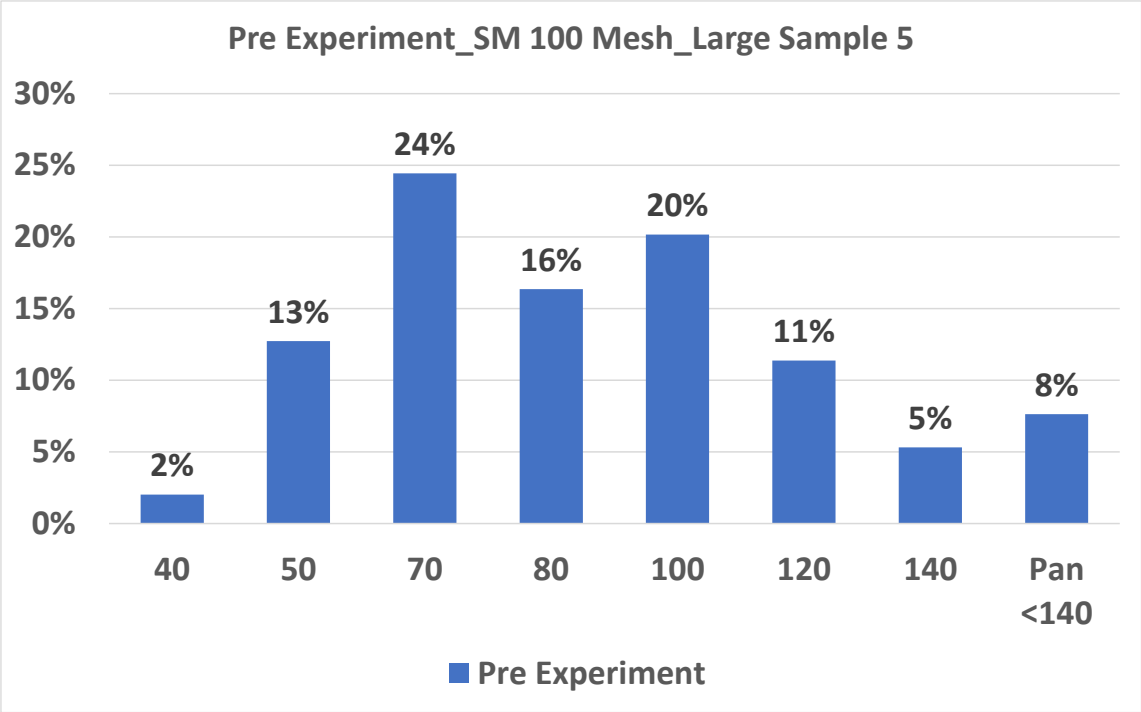

Figure 93. Sieve analysis for pre-experiment SM 100 mesh large sample 5.

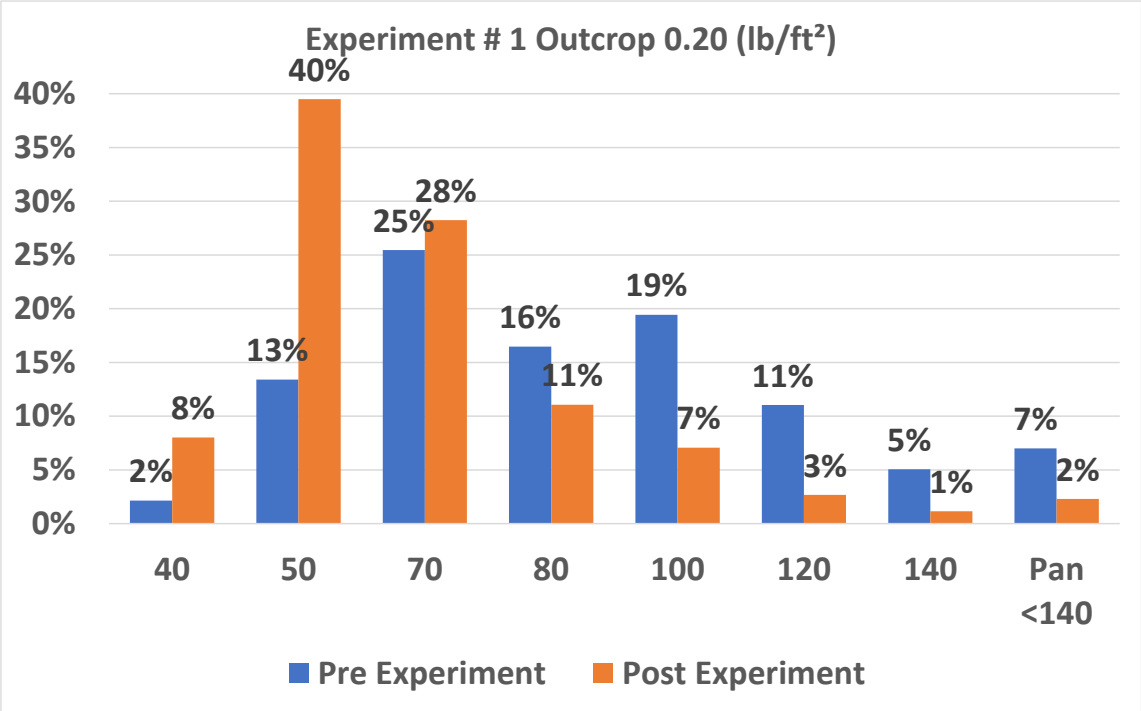

Figure 94. Sieve analysis for experiment 1.

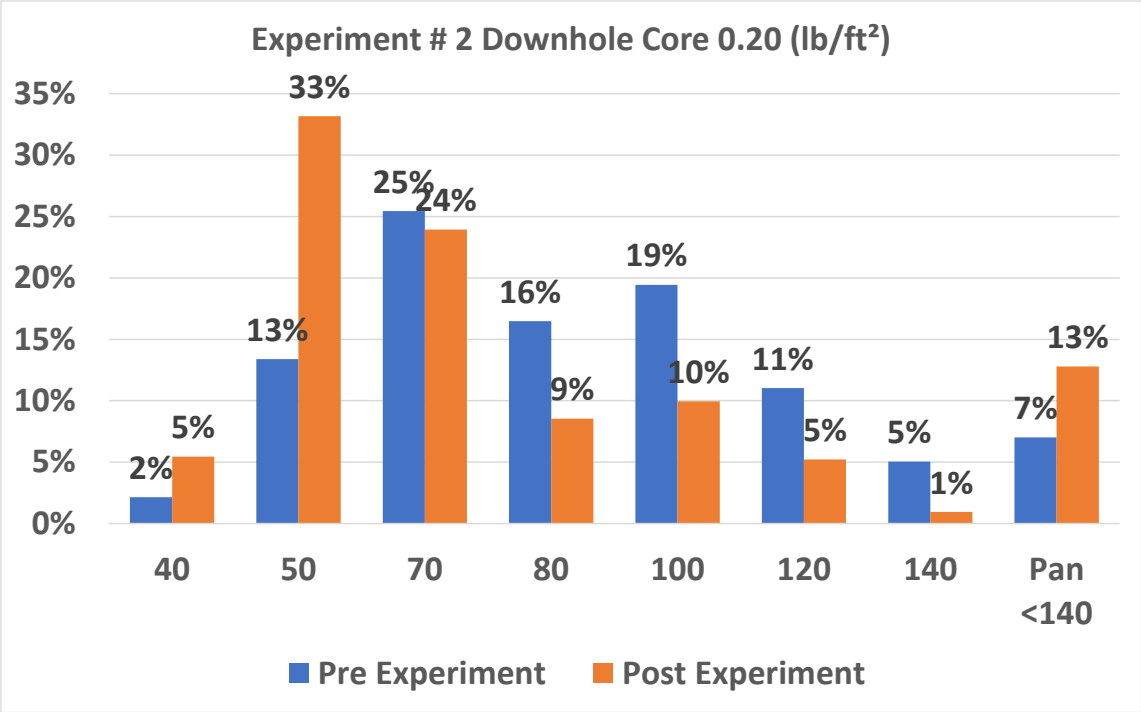

Figure 95. Sieve analysis for experiment 2.

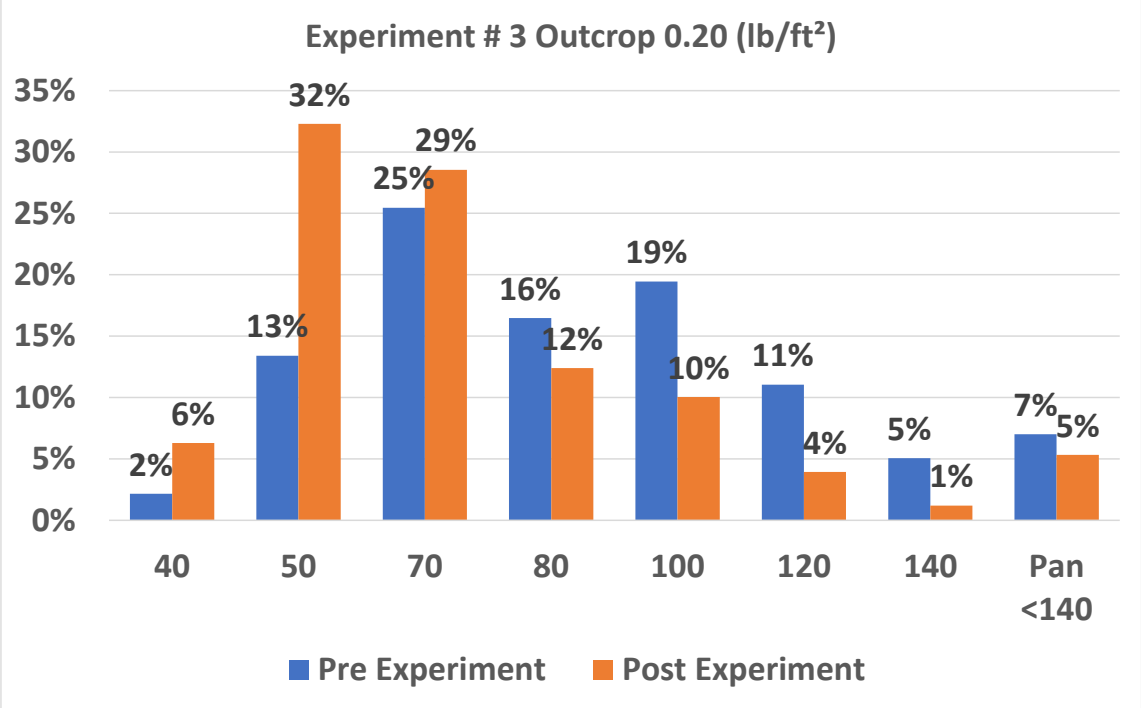

Figure 96. Sieve analysis for experiment 3.

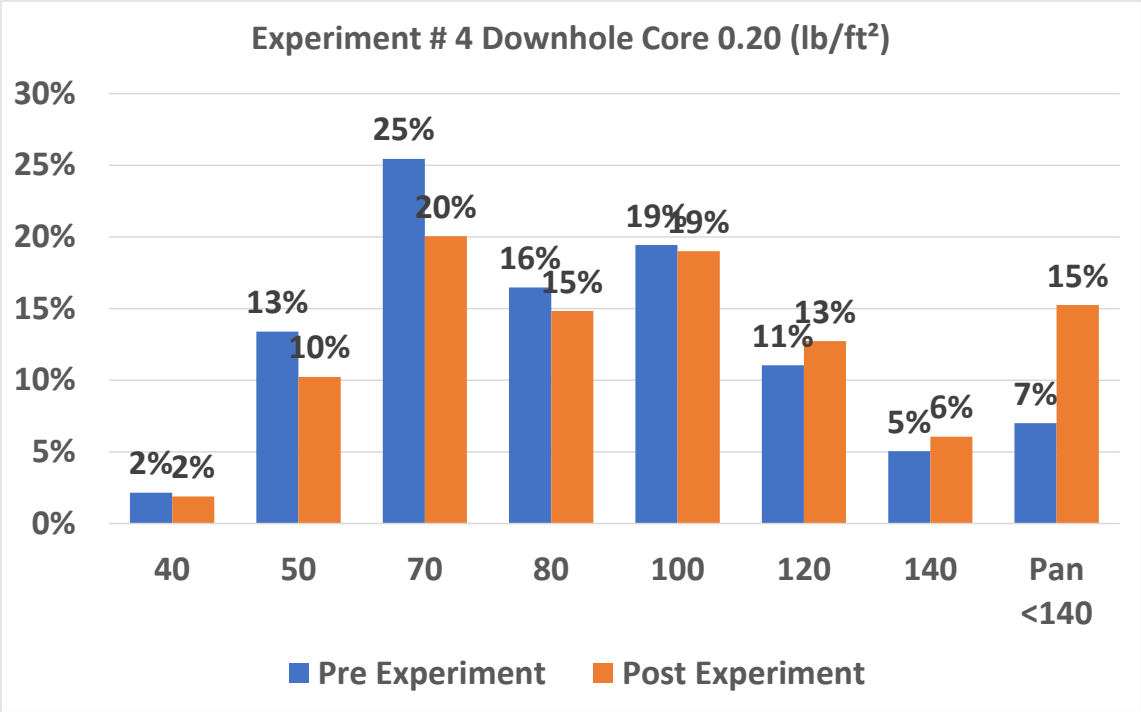

Figure 97. Sieve analysis for experiment 4.

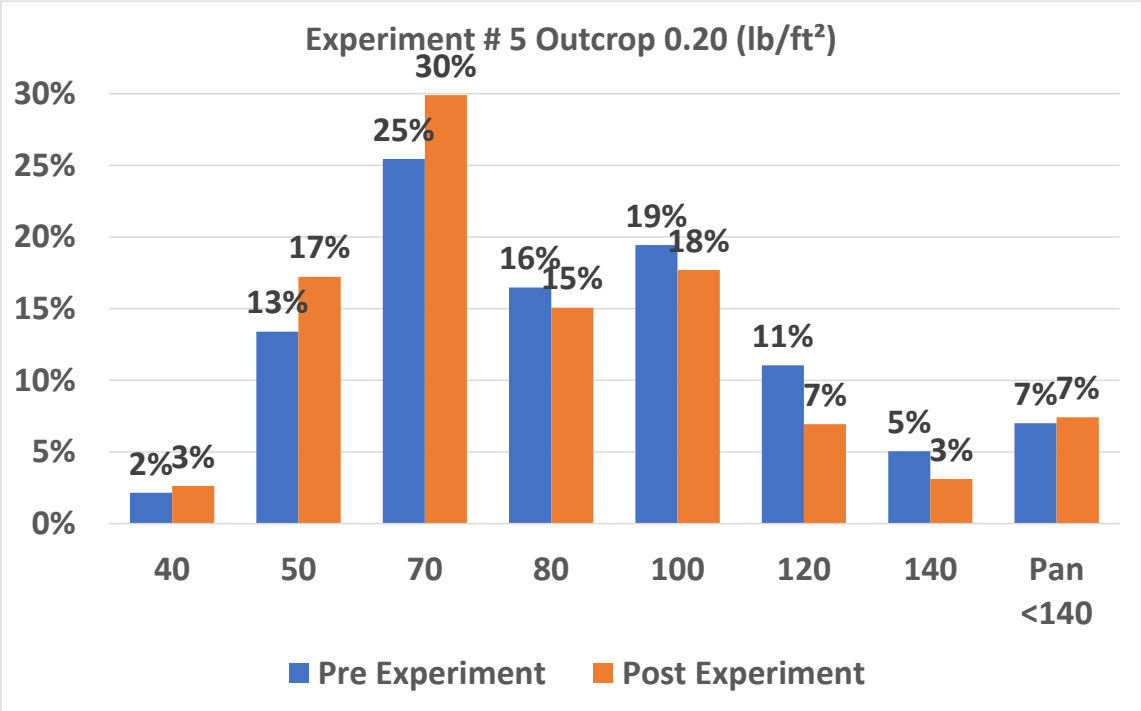

Figure 98. Sieve analysis for experiment 5.

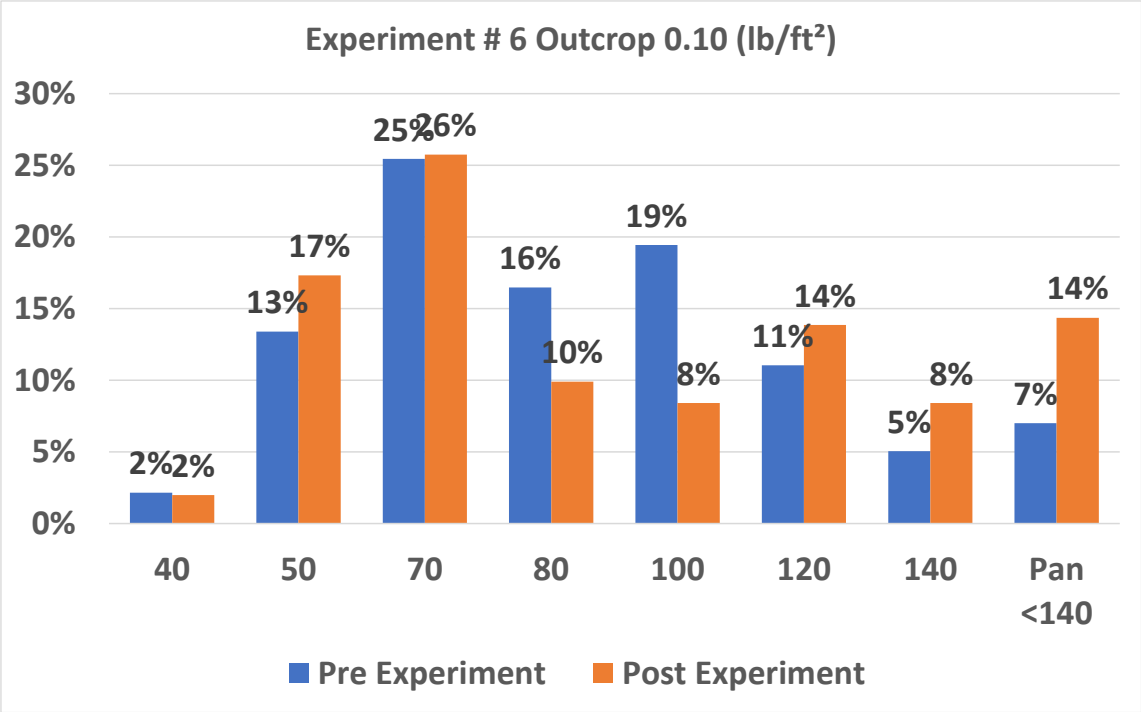

Figure 99. Sieve analysis for experiment 6.

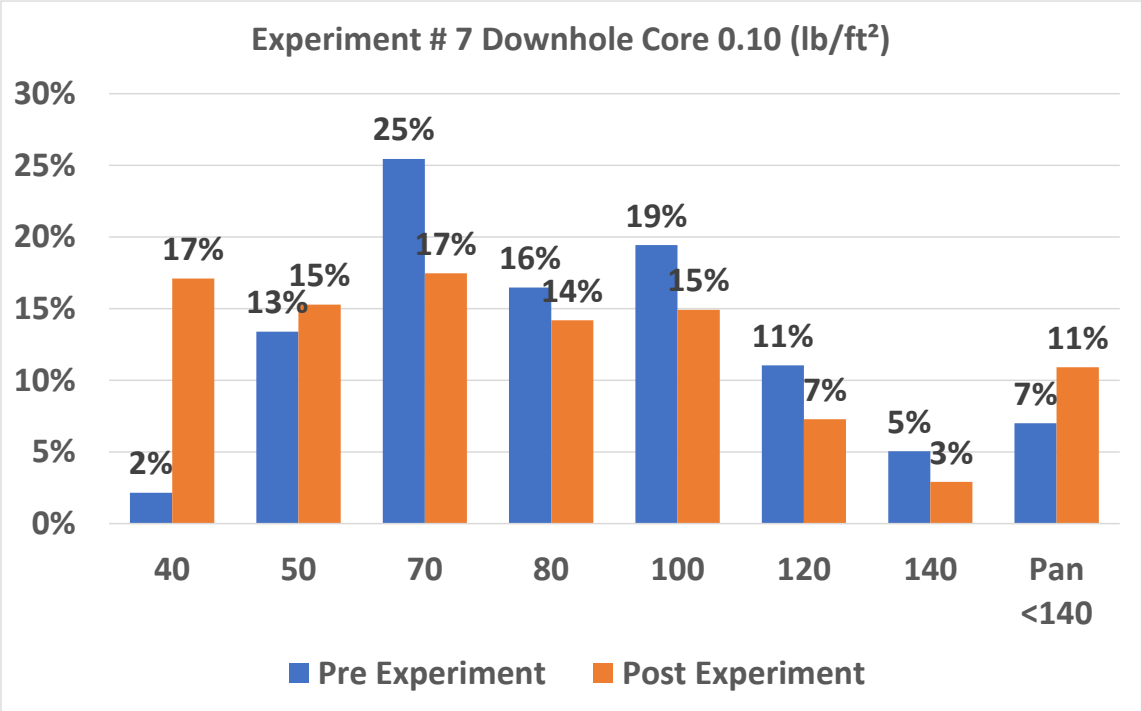

Figure 100. Sieve analysis for experiment 7.

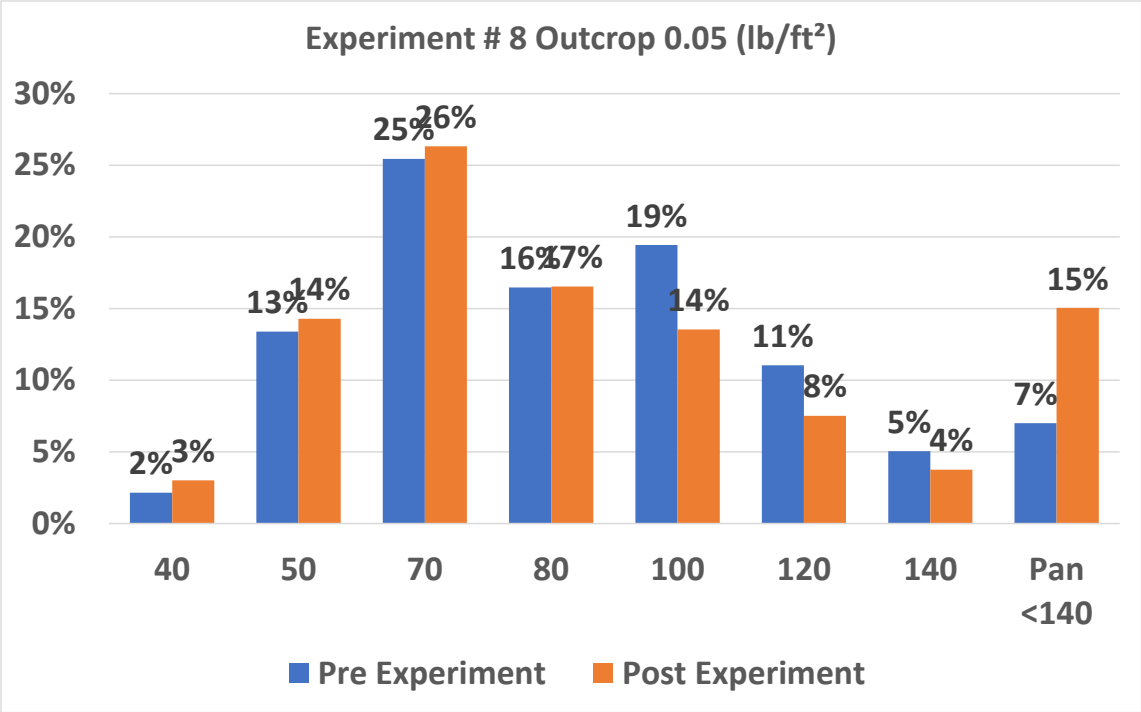

Figure 101. Sieve analysis for experiment 8.

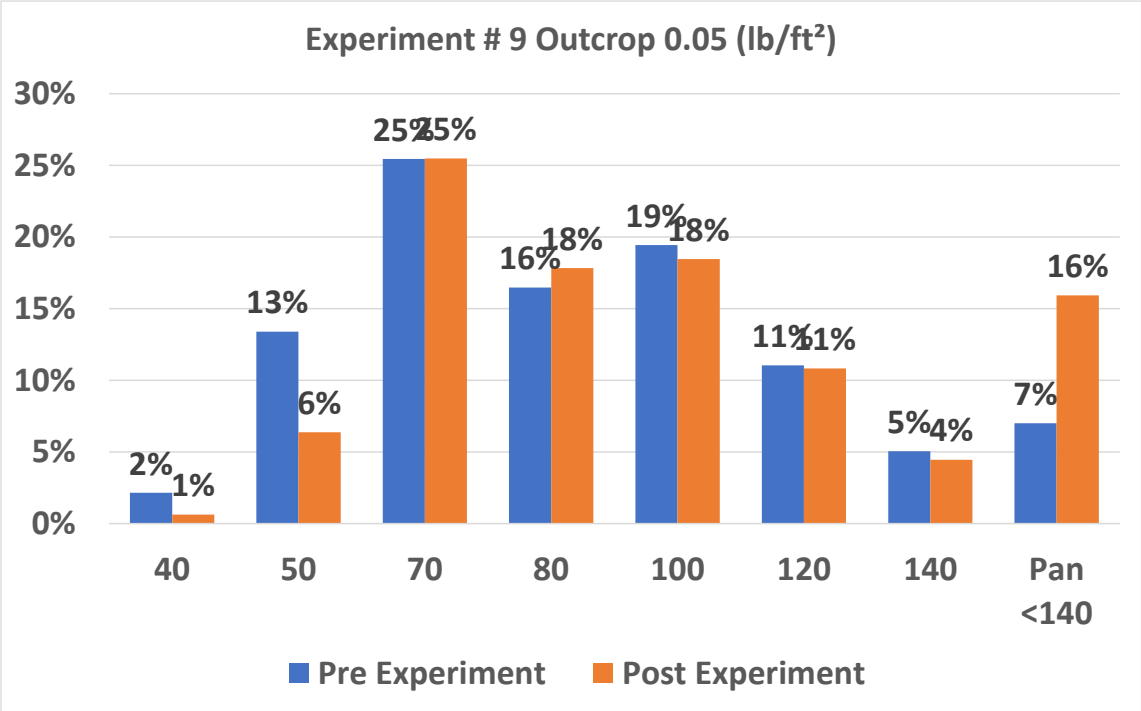

Figure 102. Sieve analysis for experiment 9.

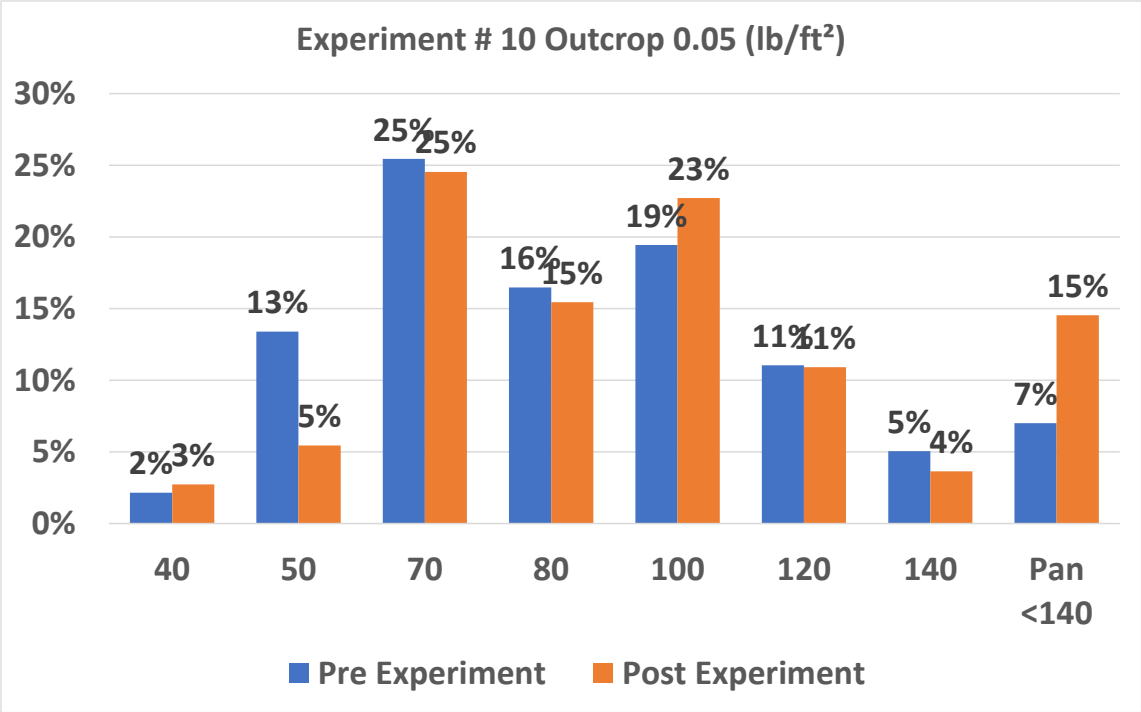

Figure 103. Sieve analysis for experiment 10.

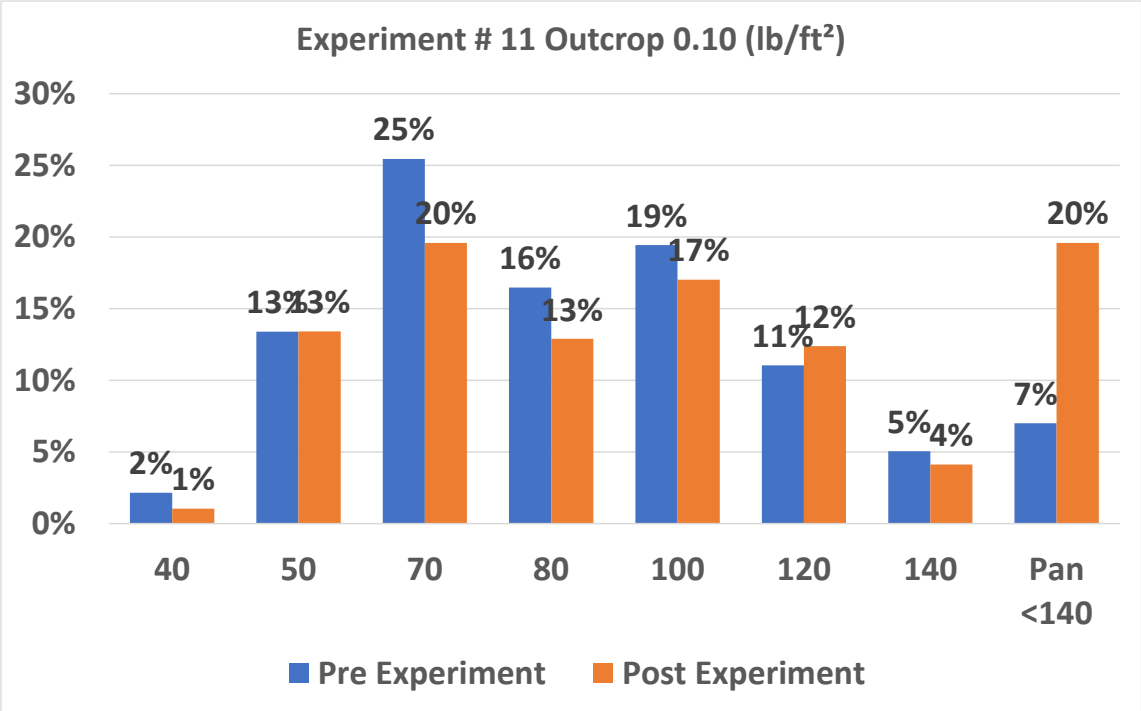

Figure 104. Sieve analysis for experiment 11.

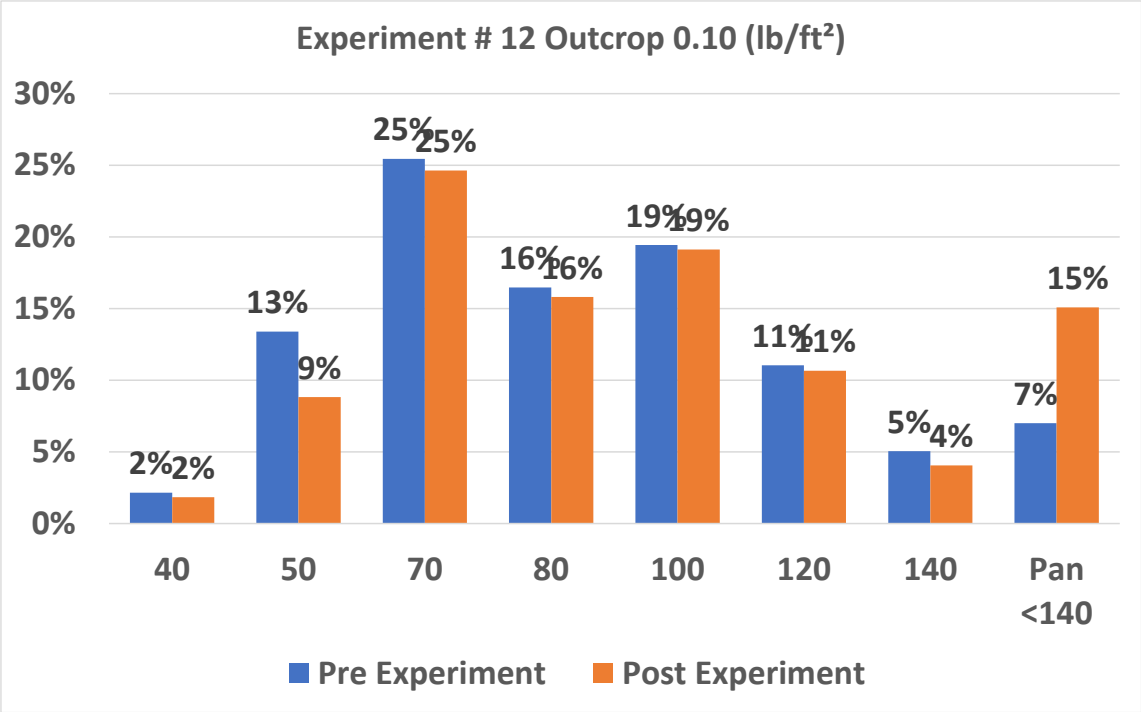

Figure 105. Sieve analysis for experiment 12.
NOTE: Experiment # 13 was an unpropped condition (0.00lb/ft^2) so there is not a proppant sieve analysis.

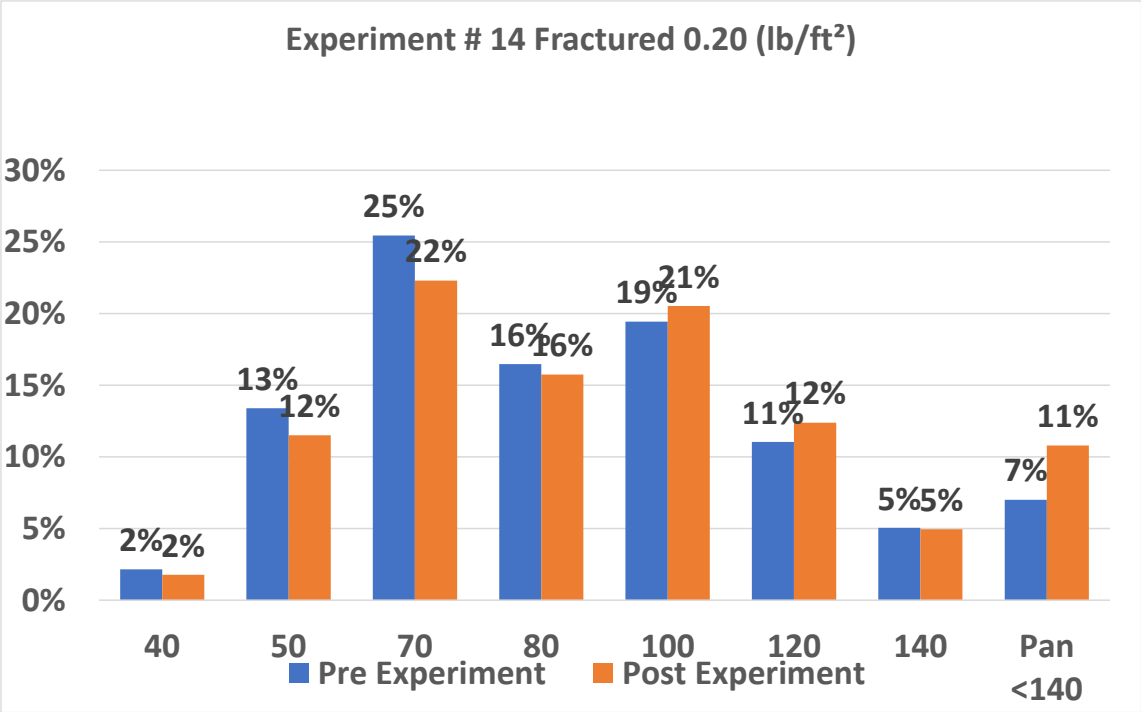

Figure 106. Sieve analysis for experiment 14.

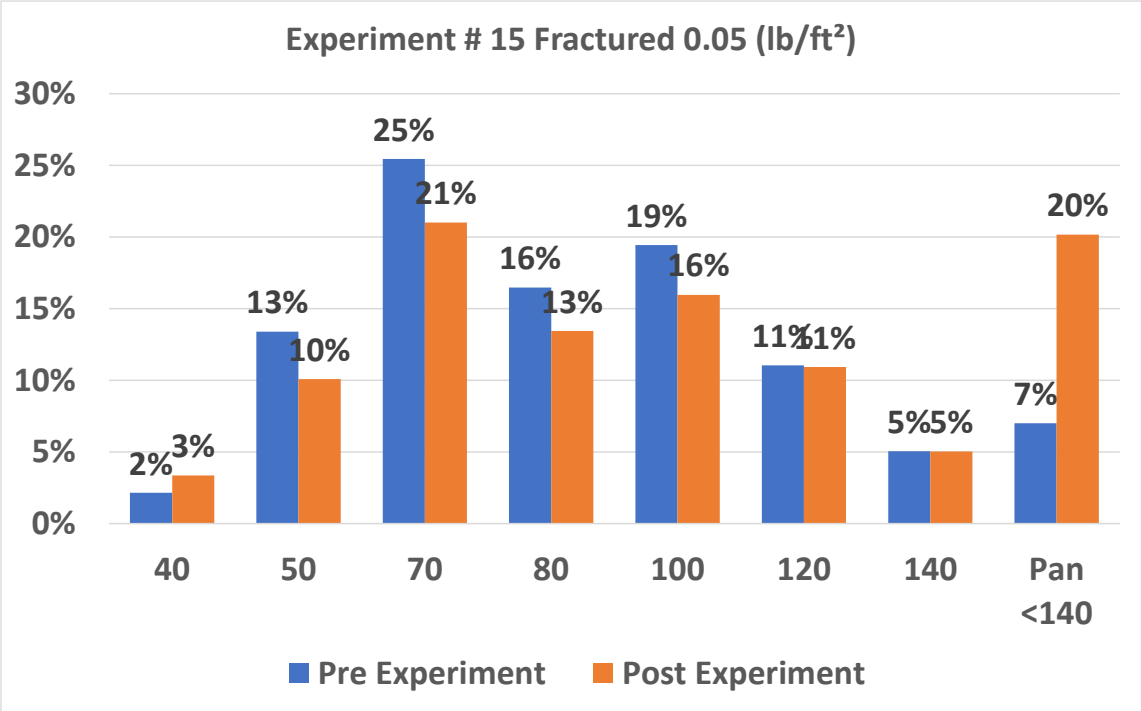

Figure 107. Sieve analysis for experiment 15.

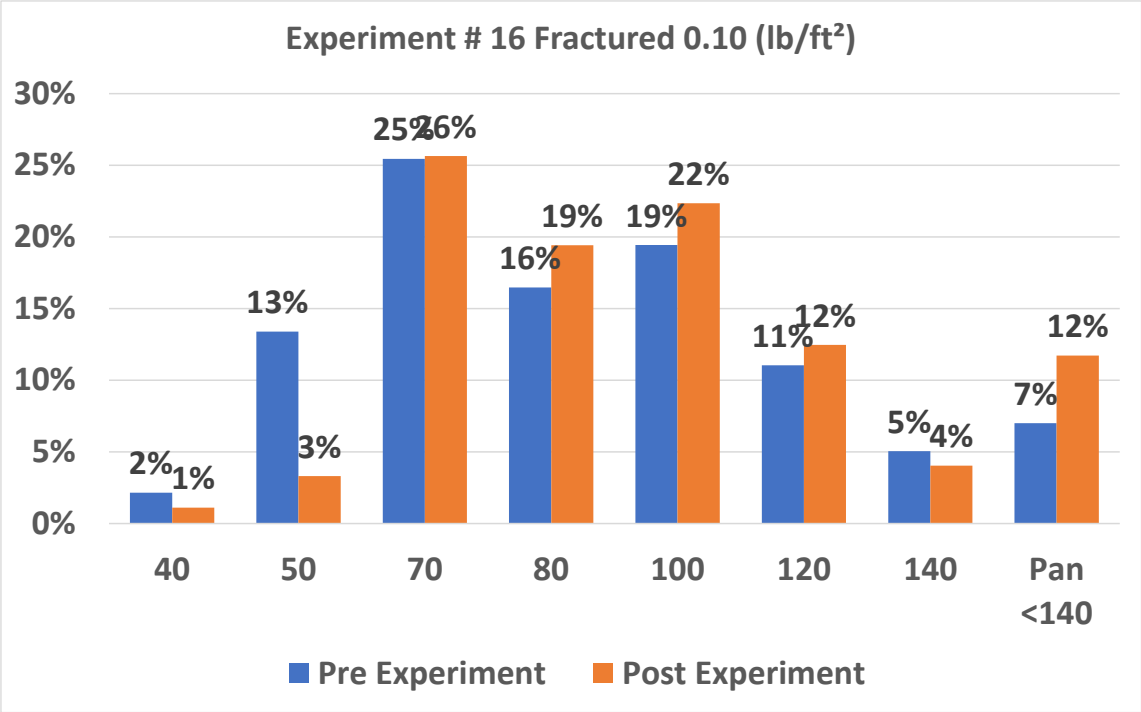

Figure 108. Sieve analysis for experiment 16.

3.5.1. Proppant concentration of 0.20lbs/ft^2

Figure 109 shows the average proppant sieve analysis for all fracture conductivity experiments with a proppant concentration of 0.20lbs/ft^2. There is a total of six test. Of these, three experiments used 100 mesh proppant from a different source than the rest of the group. Those 3 experiments were not included in this analysis. With a proppant concentration of 0.20lbs/ft^2, very little proppant crushing is observed, with only 11% of the mass ending in the pan, compared to 7% before the tests.

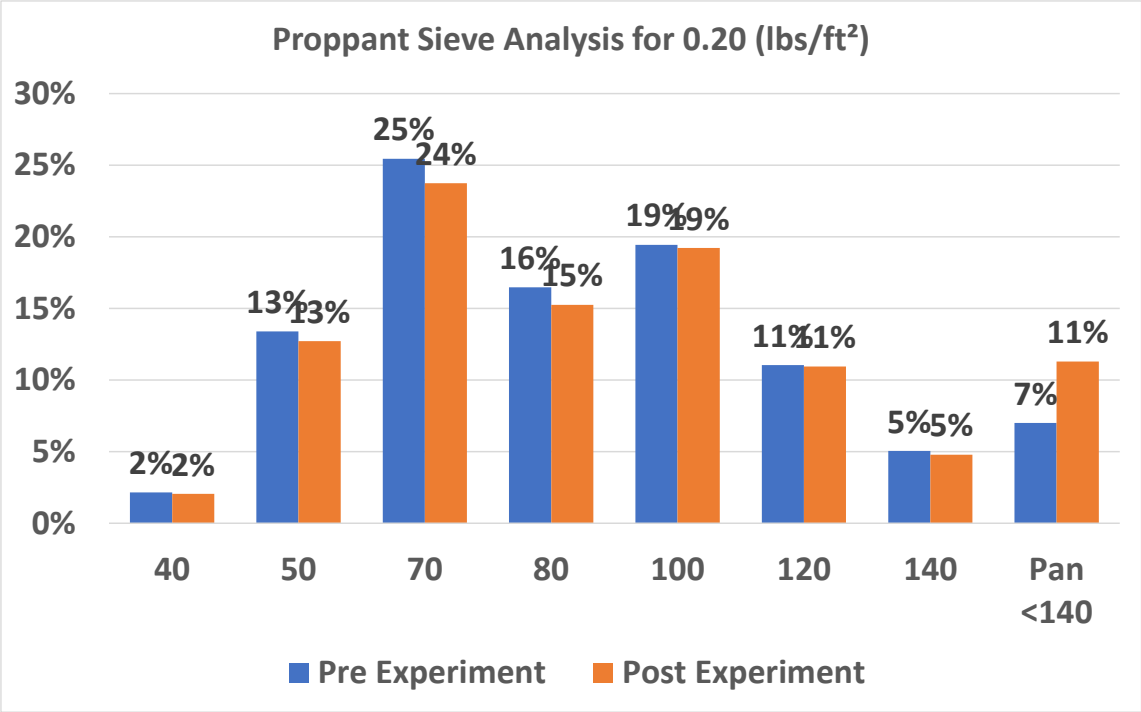

Figure 109. Proppant sieve analysis for a proppant concentration of 0.20lbs/ft^2.

3.5.2. Proppant concentration of 0.10lbs/ft^2

Figure 110 shows the average proppant sieve analysis for all fracture conductivity experiments with a proppant concentration of 0.10lbs/ft^2. Notice there is a larger post-experiment value in the 40-mesh sieve than the pre-experiment value. This is due to the experiment using downhole core which had some of the sample break out from the downhole core. The bits of sample were included in the sieve test. Only after this sieve test was preformed did it become apparent the sample chunks should obviously have been removed. Regardless, the average of all the 0.10 lbs/ft^2, yielded a higher amount of proppant crushing which can be verified by 14% of the mass ending in the pan, doubling from pre-experiment.

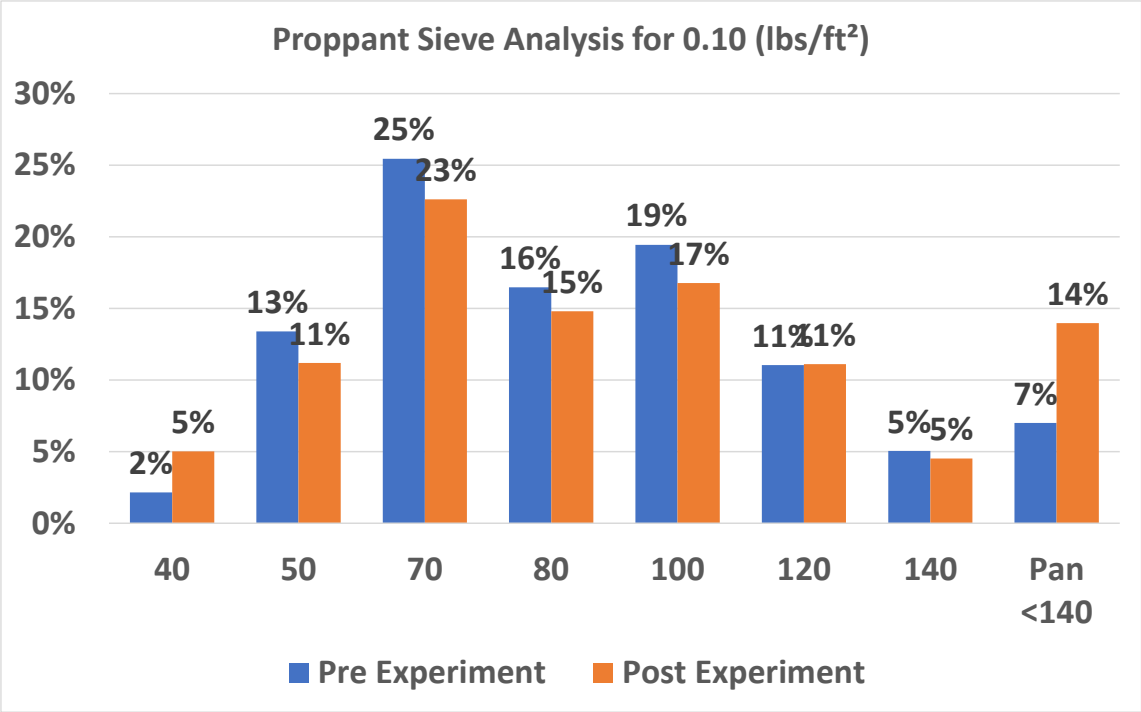

Figure 110. Proppant sieve analysis for a proppant concentration of 0.10lbs/ft^2.

3.5.3. Proppant concentration of 0.05lbs/ft^2

Figure 111 shows the average proppant sieve analysis for all fracture conductivity experiments with a proppant concentration of 0.05lbs/ft^2. Notice that the highest amount of proppant crushing occurred in the 0.05lbs/ft^2 proppant concentration, with 16% of the mass ending in the pan. One further observation, when comparing the sieve analyses of the 0.20lbs/ft^2, 0.10lbs/ft^2, and 0.05lbs/ft^2 proppant concentrations, it appears the 0.20lbs/ft^2 and 0.10lbs/ft^2 had relatively even proppant crushing throughout the different mesh sizes. However, the 0.05lbs/ft^2 seems to have a higher percentage of proppant crushing occurring in the 50-mesh sieve size.

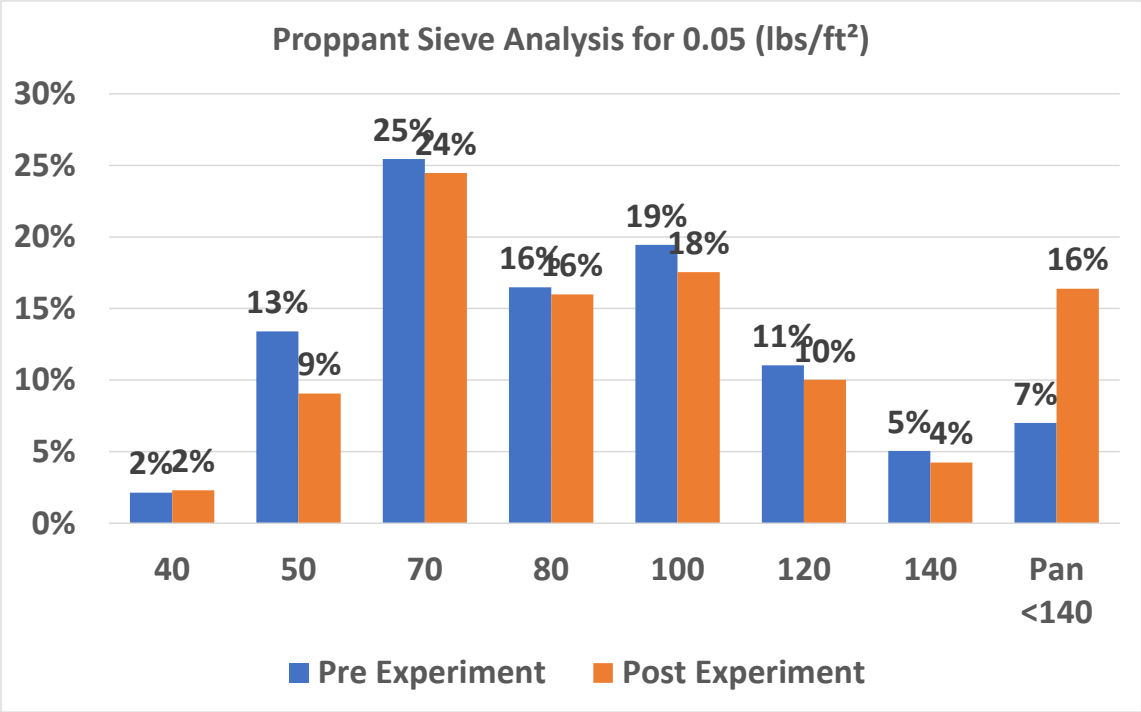

Figure 111. Proppant sieve analysis for a proppant concentration of 0.05lbs/ft^2.

4. CONCLUSIONS AND RECOMMENDATIONS*

4.1. Conclusions

This thesis presented results from multiple short term fracture conductivity experiments performed using dry nitrogen. Fracture conductivity of sawcut and fractured samples were compared, as well as samples prepared using downhole core and Austin Chalk outcrop. This study also presented the results of how fracture conductivity changed as a response to altering the proppant concentration. Finally, proppant sieve analyses were performed to quantify the amount of proppant crushing. The following conclusions were determined from analysis of the data collected:

1. The lower the proppant concentration, the higher the fracture conductivity, excluding the unpropped case. These results are due to a partial mono-layer of proppant.
2. Although 0.05lbs/ft^2 and 0.10lbs/ft^2 proppant concentrations had the highest fracture conductivities starting out, they also decreased the quickest with increasing closure stress. This is from more proppant crushing at lower proppant concentrations. This is due to less grains of proppant having to support the same closure stress which means each grain of proppant is subjected to more force.
3. Downhole core samples gave similar but higher fracture conductivity values than outcrop samples. Outcrop samples can therefore be used as proxies for downhole core samples in determining lower bounding or conservative values for fracture conductivity.

---

* Used with permission of Society of Petroleum Engineers (SPE), from Fracture Conductivity Created by Proppants and Acid in the Austin Chalk Formation, A. T. Brashear; A. D. Hill; D. Zhu; E. Kerr; R. Scofield; D. Jordan; E. Estrada; T. Tajima, 2022; permission conveyed through Copyright Clearance Center, Inc.

4. Fracture conductivities of sawcut and fractured samples were nearly identical at a proppant concentration of 0.20lbs/ft^2 but varied at proppant concentrations of 0.10lbs/ft^2 and 0.05lbs/ft^2.

4.2. Recommendations

This study only used regional 100 mesh proppant recovered directly from an SM Energy pad site to best replicate what is being used in the field. Using the lowest proppant concentration yielded the highest fracture conductivity but also yielded the highest amount of proppant crushing which would lead to fines migration and production to surface. Testing a resin coated proppant to see if the same high fracture conductivities can be achieved with less proppant crushing would be of interest. Additionally, conducting the same experiments but performing long term fracture conductivity tests would be of high interest to see how the fracture conductivity is maintained. Lastly, it is highly recommended to perform more fractured and downhole core experiments to develop a larger dataset.

REFERENCES

(2022). AUSTIN CHALK REVIVAL. Austinchalkoilgas.com. https://austinchalkoilgas.com/

(2022). Behavior of real gases. myengineeringtools.com. https://myengineeringtools.com/Thermodynamics/Behavior_Real_Gases.html

(2022). Carboxymethyl Hydroxypropyl Guar Gum (CMHPG) Used Oil Field China. made-in-china.com. https://liuheguargum.en.made-in-china.com/product/rFWAbTqUXGhd/China-Carboxymethyl-Hydroxypropyl-Guar-Gum-CMHPG-Used-Oil-Field-China.html

(2022). Fracturing Agent. Polymersco.com. https://polymersco.com/product/fracturing-agent/

(2022). Hydraulic Fracturing: Locking In Efficiencies. Hartenergy.com. https://www.hartenergy.com/exclusives/hydraulic-fracturing-locking-efficiencies-31705

(2022). hydroxypropyl Guar gum for water-base fracturing fluid of oil field. Alibaba.com. https://www.alibaba.com/product-detail/hydroxypropyl-Guar-gum-for-water-base_60348217715.html

API RP-19D. 2008. Recommended Practices for Measuring the Long-term Conductivity of Proppants. First Edition, May 1, 2008. Washington, D.C., U.S.A.: American Petroleum Institute.

API RP-61. 1989. Recommended Practices for Evaluating Short Term Proppant Pack Conductivity. First Edition, October 1, 1989. Washington, D.C., U.S.A.: American Petroleum Institute.

ASTM Standard-C136M-19. 2019. Standard Test Method for Sieve Analysis of Fine and Coarse Aggregates. West Conshohocken, Pennsylvania, U.S.A.: ASTM International.

Beckwith, Robin. "Depending On Guar For Shale Oil And Gas Development." J Pet Technol 64 (2012): 44–55. doi: https://doi.org/10.2118/1212-0044-JPT

Brannon, Harold D., Malone, Mark R., Rickards, Allan R., Wood, William D., Edgeman, J. Randall, and Josh L. Bryant. "Maximizing Fracture Conductivity with Proppant Partial Monolayers: Theoretical Curiosity or Highly Productive Reality?." Paper presented at the SPE Annual Technical Conference and Exhibition, Houston, Texas, September 2004. doi: https://doi.org/10.2118/90698-MS

Brashear, A. T., Hill, A. D., Zhu, D., Kerr, E., Scofield, R., Jordan, D., Estrada, E., and T. Tajima. “Fracture Conductivity Created by Proppants and Acid in the Austin Chalk Formation.”; Paper presented at the SPE Annual Technical Conference and Exhibition, Houston, Texas, USA, October 2022. doi: https://doi.org/10.2118/210213-MS

Cooke, C.E.. "Conductivity of Fracture Proppants in Multiple Layers." J Pet Technol 25 (1973): 1101–1107. doi: https://doi.org/10.2118/4117-PA

Copeland, A. (2020). The Impact of Proppant Grain-size Distribution on Fracture Conductivity in Shale Formations. Texas A&M University, Petroleum Engineering, College Station.

Dees, J.M., Freet, T.G., and G.S. Hollabaugh. "Horizontal Well Stimulation Results in the Austin Chalk Formation, Pearsall Field, Texas." Paper presented at the SPE Annual Technical Conference and Exhibition, New Orleans, Louisiana, September 1990. doi: https://doi.org/10.2118/20683-MS

Economides, Michael J., Hill, A. Daniel, Zhu, Ding, and Ehlig-Economides, Christine (2012). Petroleum Production Systems. 2nd. Cambridge University Press.

Fisher, M. K., Wright, C. A., Davidson, B. M., Goodwin, A. K., Fielder, E. O., Buckler, W. S., and N. P. Steinsberger. "Integrating Fracture Mapping Technologies to Optimize Stimulations in the Barnett Shale." Paper presented at the SPE Annual Technical Conference and Exhibition, San Antonio, Texas, September 2002. doi: https://doi.org/10.2118/77441-MS

Fojtasek, A. (2022). A Study of Fracture Conductivity in Carbonate Rock Created by Acid and Proppant. Texas A&M University, Petroleum Engineering, College Station.

Green, M. (2022). Happy Birthday, Fracking! api.org. https://www.api.org/news-policy and-issues/blog/2014/03/17/march-17-happy-birthday-fracking

Griffith, C., M. Pope, K. Gillespie, A. Godet, and D. Minisini, 2019, Facies in the lower Austin Chalk Group, from a roadcut on U.S. 90 and a core behind the outcrop, near Langtry, Texas: GeoGulf Transactions, v. 69, p. 79–95

Guerra, J. (2019). Fracture Conductivity Behavior in Shale Formations. PhD Dissertation, Texas A&M University, College Station, Texas, USA (August 2019).

Hollabaugh, G.S., and J.M. Dees. "Propellant Gas Fracture Stimulation of a Horizontal Austin Chalk Wellbore." Paper presented at the SPE Annual Technical Conference and Exhibition, Houston, Texas, October 1993. doi: https://doi.org/10.2118/26584-MS

Kamal, Medhat M. "Future Need of Petroleum Engineering." Paper presented at the SPE Western Regional Meeting, Virtual, April 2021. doi: https://doi.org/10.2118/200771-MS

Kyte, D.G., and D.N. Meehan. "Horizontal Spacing, Depletion, and Infill Potential in the Austin Chalk." Paper presented at the SPE Annual Technical Conference and Exhibition, Denver, Colorado, October 1996. doi: https://doi.org/10.2118/36721-MS

Martin, Ron , Baihly, Jason , Malpani, Raj , Lindsay, Garrett , and W. Keith Atwood. "Understanding Production from Eagle Ford-Austin Chalk System." Paper presented at the SPE Annual Technical Conference and Exhibition, Denver, Colorado, USA, October 2011. doi: https://doi.org/10.2118/145117-MS

Mayerhofer, M. J., Lolon, E. P., Youngblood, J. E., and J. R. Heinze. "Integration of Microseismic Fracture Mapping Results With Numerical Fracture Network Production Modeling in the Barnett Shale." Paper presented at the SPE Annual Technical Conference and Exhibition, San Antonio, Texas, USA, September 2006. doi: https://doi.org/10.2118/102103-MS

Mayerhofer, M.J., Richardson, M.F., Walker, R.N., Meehan, D.N., Oehler, M.W., and R.R. Browning. "Proppants? We Don't Need No Proppants." Paper presented at the SPE Annual Technical Conference and Exhibition, San Antonio, Texas, October 1997. doi: https://doi.org/10.2118/38611-MS

McGinley, Mark , Zhu, Ding , and A. Daniel Hill. "The Effects of Fracture Orientation and Elastic Property Anisotropy on Hydraulic Fracture Conductivity in the Marcellus Shale." Paper presented at the SPE Annual Technical Conference and Exhibition, Houston, Texas, USA, September 2015. doi: https://doi.org/10.2118/174870-MS

Palisch, Terrence, Duenckel, Robert, Bazan, Lucas, Heidt, Harmon J., and George Turk. "Determining Realistic Fracture Conductivity and Understanding Its Impact on Well Performance—Theory and Field Examples." Paper presented at the SPE Hydraulic Fracturing Technology Conference, College Station, Texas, U.S.A., January 2007. doi: https://doi.org/10.2118/106301-MS

Palisch, T.T.. T., Vincent, M.C.. C., and P.J.. J. Handren. "Slickwater Fracturing: Food for Thought." SPE Prod & Oper 25 (2010): 327–344. doi: https://doi.org/10.2118/115766-PA

Panja, Palash, and Rasoul Sorkhabi. "Geomechanical Controls on Production Performance of Austin Chalk and Eagle Ford Oil Wells in Southern Texas." Paper presented at the 56th U.S. Rock Mechanics/Geomechanics Symposium, Santa Fe, New Mexico, USA, June 2022. doi: https://doi.org/10.56952/ARMA-2022-0480

Pope, C. D., and P. J. Handren. "Completion Techniques for Horizontal Wells in the Pearsall Austin Chalk." SPE Prod Eng 7 (1992): 144–148. doi: https://doi.org/10.2118/20682-PA

Sun, Jianlei , Hu, Kyle , Wong, Joe , Hall, Bobby , and David Schechter. "Investigating the Effect of Improved Fracture Conductivity on Production Performance of Hydraulic Fractured Wells through Field Case Studies and Numerical Simulations." Paper presented at the SPE Hydrocarbon Economics and Evaluation Symposium, Houston, Texas, May 2014. doi: https://doi.org/10.2118/169866-MS

Warpinski, N.R., Mayerhofer, M.J., Vincent, M.C., Cipolla, C.L., and E.P. Lolon. "Stimulating Unconventional Reservoirs: Maximizing Network Growth While Optimizing Fracture Conductivity." J Can Pet Technol 48 (2009): 39–51. doi: https://doi.org/10.2118/114173-PA

APPENDIX A

PROPPANT SIEVE ANALYSIS

Please see below for individual proppant sieve analyses for each of the conductivity experiments that were performed, as well as 6 large pre-experiment proppant sieve analyses to develop an uncrushed proppant sieve distribution. NOTE: There were 16 fracture conductivity experiments run but only 15 proppant sieve analysis were conducted due to the unpropped (0.00lb/ft^2) fractured outcrop experiment not containing any proppant. This resulted in 21 total proppant sieve analyses.

	Pre Experiment_SM 100 Mesh_Base Line Sieve				
	Mass (g)	% Total		Starting	Ending
40	4.02	2%		4.02	
50	25.98	13%		25.96	-0.02
70	50.43	25%		50.33	-0.10
80	33.55	17%		33.50	-0.05
100	38.25	19%		38.19	-0.06
120	22.96	12%		22.98	0.02
140	9.88	5%		9.95	0.07
Pan <140	14.22	7%		14.26	0.04
Total	199.29	100%			

	Pre Experiment_SM 100 Mesh_Large Sample 1				
	Mass (g)	% Total		Starting	Ending
40	5.32	2%		7.04	1.72
50	32.25	13%		33.89	1.64
70	63.09	26%		64.68	1.59
80	40.91	17%		42.55	1.64
100	46.26	19%		47.89	1.63
120	26.11	11%		27.82	1.71
140	12.07	5%		13.81	1.74
Pan <140	17.27	7%		18.99	1.72
Total	243.28	100%			

	Pre Experiment_SM 100 Mesh_Large Sampe 2				
	Mass (g)	% Total		Starting	Ending
40	3.73	2%		5.43	1.70
50	23.08	13%		24.71	1.63
70	43.56	25%		45.17	1.61
80	27.97	16%		29.62	1.65
100	34.25	20%		35.90	1.65
120	18.97	11%		20.67	1.70
140	9.06	5%		10.81	1.75
Pan <140	11.97	7%		13.67	1.70
Total	172.59	100%			

	Pre Experiment_SM 100 Mesh_Large Sample 3				
	Mass (g)	% Total		Starting	Ending
40	5.21	2%		6.92	1.71
50	31.52	15%		33.17	1.65
70	57.51	27%		59.10	1.59
80	35.02	16%		36.66	1.64
100	40.14	19%		41.79	1.65
120	22.26	10%		23.97	1.71
140	9.81	5%		11.57	1.76
Pan <140	12.44	6%		14.13	1.69
Total	213.91	100%			

	Pre Experiment_SM 100 Mesh_Large Sample 4				
	Mass (g)	% Total		Starting	Ending
40	3.24	2%		4.92	1.68
50	21.05	13%		22.69	1.64
70	39.23	24%		40.83	1.60
80	25.91	16%		27.56	1.65
100	32.26	20%		33.89	1.63
120	18.40	11%		20.11	1.71
140	8.70	5%		10.44	1.74
Pan <140	12.31	8%		14.01	1.70
Total	161.10	100%			

	Pre Experiment_SM 100 Mesh_Large Sample 5				
	Mass (g)	% Total		Starting	Ending
40	3.67	2%		5.37	1.70
50	23.28	13%		24.93	1.65
70	44.70	24%		46.31	1.61
80	29.91	16%		31.57	1.66
100	36.89	20%		38.54	1.65
120	20.79	11%		22.52	1.73
140	9.71	5%		11.47	1.76
Pan <140	13.96	8%		15.68	1.72
Total	182.91	100%			

	Experiment # 1 Outcrop 0.20 (lb/ft²)				
	SM11_1	% Total		Starting	Ending
40	0.42	8%		2.11	1.69
50	2.07	40%		3.74	1.67
70	1.48	28%		3.07	1.59
80	0.58	11%		2.22	1.64
100	0.37	7%		2.01	1.64
120	0.14	3%		1.86	1.72
140	0.06	1%		1.82	1.76
Pan <140	0.12	2%		1.85	1.73
Total	5.24	100%			

	Experiment # 2 Downhole Core 0.20 (lb/ft²)				
	SM12_1	% Total		Starting	Ending
40	0.23	5%		1.92	1.69
50	1.40	33%		3.07	1.67
70	1.01	24%		2.60	1.59
80	0.36	9%		2.00	1.64
100	0.42	10%		2.06	1.64
120	0.22	5%		1.94	1.72
140	0.04	1%		1.80	1.76
Pan <140	0.54	13%		2.27	1.73
Total	4.22	100%			

	Experiment # 3 Outcrop 0.20 (lb/ft²)				
	SM11_2	% Total		Starting	Ending
40	0.32	6%		2.01	1.69
50	1.64	32%		3.31	1.67
70	1.45	29%		3.04	1.59
80	0.63	12%		2.27	1.64
100	0.51	10%		2.15	1.64
120	0.20	4%		1.92	1.72
140	0.06	1%		1.82	1.76
Pan <140	0.27	5%		2.00	1.73
Total	5.08	100%			

	Experiment # 4 Downhole Core 0.20 (lb/ft²)				
	SM12_2	% Total		Starting	Ending
40	0.09	2%		1.78	1.69
50	0.49	10%		2.16	1.67
70	0.96	20%		2.55	1.59
80	0.71	15%		2.35	1.64
100	0.91	19%		2.55	1.64
120	0.61	13%		2.33	1.72
140	0.29	6%		2.05	1.76
Pan <140	0.73	15%		2.46	1.73
Total	4.79	100%			

	Experiment # 5 Outcrop 0.20 (lb/ft²)				
	SM11_3	% Total		Starting	Ending
40	0.11	3%		0.10	-0.01
50	0.72	17%		0.73	0.01
70	1.25	30%		1.16	-0.09
80	0.63	15%		0.59	-0.04
100	0.74	18%		0.73	-0.01
120	0.29	7%		0.36	0.07
140	0.13	3%		0.21	0.08
Pan <140	0.31	7%		0.34	0.03
Total	4.18	100%			

	Experiment # 6 Outcrop 0.10 (lb/ft²)				
	SM11_4	% Total		Starting	Ending
40	0.04	2%		1.71	1.67
50	0.35	17%		1.96	1.61
70	0.52	26%		2.08	1.56
80	0.2	10%		1.79	1.59
100	0.17	8%		1.75	1.58
120	0.28	14%		1.94	1.66
140	0.17	8%		1.83	1.66
Pan <140	0.29	14%		1.91	1.62
Total	2.02	100%			

	Experiment # 7 Downhole Core 0.10 (lb/ft²)				
	SM12_3	% Total		Starting	Ending
40	0.47	17%		2.15	1.68
50	0.42	15%		2.04	1.62
70	0.48	17%		2.04	1.56
80	0.39	14%		2.02	1.63
100	0.41	15%		2.03	1.62
120	0.2	7%		1.91	1.71
140	0.08	3%		1.81	1.73
Pan <140	0.3	11%		1.97	1.67
Total	2.75	100%			

	Experiment # 8 Outcrop 0.05 (lb/ft²)				
	SM14_1	% Total		Starting	Ending
40	0.04	3%		1.70	1.66
50	0.19	14%		1.80	1.61
70	0.35	26%		1.92	1.57
80	0.22	17%		1.83	1.61
100	0.18	14%		1.79	1.61
120	0.10	8%		1.78	1.68
140	0.05	4%		1.77	1.72
Pan <140	0.20	15%		1.87	1.67
Total	1.33	100%			

	Experiment # 9 Outcrop 0.05 (lb/ft²)				
	SM14_2	% Total		Starting	Ending
40	0.01	1%		1.70	1.69
50	0.10	6%		1.75	1.65
70	0.40	25%		2.00	1.60
80	0.28	18%		1.92	1.64
100	0.29	18%		1.93	1.64
120	0.17	11%		1.89	1.72
140	0.07	4%		1.83	1.76
Pan <140	0.25	16%		1.96	1.71
Total	1.57	100%			

	Experiment # 10 Outcrop 0.05 (lb/ft²)				
	SM14_3	% Total		Starting	Ending
40	0.03	3%		1.72	1.69
50	0.06	5%		1.71	1.65
70	0.27	25%		1.87	1.60
80	0.17	15%		1.85	1.68
100	0.25	23%		1.92	1.67
120	0.12	11%		1.87	1.75
140	0.04	4%		1.82	1.78
Pan <140	0.16	15%		1.94	1.78
Total	1.10	100%			

	Experiment # 11 Outcrop 0.10 (lb/ft²)				
	SM15_1	% Total		Starting	Ending
40	0.02	1%		1.73	1.71
50	0.26	13%		1.90	1.64
70	0.38	20%		1.98	1.60
80	0.25	13%		1.91	1.66
100	0.33	17%		1.97	1.64
120	0.24	12%		1.95	1.71
140	0.08	4%		1.86	1.78
Pan <140	0.38	20%		2.12	1.74
Total	1.94	100%			

	Experiment # 12 Outcrop 0.10 (lb/ft²)				
	SM15_2	% Total		Starting	Ending
40	0.05	2%		1.75	1.70
50	0.24	9%		1.90	1.66
70	0.67	25%		2.27	1.60
80	0.43	16%		2.08	1.65
100	0.52	19%		2.16	1.64
120	0.29	11%		2.02	1.73
140	0.11	4%		1.90	1.79
Pan <140	0.41	15%		2.19	1.78
Total	2.72	100%			

	Experiment # 14 Fractured 0.20 (lb/ft²)				
	SM16_2	% Total		Starting	Ending
40	0.10	2%		1.82	1.72
50	0.65	12%		2.32	1.67
70	1.26	22%		2.86	1.60
80	0.89	16%		2.54	1.65
100	1.16	21%		2.81	1.65
120	0.70	12%		2.43	1.73
140	0.28	5%		2.08	1.80
Pan <140	0.61	11%		2.38	1.77
Total	5.65	100%			

	Experiment # 15 Fractured 0.05 (lb/ft²)				
	SM16_3	% Total		Starting	Ending
40	0.04	3%		1.73	1.69
50	0.12	10%		1.92	1.80
70	0.25	21%		1.84	1.59
80	0.16	13%		1.79	1.63
100	0.19	16%		1.82	1.63
120	0.13	11%		1.84	1.71
140	0.06	5%		1.83	1.77
Pan <140	0.24	20%		1.99	1.75
Total	1.19	100%			

	Experiment # 16 Fractured 0.10 (lb/ft²)				
	SM16_4	% Total		Starting	Ending
40	0.03	1%		1.74	1.71
50	0.09	3%		1.91	1.82
70	0.70	26%		2.33	1.63
80	0.53	19%		2.19	1.66
100	0.61	22%		2.29	1.68
120	0.34	12%		2.09	1.75
140	0.11	4%		1.93	1.82
Pan <140	0.32	12%		2.11	1.79
Total	2.73	100%			

Average ending cup weight	Average weight difference from first cup
1.69	
1.67	0.02
1.59	0.1
1.64	0.05
1.64	0.05
1.72	-0.03
1.76	-0.07
1.73	-0.04